Aus dem Lehrstuhl für Physiologische Chemie im Biomedizinischen Centrum
Institut der Ludwig-Maximilians-Universität München
Vorstand: Prof. Dr. Andreas G. Ladurner

The role of METTL3 and ADP-ribosylation in DNA repair

Dissertation
zum Erwerb des Doktorgrades der Naturwissenschaften
an der Medizinischen Fakultät der
Ludwig-Maximilians-Universität München

vorgelegt von
Claudia Patricia González Leal

aus
Monterrey, México

Jahr
2025

Mit Genehmigung der Medizinischen Fakultät
der Ludwig-Maximilians-Universität München

Betreuer:	Prof. Dr. Andreas G. Ladurner
Zweitgutachter:	Prof. Dr. Peter B. Becker
Dekan:	Prof. Dr. med. Thomas Gudermann
Tag der mündlichen Prüfung:	12. Dezember 2025

Table of content

Zusammenfassung (Deutsch):

Die Reaktion auf DNA-Schäden (DNA Damage Response, DDR) ist ein kritischer zellulärer Mechanismus, der die genomische Integrität aufrechterhält. Ein Versagen der DDR kann zu einem Zellzyklusarrest, Zelltod oder dem Auftreten von Krankheiten wie Krebs führen. Ein Schlüsselelement in der DDR ist die Poly(ADP-ribose) Polymerase 1 (PARP1), die DNA-Läsionen erkennt und einen schnellen Anstieg der ADP-Ribosylierung (PARylierung) auslöst. Diese posttranslationale Modifikation erleichtert verschiedene zelluläre Prozesse, einschließlich Chromatinentspannung, Rekrutierung von DDR-Proteinen, Modulation ihrer Aktivität und dem Aufbau von DDR-Komplexen.

Wachsende Beweise deuten auf eine Rolle von RNA und RNA-bindenden Proteinen in der DDR hin, wobei RNA als Vorlage für RNA-vermittelte Reparatur dient, gestoppte RNA-Polymerase als Überwachungsmechanismus der DNA-Integrität fungiert und RNA-bindende Proteine multiple Rollen in DDR-Wegen spielen. Jüngste Studien haben die Überschneidung zwischen RNA-bindenden Proteinen und PAR-Interaktoren hervorgehoben, was auf eine komplexe Wechselwirkung zwischen PARylierung und RNA-Biologie hinweist. Diese Studie konzentriert sich auf METTL3/14, einen Komplex, der für die Katalyse der N6-Methyladenosin (m6A) Methylierung von RNA verantwortlich ist und der gezeigt hat, dass er in einer PARP-abhängigen Weise zu DNA-Schadensstellen rekrutiert wird.

In dieser Studie charakterisierten wir die Rekrutierung von METTL3/14 in Echtzeit mittels Lebendzell-Imaging in Kombination mit Laser-Mikrobestrahlung. Wir bestätigten, dass METTL3/14 schnell zu DNA-Schadensstellen rekrutiert wurde und dass seine Rekrutierung von aktiver PARylierung abhängt. Unsere Assays legen nahe, dass die Methyltransferasen unabhängig voneinander rekrutiert werden, dass der C-terminale Bereich von METTL3, der die Methyltransferasedomäne enthält, für die Rekrutierung ausreichend ist und dass RNA zur Akkumulation des Komplexes an DNA-Läsionen beiträgt. Darüber hinaus liefern wir Beweise, dass METTL3/14 in vitro an PAR und RNA binden kann und dass hohe Konzentrationen von PAR RNA verdrängen können, wenn auch nicht vollständig. Außerdem zeigten METTL3-defiziente Zellen, die UV ausgesetzt waren, verzögerte 6-4PP- und CPD-Reparatur, verzögerten Transkriptionsneustart und ATF3-Akkumulation. Darüber hinaus sind diese Zellen empfindlich gegenüber Illudin S, was auf eine Rolle von METTL3 in der Transkriptions-gekoppelten Nukleotid-Exzisionsreparatur (TC-NER) hinweist. Zusätzlich untersuchten wir das therapeutische Potenzial der Kombination von METTL3- und PARP-Inhibitoren, die additive antiproliferative Effekte in Leukämie- und Brustkrebsmodellen zeigten. Unsere Ergebnisse beleuchten das

komplexe Zusammenspiel zwischen DNA-Reparatur, RNA-Biologie und PARylierung und bieten Einblicke in die Rollen von METTL3/14 sowie deren potenzielle klinische Anwendungen.

Abstract (English):

The DNA damage response (DDR) is a critical cellular mechanism that maintains genomic integrity. Failure of the DDR can lead to cell cycle arrest, cell death, or the emergence of diseases such as cancer. A key player in DDR is the Poly(ADP-ribose) polymerase 1 (PARP1), which detects DNA lesions and triggers a rapid burst of ADP-ribosylation (PARylation). This post-translational modification facilitates various cellular processes, including chromatin decompaction, recruitment of DDR proteins, modulation of their activity, and scaffolding of DDR assemblies.

Growing evidence indicates a role for RNA and RNA-binding proteins in the DDR, with RNA serving as a template for RNA-mediated repair, stalled RNA polymerase serving as a surveillance mechanism of DNA integrity, and RNA-binding proteins that play multiple roles in DDR pathways. Recent studies have highlighted the overlap between RNA-binding proteins and PAR interactors, suggesting a complex interplay between PARylation and RNA biology. This study focuses on METTL3/14, a complex responsible for catalyzing N6-methyladenosine (m6A) methylation of RNA, which has been shown to recruit to DNA damage sites in a PARP-dependent manner.

In this study, we characterized the recruitment of METTL3/14 in real-time using live-cell imaging coupled with laser microirradiation. We confirmed that METTL3/14 rapidly recruited to DNA damage sites, with its recruitment being dependent on active PARylation. Our assays suggest that the methyltransferases recruit independently of each other, that the C-terminal region of METTL3, which contains the methyltransferase domain, is sufficient for recruitment, and that RNA contributes to the accumulation of the complex at DNA lesions. Furthermore, we provide evidence that METTL3/14 can bind to PAR and RNA *in vitro* and that high concentrations of PAR can displace, although not outcompete RNA. Moreover, METTL3 deficient cells exposed to UV exhibited delayed 6-4PP and CPD repair, delayed transcription restart, and ATF3 accumulation. Moreover, these cells are sensitive to Illudin S, suggesting a role for METTL3 in transcription-coupled nucleotide excision repair (TC-NER). Additionally, we explored the therapeutic potential of combining METTL3 and PARP inhibitors, which showed additive antiproliferative effects in leukemia and breast cancer models. Our findings elucidate the complex interplay between DNA repair, RNA biology, and PARylation, offering insights into METTL3/14's roles and potential clinical applications.

List of figures

List of tables

List of abbreviations

aAM	α-Amanitin
ActD	Actinomycin D
ALKBH5	Alpha-Ketoglutarate-dependent hydroxylase homolog 5, RNA demethylase
ARTs	ADPribosyltransferases
ATF3	Activating transcription factor 3
ATM	Ataxia Telangiectasia Mutated
ATR	Ataxia Telangiectasia and Rad3-Related
BrdU	Bromodeoxyuridine
DSB	Double strand DNA break
DNA	Deoxyribonucleic acid
DNA-Pk	DNA-Dependent Protein Kinase
FRAP	Fluorescence recovery after photobleaching
FTO	Fat mass and obesity associated factor
GG-NER	Global genome Nucleotide Excision Repair
HDAC	Histone acetylases and deacetylases
IF	Immunofluorescence
IR	X-ray irradiation
K_D	Binding affinity
M6A	N6-methyladensine
METTL	Methyltransferase like
MRE11	Meiotic recombination 11
mRNA	messenger RNA
MTC	Methyltransferase complex
NBS1	Nijmegen breakage syndrome protein 1
NELF-A	Negative Elongation Factors A
NER	Nucleotide excision repair
PARP1	Poly (ADP-ribose) polymerase 1
PARG	Poly (ADP-ribose) glycohydrolase
PAR	Poly (ADP-ribose)
PARPi	PARP inhibitor. In this project, olaparib was used.
PARGi	PARG inhibitor
PBM	Poly(ADP-ribose) binding motif
PIKK	Phosphatidylinositol 3-kinase-related kinases
RBP	RNA binding proteins
RNA	Ribonucleic acid

RNAPII	RNA Polymerase II
ROS	Reactive oxygen species
RPE1	Human retinal pigment epithelial cells.
SAM	S-Adenosylmethionine
SAH	S-Adenosylhomocysteine
siRNA	small interference RNA
SSB	single strand DNA break
SUMO	Small Ubiquitin-like Modifier
T_m	Melting temperature
TC-NER	Transcription-coupled Nucleotide Excision Repair
TonEBP	Tonicity-responsive enhancer-binding protein or nuclear factor of activated T cells 5 (NFAT5)
TSA	Trichostatin A
UV	Ultraviolet light
U2OS	Osteosarcoma-derived cells
XPC	Xeroderma pigmentosum, complentation group C
XRCC1	X-ray repair cross complementing protein 1

1. Introduction

1.1 Safekeeping the genetic code

The complete set of instructions necessary for proper cellular function is contained within the DNA. However, the integrity of the genome faces continuous challenges from widespread endogenous and exogeneous sources of damage including UV light, reactive metabolites and environmental mutagens, which can cause a wide variety of DNA lesions. Additionally, errors during biological processes, such as DNA replication, can instigate DNA damage.

Genome stability, along with the accurate replication and transmission of the genetic material to succeeding generations, is achieved through a network of pathways known as the DNA damage response (DDR). This response is intricately woven into other cellular processes, such as the cell cycle. For example, by activating cell cycle checkpoints, the DDR can directly facilitate or halt cell cycle progression. Interconnections with processes including chromatin remodeling, DNA transcription, and replication, make the DDR crucial for maintaining cellular homeostasis. Consequently, failure to safeguard genome integrity can lead to cellular arrest, apoptosis, or senescence. Furthermore, this intricate network of DNA repair undergoes precise spatiotemporal regulation, ensuring the specific and coordinated action of DDR enzymes in response to different DNA lesions. The misrepair of DNA lesions and the misregulation of DDR pathways are associated with human health implications, contributing to diseases like progeria and cancer (Figure 1).

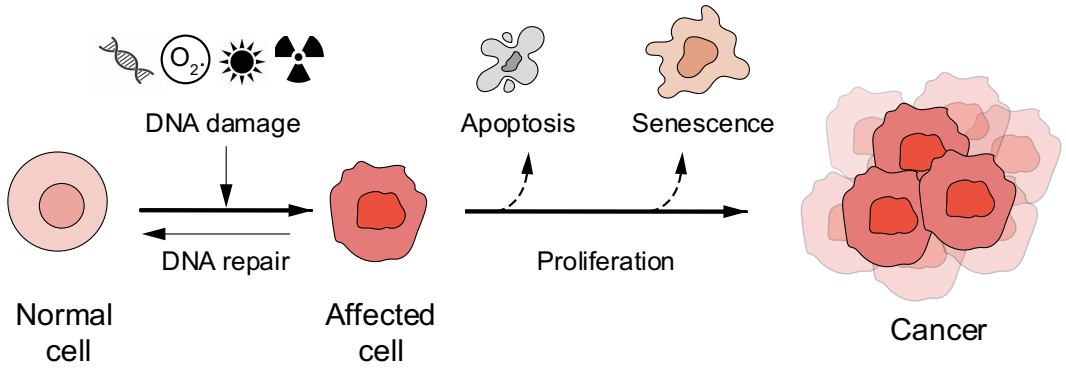

Figure 1. The DDR safeguards the genetic code. Both internal and external factors contribute to DNA damage, jeopardizing the integrity of the genome. To counteract this, cells have developed a network of repair mechanisms to ensure the restoration of genome integrity. Failure to repair DNA lesions can lead to senescence, cell death, or diseases like cancer. The figure was created with Adobe Illustrator.

Different DNA damage agents induce unique types of DNA lesions, which are repaired through distinct pathways. An overview of different DNA repair pathways is provided next, which is also represented in Figure 2. Importantly, we focus on UV-induced DNA damage repair, in particular transcription-coupled Nucleotide Excision Repair (TC-NER), as their understanding is relevant to the work described here.

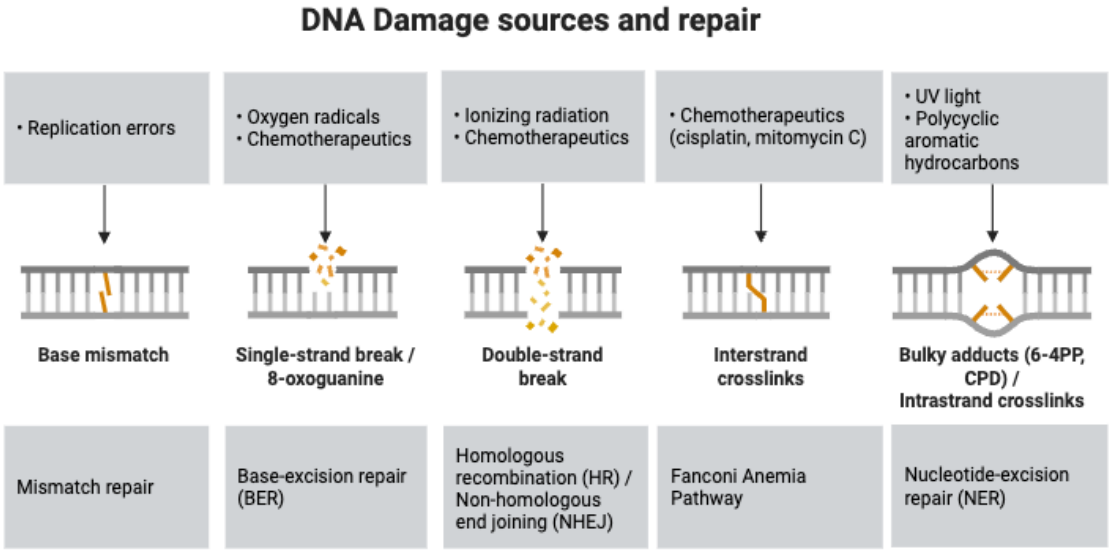

Figure 2. **Sources and repair mechanisms of DNA damage.** DNA is constantly exposed to harmful agents from both endogenous and exogenous sources (top), leading to specific types of damage (middle). If left unrepaired, these can result in mutations, senescence or apoptosis. Specialized DNA repair mechanisms (bottom) can detect and fix these lesions to maintain genetic integrity. Figure adapted from (Hoeijmakers, 2001) with Biorender.com.

1.1.1 UV-light induces DNA damage

DNA damage can originate from both endogenous and exogenous sources. One external factor that harms the DNA is the ultraviolet (UV) light. The energy of UV radiation decreases as the wavelength increases: UV-C (<280 nm), UV-B (280-315 nm), and UV-A (315-400 nm). Both UV-C and UV-B can be absorbed by the aromatic structures of nucleotides in the DNA, directly impacting the structural integrity of the DNA and inducing lesions that distort the DNA helix (Rastogi et al., 2010). The primary photolesions resulting from UV-irradiation are cyclobutene-pyrimidine dimers (CPDs) and 6-4 photoproducts (6-4PPs), both causing a bend in the DNA backbone that can lead to the interruption of RNA polymerase activity (Lima-Bessa et al., 2008).

UV-radiation can also indirectly damage the DNA by generating reactive oxygen species (ROS), which can oxidize DNA bases, forming products such as 8-oxo- 7,8-

dihydroguanine (8-oxoG) that leads to a G-T transversion during DNA replication (Rastogi et al., 2010). Besides causing base damage, ROS can interact with lipids and proteins within the cell leading to the formation of reactive aldehydes capable of forming DNA adducts. Additionally, photolesions can lead to the blockage of transcription and replication, resulting in the formation of single strand DNA breaks (SSBs), or highly cytotoxic double-strand breaks (DSBs). Specifically, UV-irradiation and ROS induction can contribute to DSBs induced by topoisomerase I cleavage complex (Strumberg et al., 2000) and the abortive activity of topoisomerase II activity (Banáth & Olive, 2003; Ohnishi et al., 2009), respectively.

1.1.2 Canonical DNA damage responses to UV-induced DNA damage

The variety of DNA lesions induced by UV irradiation triggers the response of several DNA damage repair mechanisms. These distinct pathways will be discussed next and are summarized in Figure 3.

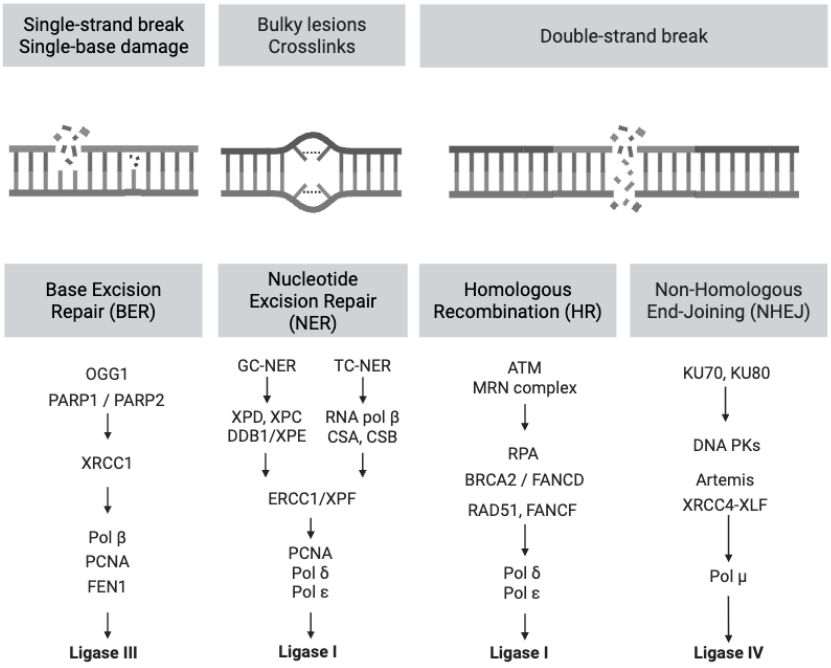

Figure 3. Summary of DDR pathways involved in the repair of UV-induced damage. UV-light can induce multiple types of DNA lesions (top), each recognized and repaired by specific DNA damage repair pathways (middle). DNA repair initiates with the recognition of the lesions by specific proteins, followed by a cascade involving various repair proteins such as DNA polymerases and ligases, ultimately leading to the repair of the DNA lesions. Figure created with Biorender.com

1.1.2.1 Base excision repair (BER)

BER is the mechanism responsible for the repair of lesions derived from base oxidation, deamination or alkylation. These lesions, which do not induce distortion to the DNA-helix, are recognized by lesion-specific DNA glycosylases. Glycosylases remove the damaged base from the sugar-phosphate backbone, generating an apurinic or apyrimidinic (AP) site. An AP-endonuclease can then excise the AP site, resulting in an SSB. Subsequently, the DNA polymerases β or δ incorporate nucleotides to the SSB, which is sealed through ligation by a DNA ligase (Hegde et al., 2008),

1.1.2.2 Homologous recombination (HR) and non-homologous end joining (NHEJ)

Repair of DSBs involves two distinct pathways known as homologous recombination (HR) and non-homologous end joining (NHEJ) (Van Gent et al., 2001). HR is an error-free mechanism that relies on the homology of the sister chromatid to repair DNA breaks. Therefore, it is exclusively performed during S and G2 phases of the cell cycle. This process requires the resection of the DNA ends at the DSB, forming 3' single-stranded DNA overhangs. These overhangs then engage in a homology-driven invasion of the sister chromatid, serving as a template for synthesizing the missing DNA fragment. The resulting DNA structure, referred to as a Holliday junction, is resolved by specific endonucleases followed by ligation of the remaining nicks, ultimately restoring the original DNA sequence (X. Li & Heyer, 2008).

In contrast, NHEJ serves as the preferred pathway for mending DSBs in the absence of a sister chromatid, rendering it particularly active during G1 phase of cell cycle. During NHEJ, the Ku heterodimer binds to DNA ends thereby preventing recession. Moreover, Ku serves as a node for the docking of nucleases, polymerases and ligases (Lieber, 2010). In contrast to HR, the processing of DNA ends involves either the excision or the addition of random nucleotides before their subsequent ligation (Lieber, 2010). While NHEJ is a time-efficient repair mechanism, it carries the potential of introducing minor insertions or deletions in the genome, thereby increasing the probability of acquiring deleterious mutations.

1.1.2.3 Nucleotide excision repair (NER)

NER is a highly versatile pathway that repairs a variety of lesions that induce distortions to the DNA helix. Thus, NER is responsible for the repair of CPDs and 6-4PPs arising from UV irradiation, as well as lesions induced by chemical adducts and UV-mimetic drugs. Two discrete NER sub-pathways, namely the global genome NER (GG-NER) and the transcription-coupled NER (TC-NER), are delineated based on how the DNA lesions are detected.

Lesions within untranscribed DNA regions, including the non-transcribed strand of active genes, undergo repair through GG-NER. The xeroderma pigmentosum complementation group C protein (XPC), which constantly probes the integrity of the DNA, binds to the opposite strand of a helix-destabilizing lesion (Marteijn et al., 2014). Notably, CPDs, exerting minimal impact on the DNA helix structure, are not directly recognized by XPC. Instead, the UV-DDB complex binds and rearranges the affected DNA, facilitating the subsequent binding of XPC (Sugasawa, 2016).

TC-NER specializes in rectifying DNA lesions on the transcribed strand of active genes, where bulky lesions stalls RNA Polymerase II (RNAPII). This impediment prompts increased interaction between RNAPII and TC-NER proteins, namely UVSSA, CSA and CSB, facilitating the recruitment of additional proteins. Remodeling of stalled transcription complexes is orchestrated by HMGN1, XAB2, FIIS and p300, thereby exposing the DNA lesion for subsequent repair (Van Den Heuvel et al., 2021).

While GG-NER and TC-NER diverge in their modes of DNA lesion recognition, they converge in their downstream machinery. After damage recognition, the XPB and XPD helicase subunits of the TFIIH complex unwind the DNA. The subsequent recruitment of XPA and the coating of the undamaged DNA by the RPA complex serve as checkpoints, confirming the presence of DNA lesions before proceeding to subsequent NER steps. After verification, the endonuclease ERCC1-XPF, followed by XPG, cleaves the damaged DNA, excising 25-30 nucleotides. Additional nucleotides are then incorporated by the coordinated action of PCNA, RFC, and DNA Polymerases ε, δ, or κ before the sealing of the DNA nicks by the activity of DNA ligase I or III (Marteijn et al., 2014).

1.1.3 DNA damage signal transduction

Although each pathway specializes in the repair of a subset of DNA lesions, some of them at specific cell cycle phases, they all share features of classic signal transduction pathways: DNA damage sensing, signal transducers and lesion repair by effectors. Members of the phospatidylinosiol 3-kinase-related kinases (PIKK), such as the ataxia telangiectasia mutated (ATM), ataxia telangiectasia and Rad3-related protein (ATR), the DNA-dependent protein kinase (DNA-Pk), as well as the poly-ADPribose polymerases (PARPs) are among the central signaling proteins that are triggered upon recognition of different DNA lesions (D'Amours et al., 1999; J. Yang, 2003). Here we provide an overview of these signaling pathways.

1.1.3.1 The PIKKs family and the DDR

Upon DNA damage, numerous proteins undergo phosphorylation at Ser/Thr-Glu motifs by the action of ATM, ATR, and DNA-Pk. Although all kinases share overlapping targets and exhibit redundant functions, *in vitro* observations suggest that ATM is predominantly activated by DSBs, whereas ATR responds to a broad spectrum of DNA lesions. Additionally, DNA-Pk selectively phosphorylates a subset of proteins involved in NHEJ (Marechal & Zou, 2013; J. Yang, 2003).

One of the extensively studied targets of the PIKKs is the phosphorylation of the histone variant H2AX, known as γH2AX, which serves as a chromatin marker for DNA breaks. This modification facilitates the recruitment of downstream repair proteins, including 53BP1 and RAD51 (Mah et al., 2010). PIKKs directly influence cell cycle progression by phosphorylating the checkpoint proteins such as Chk1, Chk2, and the tumor suppressor p53. Notably, each kinase requires a distinct protein cofactor, which serves as the DNA damage sensor, for their recruitment to DNA lesions: NBS1 for ATM, ATRIP for ATR, and Ku80 for DNA-Pk (Shiloh, 2003; J. Yang, 2003).

In contrast, the other family of DNA damage signal transducers, the poly (ADP-ribose) polymerases, can bind directly to DNA ends, triggering the subsequent signaling cascade.

1.2 The Poly (ADP-ribose) polymerases

ADP-ribosylation is a dynamic post-translational modification that is crucial for the regulation of various cellular processes, including chromatin remodeling (Poirier et

al., 1982), transcriptional regulation (D'Amours et al., 1999; Hassa & Hottiger, 2002), cell death (Chaitanya et al., 2010), and DNA damage repair (Durkacz et al., 1980, 1981; Juarez-Salinas et al., 1979). ADP-ribosylation is catalyzed by ADP-ribosylation transferases (ARTs), involving the transfer of mono- or poly (ADP-ribose) (MAR or PAR, respectively) moieties from the cofactor NAD^+ onto target proteins. Specifically, ADP-ribose can be covalently attached to serine, aspartate, and glutamate residues (Langelier et al., 2018). To date, 17 proteins have been identified as members of the poly (ADP-ribose) polymerase (PARP) family, characterized by their ability to perform MAR or PARylation. A summary of these proteins and their activity is provided in Table 1.

Table 1. ADP-ribosyltransferases and their enzymatic activity.
Adapted from (Lüscher et al., 2018).

Gene name	Alternative names	Activity
PARP1	ARTD1	PARylation
PARP2	ARTD2	PARylation
PARP3	ARTD3	MARylation
PARP4	ARTD4	MARylation
TNKS1	PARP5a, ARTD5	PARylation
TNKS2	PARP5b, ARTD6	PARylation
PARP6	ARTD17	MARylation
PARP7	ARTD14	MARylation
PARP8	ARTD16	MARylation
PARP9	ARTD9	MARylation
PARP10	ARTD10	MARylation
PARP11	ARTD11	MARylation
PARP12	ARTD12, ZC3HDC1	MARylation
PARP13	ARTD13, ZC3HAV1	Inactive
PARP14	ARTD8, BAL2	MARylation
PARP15	ARTD7, BAL3	MARylation
PARP16	ARTD15	MARylation
SIRT4		MARylation
SIRT6		MARylation

Despite sharing similarities in activity, each PARP member has distinctive structural differences and is associated with particular cellular functions. Notably, PARP1, PARP2, and PARP3 are exclusively located in the nucleus and are characterized by their contribution to DNA repair (Van Beek et al., 2021). In contrast, PARP7 has roles in both the cytoplasm (Palavalli Parsons et al., 2021) and nucleus (Kozaki et al.,

2017; Yamada et al., 2016), and its principal role is associated with immune responses. We will focus on the roles of PAR and PARP1 in the DNA damage response and RNA processes.

1.2.1 Poly(ADP-ribose) polymerase 1

Human PARP1 is one of the most extensively studied PARP enzymes owing to its abundance (Suskiewicz et al., 2020) and pivotal role in PAR formation following DNA damage (Ludwig et al., 1988). Its activity is responsible for over 90% of PAR production in primary cells following DNA damage (D'Amours et al., 1999; Shieh et al., 1998). PARP1 is a highly conserved enzyme with the three-domain structure that characterizes PARP enzymes: a DNA-binding domain at the N-terminus, an automodification domain, and a catalytic domain at the C-terminus. A schematic representation and the crystal structure of PARP1 are shown in Figure 4.

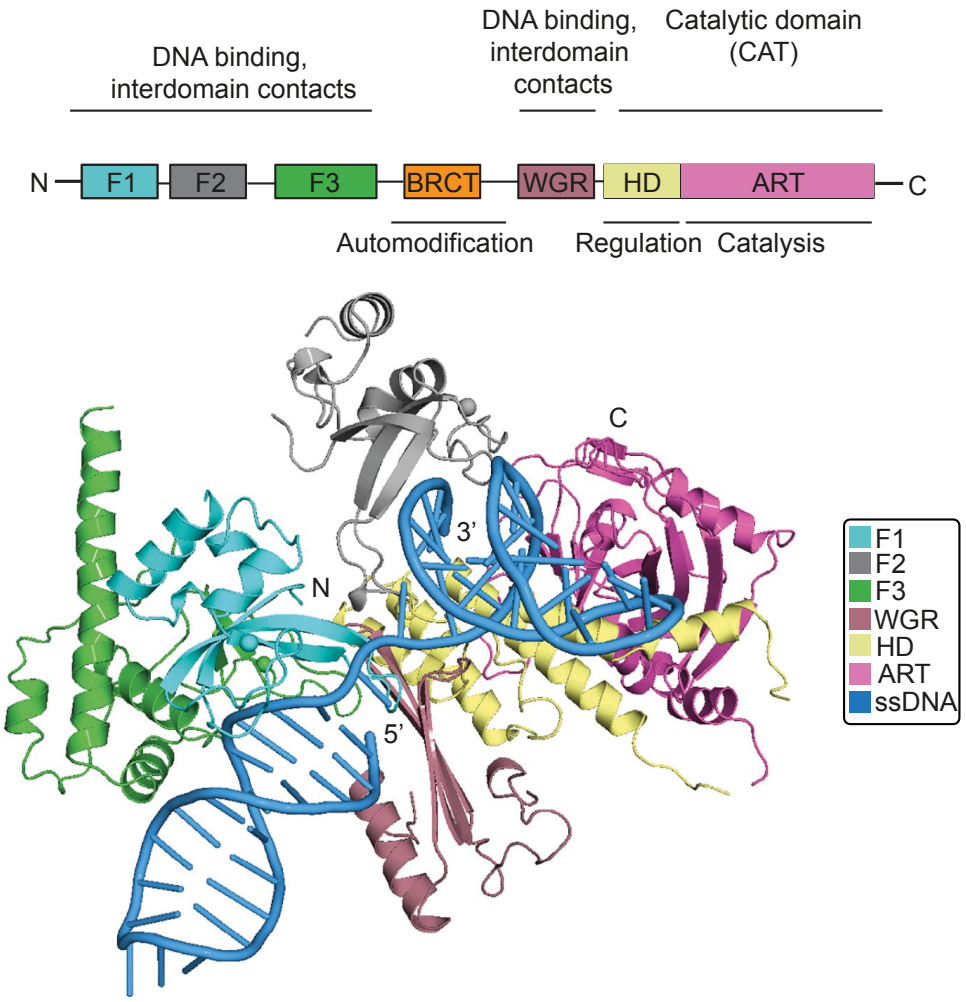

Figure 4. Structure of PARP1. (Top) Domains of PARP1. (Bottom) NMR model of PARP1 bound to a probe resembling a SSB. Adapted from (Eustermann et al., 2015) with Adobe Illustrator.

The DNA-binding domain of PARP1 contains three zinc-finger motifs. Despite their similarity, the first zinc finger motif (F1) plays a crucial role in stimulating PARP1 activity in response to DSBs. In contrast, the second zinc finger (F2) exhibits high binding affinity to SSBs (Gradwohl et al., 1990). Furthermore, F1F2 is rapidly recruited to microirradiation sites, whereas F1 and F2 alone are not recruited, suggesting collaborative interactions in lesion recognition between the zinc fingers (Ali et al., 2012; Eustermann et al., 2015). The third zinc finger (F3) contributes to both DNA binding (Buki & Kun, 1988; Eustermann et al., 2015; Langelier et al., 2012) and the chromatin rearrangement activity of PARP1 (Langelier et al., 2010).

Situated in the central region of PARP1 is an auto-modification domain rich in glutamic acid residues. Upon binding to DNA, this region undergoes extensive auto-PARylation (Langelier & Pascal, 2013). This region also houses the BRCA1 C-

terminus-like (BRCT) domain, which is characteristic of DNA damage and cell cycle checkpoint proteins (Bork et al., 1997), facilitating protein-protein interactions.

The C-terminal section of PARP1 encompasses the WGR domain and contributes to DNA binding (Eustermann et al., 2015; Langelier et al., 2012); a helical subdomain (HD), and a catalytic domain (ART) responsible for NAD^+ binding and the transfer of ADP-ribose moieties onto targets. Mutational studies have provided insights into amino acids critical for PARP1 activity. For example, the L713F mutation increases PARP1 activity (Miranda et al., 1995), whereas the E988K mutation converts PARP1 into a mono (ADP-ribose) transferase (Rolli et al., 1997). Furthermore, mutations of the tyrosine residue 986 affect the linearity of the PAR polymer, resulting in decreased branching frequency when mutated to serine and increased branching when mutated to histidine (Rolli et al., 1997; Ruf et al., 1998).

The binding of PARP1 to DNA presents an intriguing case of interdomain communication as a mechanism for activating an enzyme. In the absence of DNA, PARP1 exists in an inactive state with unengaged ART and uncommunicated globular domains. However, upon binding to DNA, the zinc fingers interact with the WGR domain, which is physically distant in the absence of DNA. In this configuration the HD is distorted, priming the ART for catalysis (Eustermann et al., 2015; Langelier et al., 2012). In addition to DNA binding, PARP1 is further regulated by its cofactor HPF1, which complements the active site of PARP1 (Suskiewicz et al., 2020), thereby allowing the polymerase to switch from its auto-modification activity to PARylation of serine residues (Langelier et al., 2021).

1.2.2 PAR metabolism

1.2.2.1 Reversal of ADP-ribosylation

PARylation is a transient post-translational modification with rapid turnover. This process involves not only the addition of ADP-ribose moieties onto proteins but also recognition, or “reading”, and the active removal or “erasing” of PAR polymers by (ADP-ribosyl) hydrolases. The chemical structure of the ADP-ribose-protein bond and the length and complexity of the PAR bound to the protein, influence the half-life of this modification and the enzyme required for its removal.

One of the key erasers of PAR is the Poly (ADP-ribose) glycohydrolase (PARG), which catalyzes the cleavage of ribose-ribose glycosidic bonds (Ikejima & Gill, 1988; Miwa et al., 1974). This implies that PARG cannot remove the terminal ribose-protein bond, for which a second (ADP-ribosyl) hydrolase, namely ARH3, is required (Rack et al., 2020). Interestingly, ARH3 and PARG colocalize with PARP1 and PARP2 after DNA damage, highlighting the regulatory role of these hydrolases during the DNA damage response (Mortusewicz et al., 2011; M. Wang et al., 2018).

The second evolutionary family of (ADP-ribosyl) hydrolases is the macrodomain. These domains can act as both “readers” and “erasers” of PAR. Macrodomains were characterized as the first modules to recognize ADP-ribose (Karras et al., 2005). Macrodomains are large evolutionary conserved modules that can bind to O-acetyl-ADP-ribose, MAR, and PAR (Barkauskaite et al., 2013; Karras et al., 2005). This domain was first identified in the core histone variant macroH2A (Pehrson & Fried, 1992), but macrodomain proteins can also be found in bacteria, archaea, eukaryotes, and RNA viruses such as coronaviruses (Leung et al., 2022; Rack et al., 2016). The hydrolytically active macrodomains include MacroD1, MacroD2 and TARG1 (Rack et al., 2020). MacroD1 and MacroD2 are MAR-hydrolyses with distinct cellular localization: while MacroD1 largely colocalizes to the mitochondria, MacroD2 can be found both in the cytosol and nucleus. In contrast, TARG1 is active in both MAR and PAR and can be found in transcriptionally active nucleoli. However, TARG1 is translocated to the nucleoplasm during DNA damage. Therefore TARG1 may contribute to the reversal of nuclear PAR after acute stimuli (Bütepage et al., 2018).

1.2.2.2 Recognition of PAR

The ability of PAR to function as a signaling modification lies in the capability of proteins to recognize this polymer and alter their activity accordingly. Hence, specific recognition of the ADP-ribose molecule is crucial. Different protein motifs have been identified to “read” PAR. Canonical PAR readers include the previously described macrodomains (1.2.2.1), the PAR-binding motif (PBM), PAR binding zinc-fingers and WWE domains (Barkauskaite et al., 2013).

PBM is a loosely defined sequence of approximately 20 amino acids, which consists of interspersed hydrophobic and basic residues (Gagné et al., 2008; Pleschke et al., 2000). Consistent with the cellular roles of PAR, PBMs can be found in proteins involved in DNA repair, chromatin structure and reorganization, transcriptional

replication, apoptosis, and cell cycle control (Barkauskaite et al., 2013; Teloni & Altmeyer, 2016). Although traditionally viewed as DNA- and RNA- interacting domains, zinc fingers can also interact with PAR when it contains a 6-8 amino acid spacer forming a Cys2-His2 type zinc finger motif. The WWE domain is rich in tryptophan (W) and glutamic acid (E) and can be found in the catalytic domain of PARPs and E3 ubiquitin ligases. Importantly, different PAR-binding domains harness specific interactions with PAR. For example, while macrodomains bind to the terminal moieties of the PAR polymer (Karras et al., 2005; Timinszky et al., 2009), the WW domain binds within the PAR chain, as it recognizes iso-ADP-ribose bonds (Z. Wang et al., 2012).

The identification of PAR motifs and PAR-interacting proteins is a growing field. For instance, a fold similar to PBM but rich in glycine and arginine, known as the GAR domain, can interact with PAR and is mainly found in proteins involved in RNA metabolism and chromatin-associated proteins (Haince et al., 2008). More recently, the RNA recognition motif (Gagné et al., 2003; Izhar et al., 2015; Ji & Tulin, 2009), the serine/arginine repeats (Isabelle et al., 2012; Malanga et al., 2008), the PAR-binding regulatory motif (Min et al., 2013) and the oligonucleotide/oligosaccharide-binding fold motif (F. Zhang et al., 2014) have also been associated with PAR interactions.

In addition to direct binding, PAR-secondary interactions may also occur. As chromatin relaxes due to the electrostatic charges of the PAR polymer (see 1.2.3.1), DNA-binding proteins can colocalize to these sites with exposed DNA (Smith et al., 2019). This colocalization to sites of active PARylation is thus PAR-dependent yet not PAR-interacting. This is the case for chromatin remodelers CHD3 and CHD4 (Smith et al., 2018). These observations offer a cautionary tale when analyzing the PAR protein-interacting network, as the timepoint and experimental conditions chosen for a readout can influence the observed PAR-interactome, potentially biasing towards enrichment of direct or indirect PAR binders.

1.2.3 The biological roles of PARP1

PARP1 contributes to cellular homeostasis and expands beyond DNA damage, contributing to DNA organization, replication, transcription, RNA metabolism, cell cycle control, and cell death. In this section, we explore PARP1's contribution to the DDR and RNA processes.

1.2.3.1 PAR-mediated chromatin decompaction

PARP1 is an early sensor of DNA damage inflicted by various sources (Ray Chaudhuri & Nussenzweig, 2017), recruiting to DNA damage sites within 1-3 seconds after damage (Satoh & Lindahl, 1992). PARP1 can directly bind to DNA ends at DNA lesions, triggering conformational changes that lead to its activation. In turn, the activation of PARP1 results in the synthesis of the ADP-ribose polymer. Each ADP-ribose unit contains two phosphate groups, which are negatively charged at physiological pH, giving the polymer a high density of negative charges. The regular, repetitive nature of the ADP-ribose polymer, together with the cumulative effect of its phosphate groups, turns PAR into a polyanionic molecule. This characteristic allows PAR to interact with other molecules, such as proteins and nucleic acids, through electrostatic interactions (Alvarez-Gonzalez & Jacobson, 1987).

Early targets of active PARP1 include itself and neighboring histones. Histones are highly basic proteins essential for DNA structure and organization, forming the protein component of chromatin around which the DNA is wrapped. Due to the polyanionic nature of the PAR polymer, PAR synthesis generates electrostatic repulsion between the DNA and the PARylated histones and with automodified PARP1 (Ferro & Olivera, 1982; Sellou et al., 2016). This results in the loosening of nucleosome packing and chromatin decompaction. A classic example of PARylation-dependent chromatin decompaction can be observed in *Drosophila* heat shock, where PAR facilitates rapid transcriptional activation. Upon temperature changes, PARP accumulates and PARylates at the heat shock loci of polytene chromosomes, leading to “puffing” (Tulin & Spradling, 2003), a process marked by the rapid removal of nucleosomes at these loci to enable transcription. In addition, the accumulation of PARylated proteins is thought to promote the formation of “transcription compartments” which enhance transcription efficiency by recycling transcription factors (Zobeck et al., 2010).

PARP1 further contributes to chromatin remodeling around DNA lesions by actively recruiting early chromatin remodelers such as ALC1 (CHD1L), CHD2, and SNF2 (Luijsterburg et al., 2016; Sellou et al., 2016; Smeenk et al., 2012). The relevance of PAR-driven chromatin decompaction to facilitate DNA repair is highlighted by the phenotypes observed when ALC1 activity is impaired. After DNA damage, the macrodomain of ALC1 guides the recruitment of this chromatin remodeler to active PAR sites, which is a key contributor to rapid chromatin decompaction (Sellou et al., 2016). In the absence of ALC1, cells are sensitive to replication stress and DNA damage

agents, including PARP inhibitors, helix-distorting agents such as cisplatin, transcription-interfering drugs like Illudin S, base alkylation agents such as methyl metanesulfonate, and DNA break-inducing agents such as X-ray irradiation, UV irradiation, and camptothecin (Ahel et al., 2009; Blessing et al., 2020; Hewitt et al., 2021; Juhász et al., 2020; Olivieri et al., 2020). The underlying molecular mechanisms of ALC1's contribution to DNA repair is a highly active research field with promising clinical insights.

In addition to the initial rapid decompaction of chromatin following a DNA insult, PAR biology is involved in chromatin re-compaction, which occurs after repair. During this process, the histone variant macroH2A1 is recruited to DNA lesions, promoting DNA compaction by inhibiting PARP1 (Timinszky et al., 2009), while the isoform macroH2A1.2 assist in the methylation of lysine 9 on histone H3 (H3K9 methylation), a modification that acts as a repressive mark in the chromatin (Khurana et al., 2014).

1.2.3.2 PARP1 is a key player in the DDR

In 1956, Roitt and colleagues reported depletion of NAD^+ levels, the substrate of PARP1, in cells exposed to the alkylating agent ethylenimine (Roitt, 1956). Inadvertenly, this represents the first report of PARPs activity following DNA damage, although PARP1 was characterized until 1963 (Chambon et al., 1963), and the PAR polymer soon after (Chambon et al., 1966; Fujimura, Hasegawa, Shimizu, et al., 1967; Fujimura, Hasegawa, & Sugimura, 1967; Hasegawa et al., 1967; Nishizuka et al., 1967; Reeder et al., 1967; Sugimura et al., 1967). Over sixty years after these observations, our understanding of how PARP1 contributes to DNA repair has expanded.

Although PARP1 can recognize nicks, single- and double-strand breaks in the DNA, SSB strongly activates it (D'Amours et al., 1999). Because of this, PARP1 was initially characterized for its role in SSB repair, particularly its contribution to the base excision repair (BER) pathway. Nonetheless, the roles of PARP1 expand to multiple DDR pathways, including nucleotide excision repair (NER), non-homologous end joining (NHEJ), and homologous recombination (HR), among others (D'Amours et al., 1999; Lüscher et al., 2018). The wide range of PAR effects in multiple DDR pathways is also evidenced by the variety of DDR proteins containing PAR-reading motifs, such as the PBMs found in the NHEJ proteins Ku80, DNA-PKcs, MRE11, ATM and the BER proteins XRCC1 and DNA Lig III; the PBZ in the histone chaperone

APLF, involved in NHEJ; and the BRCT domains of the HR protein BARD1, among many others (D'Amours et al., 1999; Lüscher et al., 2018).

1.2.3.2.1 PARP1 roles in SSB repair

The X-ray repair cross-complementing protein 1 (XRCC1) recruits to DNA lesions through the interaction of its BRCT domain binds to PAR during SSB repair (El-Khamisy, 2003; Okano et al., 2003). At the lesions, XRCC1 serves as a scaffold protein that coordinates the formation of DNA repair complexes with interacting partners required for DNA repair, such as APE1 (Vidal, 2001), DNA Polymerase β (Caldecott et al., 1996; Kubota et al., 1996), DNA polynucleotide kinase, and DNA Ligase III (Caldecott et al., 1995, 1996; Nash et al., 1997), thereby facilitating the repair of nicks and SSBs in the DNA. Moreover, the interaction of XRCC1 with DNA Ligase III is enhanced through the SUMOylation of XRCC1 by SUMO E3 TOPORS, which is recruited through PAR (Hu et al., 2018). Interestingly, XRCC1 also affects PARP1 kinetics as the absence of XRCC1 reduces the accumulation of PARP1 at DNA lesions (Reber et al., 2023) and increases the retention, or "trapping" of PARP1 at DNA lesions (Demin et al., 2021). Thus, PARP1 and XRCC1 are key reciprocal partners whose interactions guide the SSB repair.

PARP1 also mediates the resolution of single-stranded DNA nicks induced by abortive DNA topoisomerase I. PARP1 recruits and activates tyrosyl-DNA phosphodiesterase, thereby resolving the DNA-topoisomerase complex (B. B. Das et al., 2014; S. K. Das et al., 2016). This results in the repair of the nick through PAR-driven recruitment of XRCC1 (B. B. Das et al., 2014).

Finally, PARP1 contributes to the resolution of bulky DNA lesions through the NER pathway, generating intermediate SSBs. Immunoprecipitation studies have shown an interaction between PARP1 and the bulky lesion-recognizing proteins DDB2 and XPC (Blessing et al., 2022; Pines et al., 2012; Robu et al., 2013, 2017). PARylation of DDB2 contributes to its stability by preventing the ubiquitylation of DDB2 (Pines et al., 2012). Interestingly, DDB2 and XPC also stimulate PAR activity (Blessing et al., 2022; Robu et al., 2013), suggesting reciprocal modulation between PARP1 and these NER proteins. Moreover, PAR-driven recruitment of the chromatin remodeler ALC1 has been shown to affect NER efficiency, possibly by opening the chromatin adjacent to the DNA lesion, thereby facilitating lesion recognition (Blessing et al., 2022; Pines et al., 2012).

1.2.3.2.2 PARP1 roles in DSB repair

Consistent with the role of PARP1 in DSB repair, PARP1 catalytic activity can be triggered by DSBs *in vitro* (Huambachano et al., 2011), and inhibition of PARPs renders sensitivity to agents known to generate DSBs while also delaying lesion repair (Ray Chaudhuri & Nussenzweig, 2017). However, the mechanisms by which PAR affects the two main DSB repair pathways, HR and NHEJ differ.

Similar to its role in SSB repair, PARP1 activity positively impacts the recruitment of meiotic recombination 11 (MRE11) and Nijmegen breakage syndrome protein 1 (NBS1) to DSBs, which promote HR (Haince et al., 2008). However, the accumulation of PAR can be detrimental to DSB repair through HR, as evidenced by the deficient RPA protection during DNA resection observed in the absence of PARG (Illuzzi et al., 2014). On the other hand, PARP1 activity has a negative effect on NHEJ, as PARylation of Ku70-Ku80 proteins promotes their dissociation from DNA, thereby preventing DNA repair (M. Wang et al., 2006). Thus, PAR contributes to pathway selection favoring KU-independent repair processes.

1.2.4 Clinical implications of PARP inhibitors

PARP inhibitors (PARPi) are small molecule nicotinamide analogs that were first developed as tools to investigate the cellular role of PARP, particularly in relation to the DNA damage response (Purnell & Whish, 1980; Shall, 1975). However, understanding the biological consequences of PAR-mediated processes opens new therapeutic avenues. In particular, the PARPi olaparib was the first registered drug that reached the clinic based on synthetic lethality.

Synthetic lethality occurs when the impairment of two independent processes is compatible with viability; however, their simultaneous impairment results in cell death. PARPi targets the strong reliance of certain cancers on DNA damage repair, which is not observed in non-cancerous cells, thereby specifically affecting diseased cells. This strategy is particularly effective in tumors that are not derived from germline BRCA1 or BRCA2 mutations (Bryant et al., 2005; Farmer et al., 2005) because the absence of functional BRCA1/2 proteins leads to deficient HR repair and replication fork instability (Lord & Ashworth, 2016; Turner et al., 2004). Thus, in normal cells with

functional BRCA proteins, DSBs can be effectively repaired, even in the presence of PARPi. However, in cancer cells harboring BRCA1/2 mutations, the presence of PARPi leads to unresolved DNA damage, eventually leading to cell death while sparing non-cancerous BRCA1/2 proficient cells. Similar synthetic interactions have been observed between PARPi and other HR genes such as ATM, CHEK2, and CDK12 (C.-C. Chen et al., 2017; Houles et al., 2022; S. Li et al., 2022). To this date, PARPi has been approved for maintenance therapy, as single or combination therapy, for BRCA-mutated breast, ovarian, and prostate cancers (Ragupathi et al., 2023).

1.2.5 PAR and RNA metabolism

As different teams raced to characterize the polymerase responsible for the poly(A) tail synthesis of mRNAs, PARP1 was isolated (Chambon et al., 1963; Kraus, 2015). The serendipity of this event underlies a key characteristic that is sometimes overlooked: RNA and PAR biology are profoundly interconnected as PAR regulate gene expression and RNA metabolism at multiple levels. Here, we present a brief overview of the role of ADP-ribosylation in RNA metabolism.

The PARP1-driven local decondensation discussed in the context of DNA damage also occurs under homeostatic conditions. PARP1 binds near to the promoter of transcriptionally active genes, where it competes with repressive H1 (Krishnakumar et al., 2008) and excludes the histone demethylase KDM5B (Krishnakumar & Kraus, 2010), thereby preventing H3K4me3 demethylation. Moreover, PARylation of the DNA methyltransferase DNMT1 inhibits its methylation activity (Althaus, 2005). Consistently, PARP1 localizes to hypomethylated regions, with histone marks associated with active transcription (Nalabothula et al., 2015). This evidence highlights the interplay between DNA methylation and PAR, which influencing transcription activity.

Recent studies have highlighted that nuclear factors important for transcription can regulate PARP1 and PARP2 activity allosterically. These factors include HPF1 (Bilokapic et al., 2020; Langelier et al., 2021; Sun et al., 2021; Suskiewicz et al., 2020), HMGM1 (Masaoka et al., 2012), YB-1 (Alemasova et al., 2018; Naumenko et al., 2020, 2022), canonical and variant histones (Kozlowski et al., 2018; Nusinow et al., 2007; Thomas et al., 2019), and modified histones (Cohen-Armon et al., 2007; Kotova et al., 2010). The effect of PARP1 extends beyond the local chromatin architecture, as it can affect the 3D chromosomal architecture by interacting with CCCTC-binding factor (CTCF), a master regulator of the genome 3D structure. In particular,

PARP1 stabilizes the binding of CTCF to chromatin (Lupey-Green et al., 2018), while CTCF stimulates PARP1 activity in the absence of DNA damage (Guastafierro et al., 2008; W. Yu et al., 2004). These observations suggest that the chromatin context and intermediate partners can impact the effect of PARP1 in gene expression.

PARP1 can also act as a classical transcription factor, as it binds directly to the promoters of key genes such as cTnT (K. Huang et al., 2004), HTLV-I (Z. Zhang et al., 2002), and Reg (Akiyama et al., 2001), having a direct impact on transcription. Furthermore, PARP1 can act as a co-regulator by interacting with other transcription factors to either enhance or inhibit their binding to DNA (Zong et al., 2022). Moreover, PARP1 activity modulates RNAPII pausing through PARylation of the negative elongation factors A (NELF-A) and E. Modification of NELF-E abrogates its binding to RNA, which is necessary for the establishment of paused RNAPII (Gibson et al., 2016; E. A. Matveeva et al., 2019). This mechanism of PAR-mediated release of paused RNAPII was first observed in *Drosophila melanogaster* at heat shock loci (Petesch & Lis, 2008; Tulin & Spradling, 2003), where thermic stimulation triggers PARP1 activity, leading to PAR-mediated dissociation of the NELF complex, thus releasing RNAPII from its paused state. In this way, cells can rapidly activate the transcriptional program required to react to heat shock.

PARPs also play a role in RNA processing, including splicing and RNA stability. As nucleosome occupancy regulates RNA Polymerase kinetics, and slower transcription facilitates the recognition of weak splice sites (Schwartz & Ast, 2010), the chromatin remodeling activity of PARP1 and its nucleosome occupancy correlates with alternative splicing events (E. Matveeva et al., 2016). Moreover, PARP1 interacts with or modifies multiple RNA-binding proteins (RBP) involved in splicing, including heterologous ribonucleoprotein particles (Isabelle et al., 2010; Ji & Tulin, 2009; Jungmichel et al., 2013; F. Zhang et al., 2013) and serine-arginine-rich (S/R) proteins (Malanga et al., 2008).

RBP interactions with PARP proteins extend to mRNA processing beyond splicing. Key examples are the addition to the 3' end mRNA processing complex (Y. Shi et al., 2009) and the Hu antigen R (HuR), an RBP that affects the stability of lipopolysaccharide-responsive mRNAs (Ke et al., 2017). Furthermore, the catalytic activity of PARP1 also affects mRNA stability through competition between NAD+ and poly(A) polymerase, thereby decreasing the length of poly(A) tails (Di Giammartino et al., 2013).

PARP1 modulates multiple steps of ribosome biogenesis, having roles in RNA Polymerase I-dependent transcriptional regulation (Kurl & Jacob, 1985), cell-cycle dependent modulation of chromatin accessibility of ribosomal RNA genes through association with the nucleolar chromatin remodeling complex NoRC (Guetg et al., 2012), and localization of nucleolar proteins through direct PARylation (Carter-O'Connell et al., 2014; Gagné et al., 2012; Gibson et al., 2016; Kim et al., 2019), thereby affecting pre-ribosomal rRNA processing and rRNA modification.

The interplay between PAR and RNA extends beyond the interaction with intermediate proteins. PARP1 activity is required to recruit DDX18 and DHX9 helicases to resolve DNA-RNA species following DNA damage (Cristini et al., 2018; W.-L. Lin et al., 2022). Moreover, *in vitro* evidence has shown that PARP1 can directly bind to DNA-RNA species, which can arise from DNA processes or DNA damage, triggering PARylation *in vitro* (Laspata et al., 2023; H. Yang et al., 2023). PARP1 activation driven by DNA-RNA species can be explained by PARP1 binding to the DNA of these hybrids. However, biochemical approaches have confirmed that PARP1 can directly bind to and modify RNA (Munnur et al., 2019; Weixler et al., 2022). This RNA modification's frequency and cellular consequences have yet to be understood.

An additional aspect of PAR-RNA interaction that has gained attention over the last few years is the role of PAR in forming membrane-less subcompartments enriched in RBPs (Altmeyer et al., 2015; Y. Duan et al., 2019; Singatulina et al., 2019). In particular, the intrinsically disordered protein regions of RBPs are important for the formation of PAR-driven phase transition of biomolecules and are relevant in diseases such as Ataxia Telangiectasia (Lee et al., 2021; Woolley et al., 2024) and amyotrophic lateral sclerosis (Rhine et al., 2022).

In summary, PAR and RNA metabolism are intricately intertwined, with PARP1 as a key player in regulating gene expression, transcription, RNA processing, and forming membrane-less subcompartments enriched in RBPs. Understanding these interactions offers insights into various cellular processes and diseases beyond DNA repair, with implications for health and disease.

1.3 RNA in the DNA damage response

RNA has emerged as a key player in the DNA damage response by regulating gene expression and participating in DNA repair. In particular, known RNA-binding and processing enzymes have emerged as new contributors in the DNA repair process, as reviewed in (Alemasova & Lavrik, 2017; Bader et al., 2020). This section explores the multifaceted roles of RNA and the emerging role of m6A-methylated RNA in the DDR.

One of the early lines of evidence highlighting the contribution of RNA in the DDR is the contribution of key RNA-binding and processing enzymes to this network. For instance, the RNA endonucleases Drosha and DICER, which are key components of the microRNA (miRNA) processing machinery, modulate the recruitment of HR and NHEJ factors to DSBs (Francia et al., 2012; Lu et al., 2018; W. Wei et al., 2012). Interestingly, this DDR role is independent of the role of these proteins in miRNA biogenesis, as depletion of other miRNA factors did not affect DNA repair (Francia et al., 2012; Lu et al., 2018).

A key family of RNA-processing proteins that are implicated in DNA repair is the DEAD-box helicase family. Members of this group, including DHX9, DDX1 and senataxin, which traditionally unwind RNA, have been shown to directly interact with DNA-RNA species formed at the sites of DNA damage (Becherel et al., 2013; A. Jain et al., 2013; L. Li et al., 2008). In particular, DXH9 directly interacts with PARP1 and is required for DNA-RNA resolution (Cristini et al., 2018).

Other RNA-processing proteins known to mediate DDR are NONO (Krietsch et al., 2012), the exosome complex-associated protein EXOSC10 (Domingo-Prim et al., 2019; Marin-Vicente et al., 2015), and intrinsically disordered proteins including RBM14, FUS, EWS and TAF15 (Britton et al., 2014; Izhar et al., 2015; Mamontova et al., 2023; Rulten et al., 2014).

Besides the role of RNA-binding proteins in the DDR, RNA contributes to this network. Recent findings suggests that certain non-coding RNAs, including long non-coding RNAs (lncRNAs) and microRNAs, can function as sensors of DNA damage and modulate DDR signaling pathways. For instance, the lncRNA, PANDA (P21-associated ncRNA DNA damage-activated), can be induced in response to DNA damage and plays a key role in the DDR. It regulates gene expression involved in cell

cycle arrest, senescence, and apoptosis (A. K. Jain, 2020; Kotake et al., 2016; Peng et al., 2017). Additionally, specific miRNAs, such as miR-138 and miR-421, are implicated in DDR regulation by targeting key DDR genes and processes such as ATM, BRCA1, and repression of histone H2AX (Y. Wang et al., 2011). Moreover, non-coding RNAs serve as templates for homology-mediated repair or aiding the compartmentalization of DNA lesions (Francia et al., 2012; Michelini et al., 2017; Pessina et al., 2019).

Lastly, a key component of RNA metabolism, RNA Polymerase II, plays a crucial role in surveilling DNA integrity by triggering the transcription-coupled nucleotide excision repair response as described in section 1.1.2.3 (Ljungman & Zhang, 1996; Van Den Heuvel et al., 2021).

1.3.1 Post-transcriptional modification of RNA

All genetic information contained within the DNA and RNA is encoded with only four bases: cytosine, guanine, adenosine, thymine, or uracil in RNA. However, soon after the characterization of these canonical bases, analysis of the total RNA pool revealed the presence of noncanonical bases. To this date, 140 different base modifications have been characterized, stemming from post-transcriptional modification of the canonical bases. In addition to modification of the canonical bases, the ribose moieties of the RNA nucleosides can undergo modification (Dai et al., 2017; Marchand et al., 2016; Schibler & Perry, 1977), adding an additional layer of information onto the transcribed genome. The sum of all functionally relevant changes in the transcriptome that do not involve changes in the ribonucleotide sequence is known as the epitranscriptome.

The most prevalent internal chemical modification of mRNA is the methylation of the nitrogen at position 6 in the adenosine, known as N6-methyladenosine or m6A. Although its existence was first described in 1958 (Littlefield & Dunn, 1958), the available technology limited an in-depth study of this modification. It was not until the 2010s that transcriptome-wide approaches provided insights into the abundance and nature of this modification. It is now known that an average mRNA harbors 3-5 m6A nucleotides (Dominissini et al., 2012; Perry et al., 1975), and their distribution is not stochastic, being enriched within the 3'-untranscribed region (3'-UTR) and around the stop codon (Dominissini et al., 2012; Meyer et al., 2012). Moreover, adenosine methylation occurs within the degenerated consensus sequence "DRACH" (A =

methylated A; D = A, G or U, R = purine, H= A, C, or U). (Dominissini et al., 2012; Z. Lin et al., 2017; Meyer et al., 2012).

1.3.1.1 The m6A regulatory machinery

The deposition of m6A modifications on RNA molecules is catalyzed by a multicomponent methyltransferase complex, referred to as the "writer" complex. Key enzymes within this complex include methyltransferase-like 3 (METTL3), METTL14, and the accessory protein WTAP (Wilms tumor 1-associated protein). METTL3 and METTL14 are part of the MT-A70 family of S-adenosyl-L-methionine (SAM)-dependent methyltransferases. Although both enzymes possess a methyltransferase domain, SAM binds only to METTL3. METTL3 is therefore considered to be the catalytic unit of the dimer, while METTL14 provides structural support as RNA binding occurs in the interphase between the two methyltransferases (Śledź & Jinek, 2016; X. Wang et al., 2016). In contrast, WTAP is not necessary for methylation *in vitro* but mediates the localization of the heterodimer to nuclear speckles and has been functionally linked to alternative splicing (J. Liu et al., 2014; Ping et al., 2014). Other accessory proteins to the methyltransferase complex (MTC) are the Vir-like m6A methyltransferase-associated (VIRMA), RNA-Binding Motif 15 (RBM15), zinc finger CCCH domain-containing protein 13 (ZC3H13), and HAKAI (CBL photo oncogene like 1) (Dominissini et al., 2012; Knuckles et al., 2018; J. Liu et al., 2014; Wen et al., 2018). However, their roles are not yet understood.

Proteins termed "readers" recognize and bind to m6A-modified RNA, exerting regulatory effects on various RNA processes. Proteins containing the YTH domain, particularly YTHDF1, YTHDF2, YTHDF3, and YTHDC1, are prominent m6A readers involved in mRNA metabolism, including mRNA degradation, translation regulation, and alternative splicing (Dominissini et al., 2012). These proteins harbor a YTF21-B homology domain (YTH), which binds specifically to m6A (F. Li et al., 2014; X. Wang et al., 2014; C. Xu et al., 2014). Both YTHDF1 and YTHDF2 localize within the cytoplasm and interact with m6A-methylated mRNAs. While YTHDF2 destabilizes methylated transcripts by localizing RNAs into processing bodies (P-bodies) (X. Wang et al., 2014), YTHDF1 promotes mRNA translation through its association with the eukaryotic initiation factors eIF3 and eIF4G (X. Wang et al., 2015). On the other hand, YTHDF3 can affect translation by interacting with YTHDF1 while accelerating methylated mRNA decay through YTHDF2 interaction (H. Shi et al., 2017). The last

member of the YTH family, YTHDC1, acts in alternative splicing by interacting with serine/arginine-rich splicing factors (Rafalska et al., 2004; Xiao et al., 2016).

In addition to the YTH family, other m6A-binding proteins, such as HNRNPA2B1, IGF2BP1/2/3, and eIF3, contribute to the diverse regulatory functions of m6A-modified RNA. For instance, binding of HNRNPA2B1 to m6A affects microRNA processing (Alarcón, Goodarzi, et al., 2015; Alarcón, Lee, et al., 2015), binding of IGF2BPs promotes stability and storage of target mRNAs and miRNAs (M. Duan et al., 2024; H. Huang et al., 2018; Müller et al., 2019), and binding of eIF3 to 5' UTR m6A promotes cap-independent translation of mRNAs (Meyer et al., 2015).

The dynamic nature of m6A modification is regulated by demethylases, known as "erasers," which remove methyl groups from m6A-modified RNA. So far, two proteins have been discovered that can demethylate m6A-containing RNAs: the fat mass and obesity-associated protein (FTO) and the alkylation repair homolog 5 (ALKBH5).

FTO was the first enzyme identified with m6A-demethylase activity (Jia et al., 2011). As its name suggests, variants of this protein have been associated with an increased body mass index (Dina et al., 2007; Frayling et al., 2007). FTO is predominantly found within the cell nucleus, yet it can shuttle between the nucleus and cytoplasm, particularly in response to nutritional cues (Gulati et al., 2013; Vujovic et al., 2013). Similar to DNA-demethylases, FTO oxidizes m6A in a step-wise process, converting m6A into N6-hydroxymethyladenosine and then N6-formyladenosine, which is then hydrolyzed by the surrounding water, resulting in unmethylated adenosine (Fu et al., 2013).

ALKBH5 is also found in the nucleus and colocalizes with FTO to nuclear speckles (Zheng et al., 2013). Similar to FTO, ALKBH5 removes m6A methylation via oxidation. However, ALKBH5 performs direct demethylation of m6A to adenosine (Toh et al., 2020). Moreover, ALKBH5 has been implicated in spermatogenesis without reported effects on body mass index (Tang et al., 2018; Zheng et al., 2013). How the two demethylases select their substrates is not yet known.

1.3.1.2 The molecular role of m6A

As evidenced by the cellular roles of m6a readers, m6A modification exerts profound effects on various biological processes including mRNA stability and decay, RNA splicing, nuclear export, and translation efficiency (S. Wang et al., 2022). Therefore,

m6A impacts RNA metabolism, from mRNA biogenesis to post-transcriptional regulation. This is achieved by m6A serving as a docking site for reader proteins, as discussed in Section 1.3.1.1.

Beyond its function regulating RNA metabolism, m6A influences the selective expression of genes by altering the structure of the modified RNA molecule, possibly facilitating or hampering the interplay with other RNA-binding proteins and the accessibility of the translation machinery. FTO-mediated demethylation correlates with changes in transcript levels and frequency of alternative splicing (J. Wei et al., 2018), and binding of YTHDC1 to methylated regulatory RNAs, such as LINE1 and XIST, results in transcription repression (J. Liu et al., 2020; Patil et al., 2016). Furthermore, m6A has been identified as a crucial regulator of the transcriptional response to acute stimuli, such as the heat shock response, where mRNA encoding heat shock genes are hypermethylated, resulting in increased translation of these genes (Knuckles et al., 2017; Zhou et al., 2015a). Therefore, m6A modification plays a role in the adaptive stress response.

Recently, there has been growing interest in understanding the crosstalk between chromatin architecture and the deposition of m6A marks, as both processes are known to control gene expression, albeit at different stages (Song et al., 2022). For instance, METTL3 and METTL14 are involved in establishing and maintaining gene expression programs necessary for embryonic neural stem cell self-renewal. In the absence of METTL14, the mRNA of the histone acetylase CBP/p300 is hypermethylated, leading to increased protein levels and increased levels of H3K27ac (Y. Wang et al., 2018). On the other hand, depletion of METTL3 resulted in hypomethylation of the histone methyltransferase EZH2, leading to reduced protein levels and decreased H3K27me23 (J. Chen et al., 2019). The absence of methyltransferases results in decreased proliferation and premature differentiation of neuronal stem cells (J. Chen et al., 2019; Y. Wang et al., 2018), highlighting the role of m6A in neuronal stem cell self-renewal. Similar observations have been reported in other embryonic stem cell models (Batista et al., 2014; X.-M. Liu et al., 2022).

Interestingly, the relationship between histone marks and m6A deposition is bidirectional, as METTL14 was shown to recognize H3K36me3 modified histones, a marker of active transcription. This leads to the METTL3/14 complex being recruited to open chromatin regions and the subsequent methylation of transcribed RNA (H. Huang et al., 2019). These observations suggest that m6A deposition and the chromatin

landscape are interconnected through the modification of key mRNA transcripts and the direct recognition of histone marks.

1.3.1.3 M6A in cancer

Dysregulation of m6A and its main modifiers, METTL3 and METTL14, has profound implications in pathological conditions, most notably in cancer and neurological disorders. The role of m6A dysregulation in tumorigenesis has been extensively studied in recent years.

Increased METTL3 and METTL14 expression has been reported in various types of cancers, including acute myeloid leukemia (AML) (Barbieri et al., 2017; Vu et al., 2017), liver cancer (M. Chen et al., 2018; Y. Li et al., 2021; Zhong et al., 2019), glioblastoma (Cui et al., 2017; Visvanathan et al., 2018; S. Zhang et al., 2017), breast cancer (Y. Shi et al., 2020; L. Wu et al., 2019), and lung cancer (M. Du et al., 2017; W. Wei et al., 2019) and is associated with poor prognosis. Particularly, in AML, METTL3 promotes the translation of oncogene transcripts to enhance leukemogenesis (Barbieri et al., 2017).

Given the impact of m6A and METTL3/METTL14 dysregulation on diseases, many studies have explored therapeutic possibilities targeting m6A biology. The exploitation of these targets has gained traction with the advent of small-molecule inhibitors and degraders that target m6A writers (Bedi et al., 2020; W. Du et al., 2024; Y. Du et al., 2022; Yankova et al., 2021), with an ongoing phase 1 trial (TC15-22101).

1.3.1.4 M6A in the DNA damage response

In recent years, m6A-modified RNA and the METTL3/14 complex have gained interest in the DDR field, as m6A has been shown to play a role in UV-induced DNA damage repair (Xiang et al., 2017), and to mediate DNA-RNA resolution through HR (Abakir et al., 2020; E. Li et al., 2022; C. Zhang et al., 2020; J. Zhang et al., 2024). Beyond the direct role of m6A and METTL3 in DNA repair, m6A modification can indirectly impact the DDR through modulating cell-cycle checkpoint control and apoptosis (Fustin et al., 2013).

The first evidence of the role of m6A in the DDR was the report of m6A-RNA accumulation and concurrent recruitment of METTL3 to laser micro-irradiation sites by

Xiang and colleagues in 2017. This accumulation depended on active PARylation, as treatment with PARPi abrogated the recruitment of METTL3 and the accumulation of m6A. In the absence of METTL3, cells exhibit increased sensitivity to UV irradiation and impaired repair of CPD photolesions, suggesting a role for METTL3 in UV-induced DNA repair (Xiang et al., 2017). Similarly, Svobodova-Kovarikova and colleagues observed the accumulation of m6A at micro-irradiation sites, observing that METTL16, an m6A writer in snRNA, accumulated in approximately 10% of microirradiated cells, suggesting a potential interplay between different methyltransferases (Svobodová Kovaříková et al., 2020). Despite their relevance to the DDR field, these studies left some open questions, including the elucidation of the DNA damage repair pathway in which METTL3 and m6A are involved, as only Polymerase κ, but no other DDR proteins were affected by the absence of METTL3 (Xiang et al., 2017).

PAR also coordinates the recruitment of METTL3 to the DNA-RNA species induced by the topoisomerase I inhibitor camptothecin. The accumulation of these species is deleterious to cells because they induce genome instability. However, DNA-RNA species also act as intermediates in transcription-coupled repair (Petermann et al., 2022). In the context of camptothecin-induced damage, the tonicity-responsive enhancer-binding protein (TonEBP, also called NFAT5), is recruited to DNA-RNA structures in a PAR-dependent manner, while also being a substrate of PARylation (Ye et al., 2021). Binding of TonEBP to DNA-RNA species leads to the recruitment of METTL3, which methylates the RNA strand of the DNA-RNA hybrid. Moreover, m6A is required for the recruitment of RNAseH1, which resolves the DNA-RNA structure (Kang et al., 2021; J. Zhang et al., 2024).

Zhang and colleagues propose an alternative path by which m6A and METTL3 contribute to DNA-RNA resolution linking HR. In response to zeocin-induced DSBs, METTL3 is phosphorylated by ATM at residue S43, which is required for the colocalization of METTL3 with DNA-RNA hybrids. RNA methylation results in the recruitment of YTHDC1, which then recruits the HR proteins RAD51 and BRCA1. In the absence of METTL3, DNA-RNA species accumulate, leading to prolonged DNA damage signaling and increased apoptosis (C. Zhang et al., 2020). At gene expression level, METTL3 plays a role in DSBs induced by doxorubicin by promoting the expression of EGF and RAD51 (E. Li et al., 2022).

1.4 Research gap and aims of this study

Compelling evidence suggests an interplay between PAR, METTL3 and m6A methylation of RNA. However, the nature of the interactions between these proteins is unknown. This prompted us to establish the first aim of the project.

Aim 1: To dissect the interaction between PARP1 and METTL3/14 *in cellulo* and i*n vitro*.

Although there is strong evidence that METTL3 plays a role in UV-induced DNA damage repair (Xiang et al., 2017) the implicated pathways and the cellular role of METTL3/14 in response to UV damage remain to be elucidated. Therefore, we set the second aim of this study.

Aim 2: To characterize the cellular role of METTL3/14 in response to UV damage

Lastly, the growing use of PARPi in the clinic and the recent development of METTL3 inhibitors opens the possibility of synergistic therapeutic interactions that have not been explored before.

Aim 3: To explore the potential therapeutic interactions between METTL3 and PARP inhibitors in different cell models.

1.5 Significance of this work

This study describes the timing and PAR dependence of m6A accumulation and METTL3/14 recruitment at UV lesions triggered by laser microirradiation. I assessed the binding of PAR and RNA to the METTL3/14 complex and found that while both nucleic acids are recognized by the complex, high concentrations of PAR displaced but do not abolish RNA binding. Moreover, PAR did not affect the catalytic activity of METTL3/14, suggesting that PAR serves as a scaffold for METTL3/14 recruitment and RNA modification.

We further characterized the role of METTL3 in DNA repair. Consistent with previous observations (Xiang et al., 2017), METTL3 deficiency increased the UV sensitivity in the presence of BrdU. Furthermore, the absence of the catalytic subunit delays the repair of both 6-4 photolesions (64PP) and cyclobutene pyrimidine dimers (CPD), suggesting a role in early and late UV repair events. Additionally, METTL3-deficient

cells are sensitive to Illudin S, exhibit a delay in transcription restart after damage, and maintain high levels of the transcription repressor ATF3. Our research also explored the potential interaction of METTL3 inhibitors and PARPi in cancer treatment, highlighting how interfering with PAR dynamics may leverage the interplay between DNA repair and RNA modification.

2. Material and Methods

2.1 Materials

2.1.1 Chemicals and consumables

All chemicals specific for this project were purchased from Sigma (USA), Thermo Fischer Scientific (USA), VWR (USA), LifeTechnologies (USA), MedChemExpr (USA), Biomol GmbH (Germany), and Selleck Chemicals GmbH (Germany).

Commercially available kits for the isolation of nucleic acids were purchased from Metabion (Germany). Viability assay was measured using the CellTiter-Glo® kit from Promega (USA). In vitro methylation was measured using the MTase-Glo™ from Promega (USA). Cell culture media and supplements were purchased from Thermo Fischer Scientific. RNA Oligonucleotides were synthesized by Eurofins (Germany).

2.1.2 Oligonucleotides

The sequences of the oligonucleotides used in this project are listed in Tables 2- 3

Table 2. DNA oligonucleotides used for cloning

Name	Fwd/Rev	Sequence
METTL3 D395A	Fwd	GTTGTGATGGCTGCTCCACCCTGGGATATTC
METTL3 D395A	Rev	GTGAATATCCCAGGGTGGAGCAGCCATCAC
METTL3 S2A	Fwd	CAAGTCCGGAATGGCGGACACGTGGAGCTC
METTL3 S2A	Rev	CCACGTGTCCGCCATTCCGGACTTGTACAG
METTL3 H11A	Fwd	CTATCCAGGCCGCCAAGAAGCAGCTGGAC
METTL3 H11A	Rev	GCTGCTTCTTGGCGGCCTGGATAGAGCTC
METTL3 S43A	Fwd	GGCAGCATTGGCACCAACCTTCCGTAG
METTL3 S43A	Rev	CGGAAGGTTGGTGCCAATGCTGCCTCTG

GFPC1 METTL3 198	Fwd	GGACGAGCTGTACAAGTCCGGACTGAACTCTTCA-GCATCGGA
GFPC1 METTL3 352	Rev	TCGAAGCTTGAGCTCGAGATCTGAGTTACTCCTGGCTT-GGCG
GFPC1 METTL3 2	Fwd	GGACGAGCTGTACAAGTCCGGATCGGACACGTGGAGCTC
GFPC1 METTL3 219	Rev	CGAAGCTTGAGCTCGAGATCTGAGTTATGAGGCAGCAT-GTTTC
GFPC1 METTL3 351	Fwd	CGAGC GTACAAGTCCGGACAGGAGCTTGCTCTTACACAG
GFPC1 METTL3 580	Rev	CGAAGCTTGAGCTCGAGATCTGAGTTATAAATTCTTAGGTT TAGAGATG
METTL14 XhoL	Fwd	ATATATCTCGAGCGGATAGCCGCTTGCAGG
METTL14 BamHI	Rev	ATATATGGATCCTTATCGAGGTGGAAAGCC
WTAP XhoI	Fwd	ATATATCTCGAGTCACCAACGAAGAACCTCTT
WTAP bamHI	Rev	ATATATGGATCCTTACAAAACTGAACCCTGTAC

Table 3 RNA oligonucleotides used for *in vitro* assays

Name	Sequence
RNA+	GGACUGGACUGGACUGGACU
RNA-	GGGCUGGGCUGGGCUGGGCU
CY3RNA+	[CY3] GGACUGGACUGGACUGGACUGGACUGGACUGGACUGGACU

2.1.3 Vectors and plasmids

The vectors listed in Table 4 represent the plasmid backbones used for the expression of tagged proteins in mammalian cell lines, as well as the plasmids we used for the recombinant expression of proteins in Sf21 cells.

Table 4. Vectors and plasmids for protein expression

Name	TAG	Origin
EGFP-C1	GFP	Plasmid Collection Ladurner's Lab
mCherry-N1	mCherry	Plasmid Collection Ladurner's Lab
pcDNA3/Flag-METTL3	Flag	Addgene (#53739)

pcDNA3/Flag-METTL14	Flag	Addgene (#53740)
pcDNA3/Flag-WTAP	Flag	Addgene (#53741)
pFastBac-FL METTL3 + FL METTL14	GST-TEV	Provided by the Jinek Lab
pGST-METTL3	GST	Provided by the Meister Lab
EGFP-METTL3	GFP	This study
EGFP-METTL14	GFP	This study
EGFP-WTAP	GFP	This study
EGFP-FTO	GFP	This study
EGFP-METTL3 N	GFP	This study
EGFP-METTL3 M	GFP	This study
EGFP-METTL3 C	GFP	This study
mCh-PARP1	mCherry	Plasmid Collection Ladurner's Lab
mCh-PARP1 E988K	mCherry	Plasmid Collection Ladurner's Lab
His-PARP1	8XHis	Pellet of E.coli expressing His-PARP1 provided by Gunnar Knobloch

2.1.4 Antibodies

The antibodies used in this study are listed in Table 5

Table 5. Antibodies

Name	Company	Species	Applica-tion	Dilution
6-4PP	Cosmo bio; cat# NM-DND-002	mouse	IF	1: 300
ATF3	Abcam; cat# ab207434	rabbit	WB	1: 1,000
CPD	Cosmo Bio; cat# CAC-NM-DND-001 (TDM2 clone)	mouse	IF	1: 1,000
GFP	Homemade	goat	WB	1:5,000
H3	Active Motif; cat# 61475	mouse	WB	1: 1,000

m6A	Synaptic Systems; cat# 202 003	rabbit	IF	1:1,000
METTL14	Abcam; cat# ab220030	mouse	WB	1:1,000
METTL3	ABclonal; cat# A8370;	rabbit	IF/WB	1:1,000
PAR (10H)	RCB; cat# RCB1142	mouse	WB	1: 5,000
Anti-PAR (pan-ADPr binding reagent)	Millipore; cat# MABE1016	rabbit	IF/WB	1:1,000
PARP1	Homemade	rabbit	WB	1: 10,000
RBP1 (clone 4H8)	Active Motif cat# 39497	mouse	WB	1:1,000
RBP1 pS2	Abcam cat# ab5095	rabbit	WB	1:1,000
Tubulin	Sigma; cat#T6199	mouse	WB	1: 1,000
γH2AX	Abcam; cat# ab11174	rabbit	IF	1:1,000
γH2AX	Millipore; cat# 05-636	mouse	IF	1:1,000
anti-Mouse IgG (H+L) Cross-Adsorbed Secondary Antibody, Alexa Fluor 488	Thermo Fisher Scientific; cat# A-11001	goat	IF	1:2,000
anti-Rabbit IgG (H+L) Cross-Adsorbed Secondary Antibody, Alexa Fluor 568	Thermo Fisher Scientific; cat# A-10042	donkey	IF	1:2,000
Highly cross-adsorbed; CF 680 antibody (mouse/ rabbit)	Sigma; cat#SAB4600205/ SAB4600200	mouse/rabbit	WB	1:10,000
Highly cross-adsorbed, CF 770 antibody	Sigma; cat#SAB4600214	mouse	WB	1:10,000
Highly cross-adsorbed, CF 750 antibody	Sigma; cat#SAB4600373	rabbit	WB	1:10,000

2.1.5 Buffers and media

I specify the composition of the different buffers used under each method.

The U2OS and MDA-MB-231 BRCA-proficient triple-negative breast cancer cells were maintained in DMEM low glucose media with 10% FBS and 1% penicillin/streptomycin. We generated stably transfected cells, which are described in section 2.2.2.3. We sustained the expression of the transfected constructs using DMEM low glucose media with 200 µg/mL G418. MOLM-13, DLD1 wild-type and DLD1 x-man cells were maintained in RPMI media with 10% FBS and 1% penicillin/streptomycin. SUM149PT BRCA1-mutant triple-negative were maintained in Ham's F12 medium supplemented with 10% FBS and 1% penicillin/streptomycin.

As phenol-red can interfere with luminescence and fluorescence measurements, we used phenol-red free DMEM and RPMI media when seeding viability assays. Similarly, we used Leibowitz L-15 for live-cell imaging microscopy, as this formulation is free of phenol-red and is CO2-independent.

2.2 Methods

2.2.1 Cloning

2.2.1.1 Generation of constructs

We purchased FLAG-METTL3, FLAG-METTL14, and FLAG-WTAP DNA from Addgene (see Table 4). FTO was amplified from U2OS wild-type cDNA. These proteins were sub-cloned into EGFP-C1 vectors using conventional restriction cloning.

2.2.1.2 Site-directed mutagenesis

We used site-directed mutagenesis to generate the catalytic mutant METTL3_D395A. We designed the primers to be complementary to each other and complementary to the DNA template with the desired amino acid mutation. We used the DNA polymerase PfuUltra™ from Stratagene, as it exhibits a low error rate thus reducing the risk of incorporating unwanted mutations. We run the reactions for 18 PCR cycles and digested with DpnI endonuclease to cleave the unmutated template DNA. E.coli DH5α cells were transformed with the PCR product. We confirmed the introduction of the desired mutation using DNA sequencing (see 2.2.1.5).

2.2.1.3 Heat-shock transformation of *E. coli*

We used heat shock-competent E. coli DH5α to produce and isolate DNA plasmids. For this, 10 pg to 100 ng of DNA were incubated with 50 µL of thawed competent cells for 20 min on ice. Next, the cells were incubated for 60 seconds at 42°C and placed on ice for 2 min. Then, we allowed the cells to recover and to start the production of antibiotic resistance by incubating for 30 min at 37°C in 800 µL of LB-media. Lastly, we plated the cells in agar plates containing the antibiotic needed and incubated overnight at 37ºC.

2.2.1.4 Isolation of plasmid DNA from *E. coli*

Putative positive clones expressing the desired plasmids were selected from agar dishes containing the necessary antibiotic selection. We inoculated the selected clones in LB medium supplemented with the appropriate selection antibiotic. We isolated the plasmids using the mi-Plasmid miniprep kit (Metabion) or the Pureyield™ Plasmid Midiprep system (Promega) following the manufacturer's guidelines.

2.2.1.5 DNA sequencing

We used DNA sequencing to verify the construct's integrity after subcloning and site-directed mutagenesis. GATC Biotech AG performed the sequencing, which was analyzed using SnapGene Viewer.

2.2.2 Cell culture

2.2.2.1 Culture of human cell lines

We used osteosarcoma-derived human U2OS cells (ATCC HTB-96^{TM}) as the primary cell model for this project. The sizeable nuclear size and the adherent nature of these cells make them ideal for imaging assays. In particular, we used CRISPR-generated METTL3 knockout cell, together with its parental control, that the Yang Shi Lab kindly provided (Xiang et al., 2017). CRISPR-knockout PARP1 deficient cells were previously generated in our lab, as previously reported (Sellou et al., 2016). For testing the effect of METTL3 inhibition, we used the MOLM13 leukemia cell line (DSMZ ACC 554).

We maintained the cells in the media described in section 2.1.5, in 10 cm or 15 cm cell culture dishes and kept at 37°C in a humidifier incubator with 5% CO_2. We passaged the U2OS cells every 3 days and maintained in culture for up to two months. Passaging was done by adding trypsin to the cells for 5 minutes at 37°C and seeding in a 1:10 ratio. For passaging the non-adherent MOLM13 cells, the cells were resuspended and seeded in fresh media in a 1:10 ratio.

Cells were counted and the viability was measured with the Vi-CELL XR Cell Viability Analyzer (Beckman Coulter). For this, we washed the cells with PBS, trypsinized, and resuspended in fresh media. A sample of 0.5 mL was taken for each cell type, mixed with 0.5 mL of PBS, and placed into the autosampler cue.

2.2.2.2 Transfection of plasmid in human cell lines

To express tagged proteins, we transfected different constructs using the X-treme-GENE™ HP reagent following the manufacturer's instructions. For this, cells were seeded one day before transfection. The next day, we prepared the transfection mixes according to Table 6 using the plasmid of interest. Mixes were incubated for 5 min at room temperature before being added drop-wise to cells with fresh media. Plasmids used in this project are listed in Table 4.

Table 6. Transfection of plasmids

Format	Cells/well	OptiMEM : DNA	XtremeGENE
8 well Labtek	80,000	100 µL : 300 ng	0.8 µL
6 well plate	200,000	500 µL : 6 µg	6 µL

2.2.2.3 Generating stable cell lines

We generated cell lines expressing the transgene of interest by transfecting cells with the plasmid according to the previously described protocol. We selected the successfully transfected cells by adding G418 to the media for the following two weeks. After selection, cells were expanded, and the expression of the transgene was confirmed via Western blot.

In the case of METTL3-deficient cells transfected with a catalytic mutant METTL3 D385A, the level of expression of the transgene was significantly different among transfected cells. To facilitate further studies, cells were monoclonalized using limiting dilution.

2.2.2.4 siRNA-mediated knockdowns

Transient depletion of a protein using silencing RNA allowed us to investigate the role of a protein before the cell develops coping mechanisms in the absence of the targeted protein. To do this, we seeded 200,000 U2OS cells in a 6-well plate and allowed them to adhere overnight. Next day, we prepared transfection mixes containing 500 µL OptiMEM, 10 nM of siRNA targeting the desired protein (see Table 7), and 4 µL of Lipofectamine RNAiMAX (Invitrogen). Mixes were incubated for 15 min before being added drop-wise to cells with fresh media. We performed a second transfection after six hours. We

confirmed the depletion of the desired proteins 48 h after transfection using Western blot. All siRNA experiments were performed at this time point.

Table 7. siRNA sequences

Name	Sequence	Company	Catalogue
siRNA METTL3	GCAAGUAUGUUCACUAUGATT	Horizon Discovery	Custom
siRNA METTL14	GGAUGAGUUAAUAGCUAAATT	Horizon Discovery	Custom
siRNA XPC	N/A	Thermofisher Scientific	4392420
siRNA XPA	N/A	Thermofisher Scientific	AM16708
siRNA CSB	N/A	Thermofisher Scientific	4392420
siTONEBP #1	CAACAUGCCUGGAAUUCAA	Horizon Discovery	Custom
siTONEBP #2	GCAGUAUGAUUAAGAGUGA	Horizon Discovery	Custom
siNT	AATTCTCCGAACGTGTCACGT	Qiagen	1022076

2.2.2.5 Colony formation assay

We used colony formation assays to assess the survival of cells after treatment with UV-C (254 nm). Cells were trypsinized, seeded at low density (500-750 cells per well), and mock-treated or exposed to an increasing dose of UV light (1, 2, 4, 6, 8 J/m2 of UV-C). After 10 days, the plates were washed with PBS, fixed and stained using a solution containing 50% methanol, 7% acetic acid, and 0.1% Brilliant Blue R. We scanned the stained plates and analyzed using the ColonyArea plugin in ImageJ (Guzman et al., 2014), applying a manual threshold of 180. We estimated the number of surviving colonies from the colony area coverage.

2.2.2.6 Viability assay

We performed viability assays using CellTiter-Glo®, which measures ATP after cell lysis, to test the cell health after exposure to Illudin S, Olaparib, or STM2457. To test sensitivity against Illudin S, we seeded 11,000 UO2S cells per well of a 96-well plate using phenol-red free media (50 µl per well). The next day, 50 µl of a 2X Illudin S was added (0-316 ng of Illudin S). We incubated the cells for 48 hours and harvested by adding 100 µL of the CellTiter-Glo reagent mix. After 10 min, luminescence was measured using a Tecan Infinite M1000 PRO. Cell viability was measured by normalizing the luminescent signal against signal from non-treated cells.

We used the same procedure to test synergy between Olaparib and STM2457 with the following modifications: 10,000 MOLM-13 cells were seeded per well of a 96-well plate. The next day, we prepared two plates of 10X solutions of the desired final concentrations: one for olaparib (final 0 – 50 μM) and one for STM2457 (final 0-50 μM). 10 µL of each pre-mix was added per well, together with 30 µL of fresh media. We measured the luminescence signal after 72 h of treatment. We estimated the percentage of inhibition as follows:

$$\%\ inhibition = \left(1 - \frac{Luminescence\ of\ sample - All\ dead\ sample}{All\ alive\ sample - All\ dead\ sample}\right) * 100$$

All dead and all alive samples correspond to DMSO conditions in which all cells were dead or viable correspondingly.

2.2.2.7 Cell cycle analysis by flow cytometry

We used propidium iodine staining to assess cell cycle of U2OS cells after UV irradiation. After recovery for the determined time points, cells were trypsinized and washed in FACS buffer. $1x10^6$ cells per sample were fixed using 70% ice-cold ethanol, added drop-wise while vortexing overnight at 4°C. The following day, we centrifuged the cells (200xg for 15 min at 4°C) and washed with FACS buffer before incubating for 1h at RT in PI solution. Samples were filtered before using the BD LSRFortessa, and data was analyzed using the Flowing software (Turku Bioscience). At least 5,000 events were collected per sample of 3 independent experiments.

FACS buffer	1x PBS pH 7.5, 2% FCS, 2 mM EDTA
PI solution	1x PBS pH 7.5, 0.1% TritonX-100, 100 µg/mL RNase A, 20 µg/mL propidium iodine

2.2.2.8 Culture of Sf21 cells

We used Sf21 insect cells, derived from *Spodoptera frugiperda,* to express and purify recombinant METTL3 using baculovirus. This work was performed in collaboration with the Meister Lab at the University of Regensburg. Briefly, we cultivated the cells in Sf-

900™II SFM (Thermo Fischer Scientific) at 27°C with constant agitation (55 to 70 rpm). Cells were maintained at a density between 1-4 x 106 cells/mL, sub-cultivating by diluting to 1x10^6 cells/ml of Sf-900 medium. Of note, the expression of the METTL3/METTL14 complex was done similarly by the Jinek Lab in Zurich.

2.2.3 Protein-based methods

2.2.3.1 Expression of recombinant proteins in Sf21 cells

For the expression of METTL3, we cultured Sf21 cells in 500 mL at a concentration of 1 x 10^6 cells/mL. Cells were then infected with 10 mL of passage 2 viral stock, which Prof. Gunter Meister at the University of Regensburg kindly provided. After infection, we incubated the cells at 27°C for 72 h with constant agitation. Cells were harvested by centrifuging at 700 xg for 10 min, and lysates were prepared from the pellets.

2.2.3.2 Lysate preparation for protein purification

We harvested the cells by centrifugation (700 xg for 10 min at RT) and washed twice in PBS buffer (pH 7.0) before resuspending in GST-lysis buffer. We lysed the cells on ice using sonication (output setting: 4-5; duty cycle 50%). Cell debris was removed by centrifuging at 48 000 xg for 45 min at 4°C. The supernatant was then filtered using a 0.45 µM diameter filter.

GST lysis buffer	1x PBS pH 7.5, 1.5 M NaCl, 2 mM DTT, 2 µL/L Benzonase

2.2.3.3 Purification of METTL3

I wrote the HPLC purification program with the support of Dr. Dr. Eva Schöller (University of Regensburg), who also helped operating the Aekta purification system (GE Healthcare). For GST-METTL3 purification, the filtered lysate was loaded onto a 5 mL GST column. We washed the bound protein with 3 column volumes of GST lysis buffer, followed by the elution with three column volumes of elution buffer. We collected the fractions and analyzed using SDS-PAGE with Coomassie staining. We pulled together the fractions containing the protein of interest and concentrated using a Vivaspin concentrator (30 kDa Sartorius). Then, the sample was loaded into a Superdex 200 10/300

resin (GE Healthcare) for size exclusion. The column was first equilibrated with SEC buffer before loading the sample. Fractions containing GST-METTL3 were pooled, and protein concentration was measured. Glycerol was added (end concentration 50%) before flash-freezing the protein and stored at -80°C to freeze the proteins.

GST-elution buffer	50 mM Tris-HCl pH 8.0, 10 mM glutathione, 150 mM NaCl
SEC buffer	HEPES pH 7.4, 200 mM NaCl, 2 mM DTT

2.2.3.4 Purification of PARP1

Purified recombinant PARP1 ΔHD was kindly provided by Dr. Gunnar Knobloch (Eisbach Bio), and a pellet of E. coli expressing His-PARP1 full-length. The recombinant protein was purified according to Langelier and colleagues (Langelier et al., 2010), with the help of Matin Moschref. We thawed the pellet into 4 times the cell pellet volume of lysis buffer and sonicated using 6-8 cycles of 1 minute ON, 2 min OFF (output setting 4; duty cycle: 70%). Then, the lysate was centrifuged at 40 000 xg for 30 min at 4°C. Ni-NTA beads were washed once with water and 2 times with wash buffer and centrifuged at 3 000 rpm, 4°C, 2 min). We incubated the centrifuged cell lysate with the washed His beads at 4°C for 1h under constant rotation. After incubation, the beads were centrifuged (3 000 rpm, 4°C, 2 min) and washed 2 times with wash buffer, one time with wash buffer 2, and one additional time with wash buffer. Elution of bound protein was done by incubating the beads with 1 volume of elution buffer, incubated for 5 minutes, and centrifuged (3 000 rpm, 4°C, 2 min). Elution was performed 3 times, and all fractions were tested for protein content. Protein content was estimated using the Protein Assay Dye Reagent (Bio-Rad). We pulled the fractions enriched with protein and diluted with no salt buffer to achieve a final concentration of 250 mM NaCl. We loaded the diluted protein into a 5 mL heparin column (GE Healthcare) and run in the Aekta purification system in a gradient with 40 column volumes from 0 to 100% Heparin Buffer B. We collected the fractions and run in an SDS gel. We pulled the fractions containing the protein of interest and concentrated using a Vivaspin centrifuge concentrator (cut-off 30 kDa, prewet with SEC buffer, Sartorius). We loaded the concentrated protein into a HiLoad 26/60 Superdex 200 pg (GE Healthcare) preequilibrated before with SEC buffer. We collected the fractions and confirm the presence of the protein using SDS gel. We pulled together the fractions containing the protein of interest and concentrating once more using a fresh Vivaspin centrifuge concentrator.

Lysis buffer	20 mM HEPES pH 8.0, 500 mM NaCl, 0.1% NP-40, 20 mM Imidazole pH 7.5, 0.5 mM TCEP, pH 7.0
Wash buffer	20 mM HEPES pH 8.0, 0.5 mM NaCl, 20 mM Imidazole pH 7.5, 0.5 mM TCEP, pH 7.0
Wash buffer 2	20 mM HEPES pH 8.0, 1 M NaCl, 20 mM Imidazole pH 7.5, 0.5 mM TCEP pH 7.0
Elution buffer	20 mM HEPES pH 8.0, 500 mM NaCl, 400 mM Imidazole pH 7.5, 0.5 mM TCEP pH 7.0
No salt buffer	20 mM HEPES pH 8.0, 0.5 mM TCEP pH 7.0
Heparin buffer A	50 mM Tris pH 7.0, 250 mM NaCl, 1 mM EDTA, 0.1 mM TCEP pH 7.0
Heparin buffer B	50 mM Tris pH 7.0, 1 M NaCl, 1 mM EDTA, 0.1 mM TCEP pH 7.0
SEC buffer	20 mM HEPES pH 8.0, 150 mM NaCl, 0.1 mM EDTA, 0.1 mM TCEP pH 7.0

2.2.3.5 Purification of PAR polymer

The PAR polymer was produced by triggering a PARylation reaction using purified PARP1ΔHD, as previously described (Fahrer et al., 2007). We carried out the reaction in 20 mL of 50 mM Tris-HCl pH 8.0, 4 mM $MgCl_2$, 20 mM NaCl, 5 mM NAD+, 250 µM DTT, 150 µg/mL of salmon sperm DNA, and 150 nM human PARP1 at 37°C for 60 minutes. The reaction was stopped by adding 20 mL of cold 20% (wt/vol) TCA and incubated on ice for 15 min. We centrifuged the protein mix for 10 min at 9000g at 4°C, and the pellet was resuspended in 20 mL of ice-cold 99.8% ethanol followed by 10 min incubation on ice. The pellet was centrifuged and rewashed with ice-cold ethanol before centrifuging at 9000g for 20 min. We removed the ethanol and air-dried the pellet. The polymer was cleaved from PARP1 by treating the pellet with 9 mL of 0.5 M KOH/50 mM EDTA for 10 min at 37°C in a shaking water bath. Then, we added 1 mL of Tris-HCl pH 8.0 to achieve a final concentration of 100 mM Tris-HCl. We aliquoted the mix into 1 mL Eppendorf tubes after adjusting the pH to 8.0. Each aliquot was then supplemented with 25 uL of 2M $MgCl_2$ and 55 µL of DNAse I (2 mg/mL). Samples were incubated for 2 hours at 37°C while shaking. Proteinase K was added (11 µl of a 20 mg/mL stock solution) with 10 µL of 100 mM $CaCl_2$ to digest overnight. The next day, we added 600 µL of phenol to each tube, and centrifuged the samples for 10 min at 14,000g. The aqueous phase was transferred into DNA LoBind tubes, and 600 µL of phenol/chloroform/isoamyl alcohol (25:24:1 v/v/v) was added. Samples were centrifuged, and we collected the supernatant

of all samples. Then, 99.8% ethanol stored at -20°C was added to achieve a final concentration of 70% (v/v). The ethanol mix was incubated overnight at -20°C. The next day, the mix was centrifuged for 30 min at 9000g at °C. We air-dried the pellet before resuspending in 100 uL of Milli-Q water. We estimated the concentration of the polymer based on the absorption coefficient of mono(ADP-ribose) monomers measured at 258 nm and using the Lambert-Beer equation:

$$[PAR] = A_{258nm}\ cm^{-1} / 13{,}500\ cm^{-1}\ M^{-1}$$

2.2.3.6 Slot blot assay

Binding to PAR was assessed using a slot blot approach. We equilibrated the nitrocellulose membrane for 5 min with TBS-T buffer. The member was air-dried before spotting increasing concentrations of recombinant METTL3/14, BSA, and MacroH2A1/H2B (kindly provided by Imke Mandemaker). The membrane air dried before incubating with 1 µM PAR in TBS-T overnight at 4°C. The next morning, the PAR solution was removed, and the membrane was washed 5 times with TBS-T before blocking for 1 h with 5% milk in TBS-T. The binding of PAR to spotted proteins was detected using the pan-ADPribose reagent.

TBS-T buffer	10 mM Tris pH 7.4, 150 mM NaCl, 0.05% (v/v) Tween 20™

2.2.3.7 Electrophoretic mobility shift assay

We incubated purified METTL3 and 20 ng of Cy3-labeled RNA in 25 µL EMSA buffer for 15 min at 26°C. For the competition assay, different amounts of PAR was further incubated with this reaction mix for 75 min at 26°C. Samples were separated on a 6% native polyacrylamide gel (pre-run at a constant current of 80V for 45 min) in 0.4x TBE buffer at a constant current of 80V for 70 min. We imaged the gels using a ChemiDoc MP (Bio-Rad).

EMSA buffer	20 mM Tris pH 7.6, 1.5 mM $MgCl_2$, 40 mM KCl, 0.5 mM EGTA, 10% glycerol, 200 ng/µL BSA, 1 mM DTT, 1 U/µL of RiboLock
0.4x TBE buffer	90 mM Tris, 90 mM boric acid, 2 mM EDTA

2.2.3.8 Nano differential scanning fluorimetry

We used Prometheus NT.48 (NanoTemper GmbH, Munich, Germany) to perform dye-free thermal shift assays. Capillaries were filled with 10 µL of binding buffer containing 1 µM of recombinant protein and increasing ligand concentrations. The excitation light was adjusted to get readings above 2000 arbitrary units, and samples were measured in a temperature range of 20-80°C with a temperature slope of 1°C/minute. Three technical replicates were analyzed per run; scattering information was used to exclude aggregate formation. For visualization, data was normalized to min and max values of the first derivative of the 350/330 nm ratio. The T_m values were obtained from the NT.48 Software.

Binding buffer 20 mM Tris pH 7.5, 50 µM $ZnCl_2$, 1% glycerol and 1 mM DTT

2.2.3.9 Microscale thermophoresis

We used Monolith NT.115 (NanoTemper GmbH, Munich, Germany) to assess recombinant METTL3/14 binding to fluorescently tagged RNA and PAR. Capillaries were filled with 10 µL of binding buffer containing 100 nM of RNA or PAR probe and increasing concentrations of recombinant protein. The excitation light was adjusted to get readings above 2000 arbitrary units. Two technical replicates were analyzed per run and quality of the traces was used to exclude anomalies such as aggregates or air bubbles. Data was analyzed using the NT Analysis Software and K_d values were calculated by fitting a Hill slope model in GraphPad Prism8. The accuracy of the model is reported as the R^2 value for each condition.

Binding buffer 20 mM Tris pH 7.5, 50 µM $ZnCl_2$, 1% glycerol and 1 mM DTT

2.2.3.10 Dye protein assay, SDS-PAGE, Coomasie staining, Western blotting

To quickly assess protein content in elution fractions, the Bio-Rad protein Assay was used, a colorimetric assay based on the Bradford method, was used. For this, an initial 1:5 dilution of the concentrated reagent was prepared. 2 µL of the eluate were then added to 200 µL of the reagent. Samples are mixed, and we wait for color development. Samples with higher protein content, as seen by the change of color into dark blue tones, were combined for further analysis.

We used sodium dodecyl sulphate polyacrylamide gel electrophoresis (SDS-PAGE) to separate proteins based on their molecular mass. The acrylamide concentration was selected based on the mass of the protein of interest, choosing between 10% polyacrylamide gels (self-made) or 4-20% gradient gels (Bio-Rad). To prepare the samples, they were supplemented with sample buffer, boiled for 10 min at 95°C and allowed to cool down before loading. Once loaded, the gels were run at 180 V or 250 V (self-made and gradient gels respectively). Separation was stopped when the protein ladder was fully resolved.

Stacking gel	5% Acrylamide/Bis acrylamide solution (30% / 0.8% w/v), 130 mM Tris-HCl pH 6.8, 0.1% SDS, 0.1% APS, 0.1% TEMED
Separation gel	10% Acrylamide/Bis acrylamide solution (30% / 0.8% w/v), 390 mM Tris-HCl pH 8.8, 0.1% SDS, 0.1% APS, 0.1% TEMED
SDS running buffer	25 mM Tris-HCl pH 7.5, 200 mM glycine, 1% SDS
2x sample buffer	80 mM Tris-HCl pH 6.8, 4% SDS, 0.02% bromophenol-blue, 10% glycerol, 10% β-mercaptoethanol

For protein purification, SDS-PAGE gels were followed with Coomassie staining, while protein expression for cellular assays were followed by Western blotting. Coomassie staining was performed by incubating the gel for 1 to 2 h, at RT with Coomassie staining solution. After staining, the gels were rinsed three times with Milli-Q grade water and destained with destaining solution at RT. The solution was changed multiple times, until bands were visible.

Coomassie staining	10% acetic acid, 30% ethanol, 0.25% Coomassie R 250
Destaining solution	10% acetic acid, 30% ethanol

For Western blotting, proteins were transferred onto a 0.45 µM PVDF membrane (Merck) using the Trans-Blot Turbo Transfer System from Bio-Rad with 1x transfer buffer (Bio-Rad) for 25 min at 15 V, 1.5 A. After transfer, blots were blocked in TBS-T containing 5% skim milk for 30 min at RT. After washing three times with TBS-T, blots were incubated overnight with the corresponding primary antibody diluted TBS-T at 4°C. The next morning, blots were washed 3 times with TBS-T and incubated for 1 h at RT with the secondary antibody diluted in TBS-T. The membrane was washed three times before developing

using Pierce™ ECL substrate or fluorescence and documenting the results using the ChemiDoc Imaging System (Bio-Rad) or the Odyssey scanner system (Li-COR Bioscience).

TBS-T 150 mM NaCl, 10 mM Tris-HCl pH 7.5, 0.1% Tween

For re-probing blots developed using ECL, membranes were stripped using stripping buffer. For this, we incubated the membrane 3x with stripping buffer, refreshing the buffer every 10 minutes. We then washed 2x with PBS for 10 min each, followed with 2 washes with TBS-T buffer for 5 min each. After washing, membrane was re-blocked with 5% milk in TBS-T and probed with primary antibody as previously described.

Stripping buffer 1.5% w/w glycine, 0.1% SDS, 1% Tween 20™, pH 2.2

2.2.4 Cell and microscopy-based methods

2.2.4.1 Cell cycle analysis with flow cytometry

Flow cytometry was used to determine the cell cycle profile of cells after UV exposure. For this, 300,000 cells were seeded in 10 cm cell culture dishes. On the next day, cells were exposed to 10 J/m^2 of UV-C and allowed to recover for 20 and 6 h. After recovery, samples were trypsinized and counted, taking 1,000,000 cells for analysis. Samples were centrifuged and resuspended in 1 mL of flow cytometry buffer. Samples were centrifuged to remove cell debris and fixed overnight in 1 mL of 70% ice-cold ethanol at 4°C. Next morning, the samples were centrifuged at 4°C, 200xg for 15 min. Pellets were washed with flow cytometry buffer, centrifuged at 4°C, 300xg for 5 min, resuspended in 1 mL propidium iodine solution, and incubated for 30 min. Before analysis, samples were filtered through a 35 µm cell strainer cap to prevent clump formation. Data was collected using a BD LSRFortessa™, using a low flow setting and collecting a minimum of 10,000 events. The cells were gated to exclude debris and doublets based on forward and side scatter during the data acquisition.

Flow cytometry buffer PBS, 2% FBS, 2 mM EDTA

Propidium Iodine solution PBS, 0.1% Triton X-100, 100 µg/mL RNAse A, 20 µg/mL propidium iodine

2.2.4.2 Co-immunoprecipitation

HEK293T cells were seeded to a 15-cm dish at a density of 2.5×10^6 and transfected with 12 µg GFP-METTL3 plasmids the following day. Following 48 h of incubation, we treated the cells with 0.5 µg/mL Actinomycin D for 2 hours and harvested in cold PBS. We first lysed the cells in 1 mL EBC-1 buffer for 20 min, and the pellet was further lysed in 300 µL EBC-1 buffer with 500 U Benzonase, 5 µL goat anti-GFP antibody (homemade), 1 µM Olaparib, and PARGi for 3 h while rotating. The supernatant was taken 1% as input and incubated with 300 µL Dynabeads for another 1.5 h. We then washed the beads 6x with 1 mL EBC-2 buffer and prepared for SDS-PAGE electrophoresis.

EBC-1 buffer	50 mM Tris pH 7.5, 150 mM NaCl, 0.5% NP-40, 2 mM $MgCl_2$, 1x protease inhibitor cocktail.
EBC-2 buffer	50 mM Tris pH 7.5, 150 mM NaCl, 0.5% NP-40, 1 mM EDTA, 1x protease inhibitor cocktail.

2.2.4.3 Imaging system

All imaging experiments were conducted using a Zeiss AxioObserver Z1 confocal spinning-disk microscope with a sCMOS ORCA Flash 4.0 camera (Hamamatsu). A C-Apo 63x water immersion objective was used for live-cell imagining, whereas fixed cells were imaged with a 40x C-Apochromat/1.2 Korr water objective (Olympus).

2.2.4.4 Microirradiation with live-cell imaging

Cells were seeded in 8-well Nunc Lab-Tek chambers (Thermo Fisher Scientific) and transfected as described in section 2.3.2.2. To pre-sensitize cells, samples were incubated with 1 µM BrdU for 16 h. Cells were recorded in Leibovitz's L-15 media at 37ºC and no CO_2. DNA damage was induced through a line of 88 pixels using 15% power of a 355 nm laser operated through a single-point scanning head (UGA-42 firefly, Rapp OptoElectronics) with 20-22 runs per object. Images were recorded for 5 min following irradiation at 5 s intervals. For treatments, cells were incubated as follows: 1:500 DMSO for 1 h, 1 µM Olaparib (PARPi; SelleckChem) for 1 h, 1 µM PDD00017273 (PARGi; Sigma) for 1 h, 2 µg/mL αAmanitin (Sigma) for 4 h, and 0.5 µg/mL Actinomycin D (Applichem) for 2 h.

2.2.4.5 Microirradiation with immunofluorescence staining

Cells were prepared and micro-irradiated as described for live-cell imaging. After microirradiation, we incubated the cells for the indicated times, fixed, and stained as described in (Mandemaker et al., 2020). In brief, samples were washed with ice-cold PBS, fixed with 2% paraformaldehyde in PBS + 0.1% Triton X-100 for 15 min at room temperature, followed by 2x 10 min of permeabilization at room temperature using PBS + 0.1% Triton X-100. Samples were washed with PBS+ and incubated for 5 min with 0.07 M NaOH to denature the DNA. After washing with PBS+, the cells were incubated with diluted primary antibody overnight at 4°C. Samples were washed 5x with PBS + 0.1% Triton and 2x with PBS+ to remove unbound antibody. Samples were incubated for 1 h at room temperature in the dark with Alexa Fluor 488 or Alexa Fluor 568-conjugated fluorescent antibodies (Thermo Fisher Scientific) and Hoechst 33342 (Termo Fischer Scientific) diluted in PBS+. Unbound antibody was removed by washing 5x with PBS + 0.1% Triton and 2x with PBS+, and samples were mounted using Aqua-poly mount (Polysciences Inc).

PBS+ PBS, 0.5% BSA, 0.15% glycine

2.2.4.6 Immunofluorescence staining

Cells were grown in coverslips for all stainings after global UV-C irradiation, and irradiated with 10 J/m^2. For local UV-C irradiation, cells were covered with an Isopore™ filter (0.22 µM, Merck) before irradiating with 10 J/m^2. For 6-4 PPs staining, cells were fixed with 4% paraformaldehyde in PBS, washed 3x with PBS, and permeabilized for 5 min with PBS + 0.5% Triton X-100 on ice. After washing 3x with PBS, samples were denatured with 2M HCl for 30 min at room temperature. We washed 5x with PBS and blocked the samples using PBS + 20% FBS for 1 h at room temperature while gentle tilting. Next, samples were washed 5x with PBS and incubated with primary antibody diluted 1:300 in PBS + 5% FBS for 1 h. After washing 5x with PBS, samples were incubated with secondary antibodies, as described before. Samples were washed 5x with PBS and mounted. CPD staining samples were processed as described for immunofluorescence staining after microirradiation (see 2.3.4.5). For ATF3 staining, samples were fixed for 15 min with 2% PFA in PBS +0.2% Triton X-100 and permeabilized for 3x short washes and 2x 10 min washes with 0.1% Triton X-100 in PBS. Samples were blocked with 5% BSA in PBS with 0.1% Tween for 30 min at room temperature, and primary was diluted

1:500 in 1% BSA in PBS + 0.1% Tween and incubated overnight at 4°C. Next, samples were washed for 10 min 2x with 0.1% Triton X-100 in PBS and 1x with 1% BSA in PBS with 0.1% Tween. The secondary antibody was diluted in 1% BSA in PBS with 0.1% Tween and incubated for 1h at RT in the dark. Samples were washed 2x 10 min in 0.1% Triton X-100 in PBS and 1x in 1% BSA in PBS with 0.1% Tween before mounting using Aqua-poly mount (Polysciences Inc).

2.2.4.7 Fluorescence recovery after photobleaching

We seeded the cells in 8-well Nunc Lab-Tek chambers (Thermo Fischer Scientific) and changed them to Leibovitz's L-15 media at 37ºC and no CO_2 before starting the experiments. Recovery after photobleaching analysis of METTL3 was performed in cells stably expressing GFP-METTL3. We used transient transfection to analyze METTL14. After 30 frames, a circle with a radius of 40 pixels was bleached using a 488 nm, 100% laser power. We monitored the recovery of the GFP signal in the bleached area for 30 frames taken at 2 s intervals.

2.2.4.8 EdU labeling for recovery of mRNA synthesis after UV irradiation

Cells were seeded in coverslips in DMEM supplemented with 1% FBS, exposed to UVC irradiation (10 J/m^2), and allowed to recover in DMEM supplemented with 10% FBS for the desired times. We then incubated the cells in DMEM media with 0.5 mM ethynyluridine (EU) for 2 h at 37°C, washed with PBS and fixed for 15 min with 4% paraformaldehyde in PBS. Samples were rinsed 2x with 3% BSA in PBS and permeabilized for 20 min with PBS + 0.5% Triton X-100. We performed a Click-iT reaction to couple the secondary antibodies using the Click-iT® RNA Alexa Fluor® 594 Imaging Kit (Thermo Fischer Scientific). Samples were rinsed 2x with 3% BSA in PBS, followed by 2x PBS, and mounted as described before.

2.2.5 Data analysis

2.2.5.1 Microirradiation live-cell imaging analysis

We cropped the images to generate image files containing one single cell per file. Localization of the cell through time was registered using the StackReg plugin (Thevenaz et

al., 1998). We used the HiLo look-up table to classify pixels based on their fluorescence intensity. This visualization guided the selection of the region of interest, and a background region was used for downstream data processing. Then, we used the Li auto threshold algorithm to select the whole nucleus. Results containing the intensity of the three selected regions were transferred to Microsoft Excel, where the relative fluorescence intensity was calculated by normalizing to the signal before irradiation and using the following formula:

$$RFI = \frac{(\frac{X - B}{\bar{X}})}{\frac{N - B}{\bar{N}}}$$

where X stands for the region of interest, B to the background, $\bar{X}$ to the average fluorescent signal of the region of interest before damage, N to the whole nuclear signal and $\bar{N}$ to the average fluorescent signal of the whole nucleus before damage.

2.2.5.2 Microirradiation with fixed immunofluorescence imaging analysis

Dr. Imke Mandemaker provided the original script to analyze the intensity of a signal inside and outside a damaged region, which was adapted to the particular conditions used in this project. First, a nuclear mask and a DNA damage mask were generated based on Hoechst 33342 and CPD stainings, respectively. A non-damaged area mask was generated by subtracting the DNA damage mask from the nuclear mask, a real damage area was determined by conditioning the DNA damage mask to be contained within the nuclear mask, a background mask was created as the inverse of the nuclear mask. We applied these masks to the channel containing the signal of interest. The area and integrated signal density of the damaged site and the non-damaged nuclear region were measured and corrected for the background signal. We calculated the accumulation as the mean intensity signal of the damaged region against the nuclear signal. The signal was filtered based on the area of the damage site, where area had to be greater than 10 pixels.

2.2.5.3 Immunofluorescence analysis

To measure nuclear fluorescent signal after global irradiation, a nuclear mask was generated using the Li auto threshold algorithm in the channel containing Hoechst 33342 signal. Particles with size between 100-1000 pixels and circularity > 0.3 were selected for analysis. To analyze accumulation at the LacO foci, mCh-MacroH2A1.1 were

selected. Accumulation was calculated using the formula described for live-cell imaging after microirradiation.

2.2.5.4 Fluorescence recovery after photobleaching analysis

To monitor the recovery of the fluorescent signal after photobleaching, the bleached cell was selected and duplicated. Localization of the cell through time was registered using the StackReg plugin (Thevenaz et al., 1998), and we used the HiLo look-up table to color-code pixels based on their fluorescence intensity. Then, we manually fitted a circle of 28 pixels to the bleached nuclear region. We recorded the fluorescence intensity of the bleached region, a background control, and a nuclear control from a neighboring cell (used as control for photobleaching of the imaging system) were recorded over all time frames and transferred to Microsoft Excel. We calculated the relative fluorescence intensity with the following formula:

$$RFI = \frac{(\frac{X - B}{\bar{X}})}{\frac{P - B}{\bar{P}}}$$

where X stands for the bleached region, B for the background control, $\bar{X}$ for the average fluorescent signal of the area of interest before bleaching, P for the photobleaching control, and $\bar{P}$ for the average fluorescent signal of the photobleaching control before photomanipulation. The fluorescent intensity was then normalized to the intensity signal before and after photomanipulation. We calculated the immobilized fraction as 1 minus the maximum recovery.

2.2.5.5 Statistics

We used Microsoft Excel for data processing, and Prism GraphPad for data visualization and statistical analysis. A one-way ANOVA was performed to compare multiple conditions, followed by either Turkey's post-hoc test (for comparing all means) or Dunnett post-hoc test (for comparing means against a control). A two-way ANOVA was used for cell cycle analysis, followed with Turkey's post-hoc test to evaluate differences based on genomic background, treatment, and cell cycle phase. Significance levels were defined as follows: not significant (ns) $p > 0.033$, * $p < 0.033$, **$p < 0.002$, *** $p < 0.001$, **** $p<0.0001$. I provide the specific number of cells and replicates analyzed per experiment in each figure legend, together with data representation (mean ± SEM or SD) and the specific statistical test used. Significant differences between conditions are indicated in the figures with lines connecting the compared groups.

3. Results

3.1 METTL3/14 complex and m6A accumulate at DNA damage sites

3.1.1 M6A accumulates at DNA lesions in BrdU-treated cells

We first characterized the accumulation of m6A at UV-induced DNA damage sites. In agreement with previous reports (Svobodová Kovaříková et al., 2020; Xiang et al., 2017), we observed that pre-sensitization with BrdU is required for nuclear m6A accumulation after UV treatment using both laser microirradiation (Figure 5 A) and local UV-C irradiation through a micropore membrane (Figure 5 B). Of note, m6A signal at local irradiation sites is observed in METTL3-deficient cells (ΔMETTL3), suggesting unspecific binding of the antibody as the absence of METTL3 was confirmed by western blotting (Figure 5 C), contribution of other methyltransferases, or residual METTL3 spliced variants not detected by our antibody, as suggested by (Poh et al., 2022).

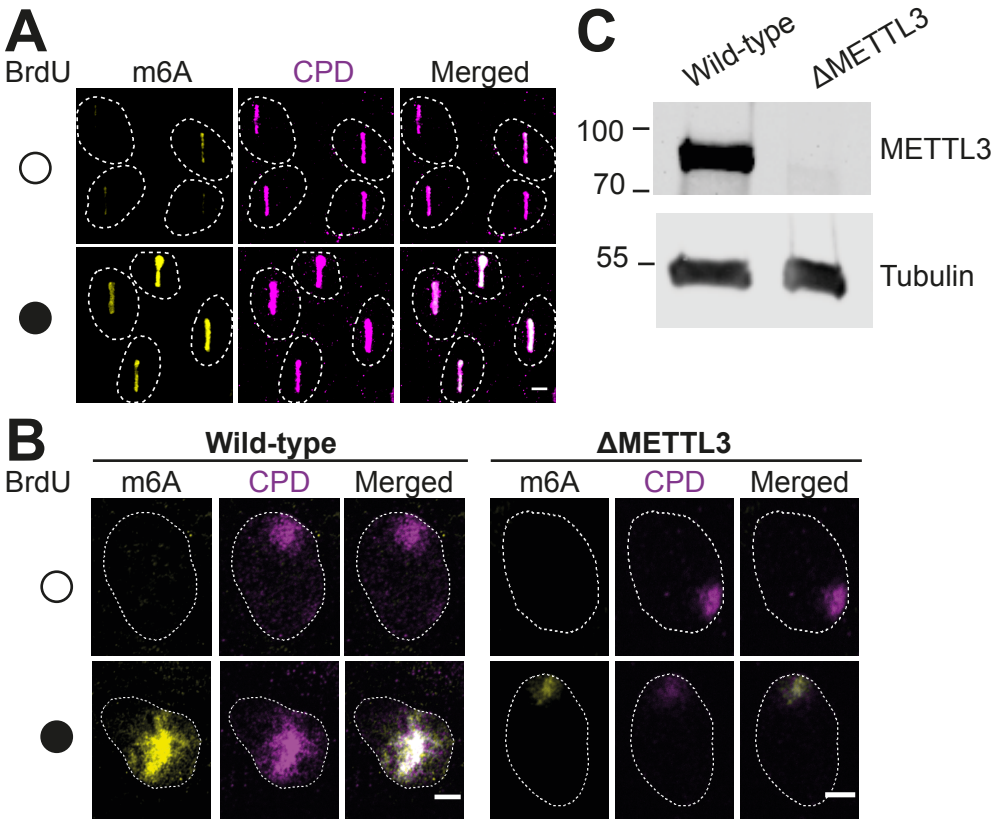

Figure 5. BrdU is required for m6A accumulation after UV damage. Immunofluorescence staining of m6A following (**A**) microirradiation and (**B**) UV-C (10 J/m^2) local irradiation in the presence and absence of BrdU. M6A signal was detected in BrdU-treated samples and co-localized with CPD photolesions. M6A was also observed in ΔMETTL3

cells, indicating possible antibody cross-reactivity. (**C**) Western blot to confirm the absence of METTL3 in ΔMETTL3 cells. The scale bars in (**A**) and (**B**) represent 5 µm.

Using microirradiation followed by immunofluorescence staining, we confirmed the rapid and transient accumulation of m6A at DNA-damaged sites, as previously reported (Svobodová Kovaříková et al., 2020; Xiang et al., 2017). In our hands, m6A was observed immediately after damage and disappeared 6 min after photomanipulation (Figure 6 A-B).

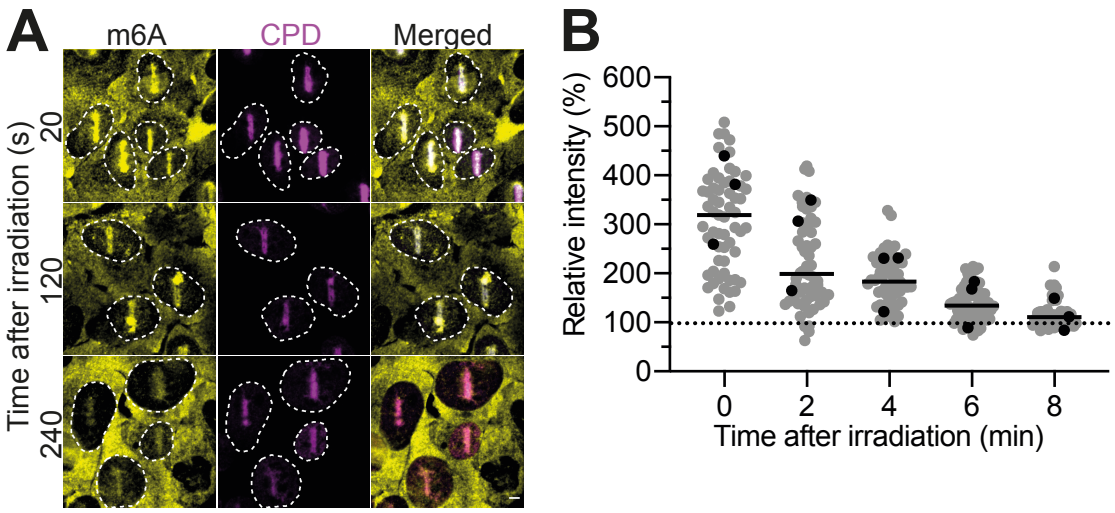

Figure 6. Kinetics of m6A accumulation at DNA damage sites. (A) Representative images and (**B**) quantification of the m6A immunofluorescence signal following microirradiation. More than 100 cells per condition were analyzed across three independent experiments. Each nucleus is represented as a data point. The black points represent the means of the three independent experiments, with the bar indicating the median signal of all nuclei. The scale bar in (**A**) represents 5 µm.

3.1.2 METTL3 and METTL14 accumulate at DNA lesions

To characterize the dynamics of METTL3 at DNA photolesions, we generated a stably expressing GFP-METTL3 U2OS cell line. In contrast, we used transient transfection of GFP-METTL14 to study the dynamics of this protein in U2OS cells. The kinetics of METTL3 and METTL14 enrichment at DNA damage sites were monitored using live-cell imaging (Figure 7 A). This approach allows us to directly monitor the localization of the desired proteins with better time resolution than immunofluorescent staining. The accumulation of both GFP-METTL3 (Figure 7 B) and GFP-METTL14 (Figure 7 C) in presensitized cells was transient, with maximum recruitment observed approximately 60 s after microirradiation.

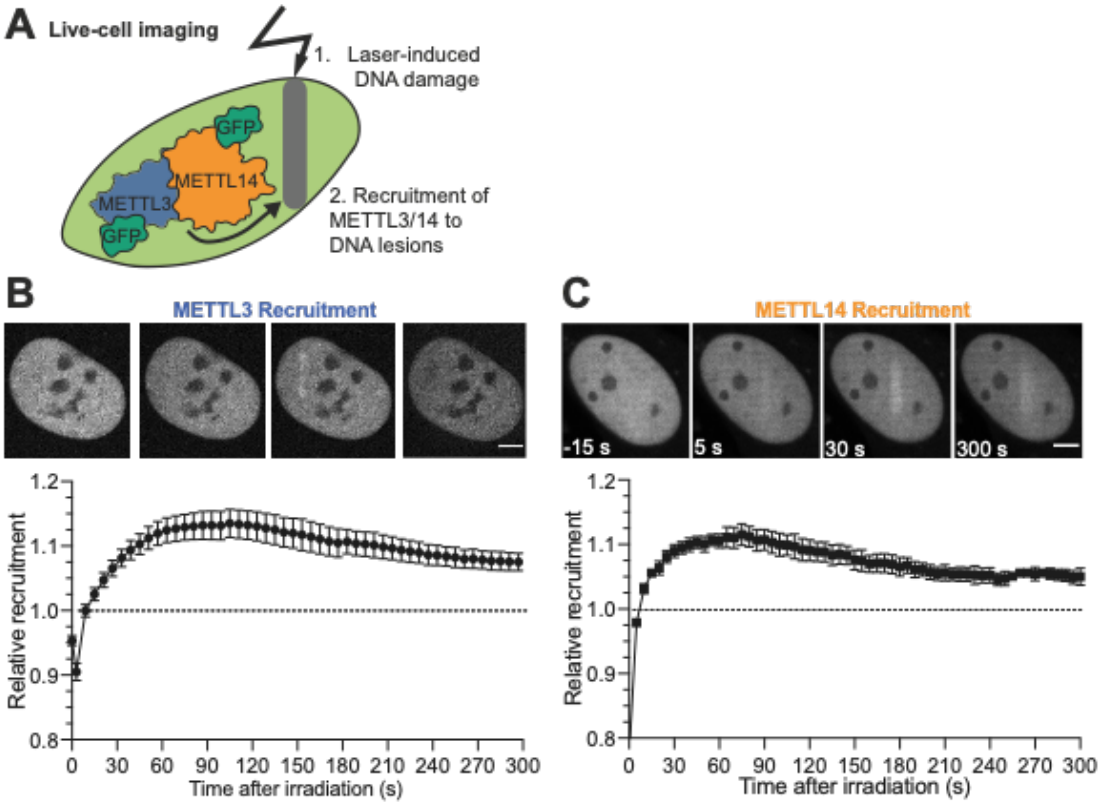

Figure 7. Recruitment kinetics of METTL3 and METTL14 to DNA damage sites. (**A**) Schematic representation of the live-cell imaging recruitment experiments. (**B**) Representative images (top) and quantification (bottom) of GFP-METTL3 recruitment and (**C**) GFP-METTL14 recruitment kinetics to 355-nm microirradiation sites, measured over 5 min. More than 30 cells were analyzed per condition across three biological replicates. Data are presented as the mean ± SEM. The GFP signal is normalized to the pre-damage intensity at the microirradiation sites. The scale bar represents 5 µm.

3.1.3 WTAP recruits to DNA lesions, but FTO does not

We further characterized the recruitment of the m6A demethylase FTO and the accessory protein WTAP. Using the same experimental conditions, we did not observe recruitment of GFP-FTO to microirradiation sites (Figure 8A). However, low levels of GFP-WTAP were observed at DNA damage sites. In contrast to the METTL3/14 complex, the GFP-WTAP signal at microirradiation falls below nuclear levels 2 min after photomanipulation (Figure 8B). This difference in kinetics suggests that the recruitment mechanism of WTAP differs from that of METTL3/14. Thus, it is not likely that WTAP recruits alongside METTL3/14 as a holocomplex.

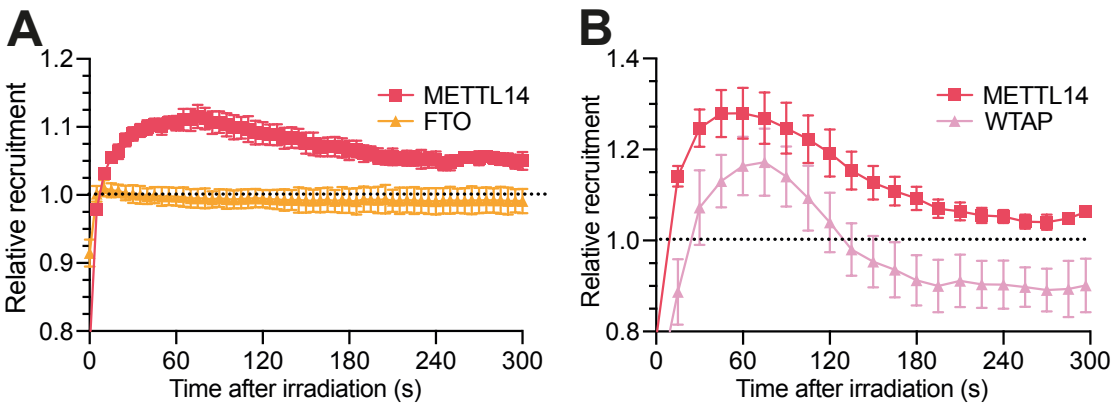

Figure 8. Kinetics of recruitment of the demethylase FTO and WTAP. (**A**) The recruitment kinetics of GFP-FTO and (**B**) GFP-WTAP to DNA damage sites were measured over 5 min following irradiation. GFP-METTL14 recruitment was used as a positive control. More than 30 cells per condition were analyzed across three biological replicates. Data are presented as the mean ± SEM. The GFP signal is normalized to the pre-damage intensity at the microirradiation sites.

3.1.4 METTL3 and METTL14 recruit independently to DNA damage sites

Despite METTL3 being the catalytic subunit of the METTL3/14 complex, RNA methylation *in vitro* can only occur in the presence of the heterodimer (J. Liu et al., 2014; X. Wang et al., 2016). Therefore, we asked whether each methyltransferase requires its interacting partner to recruit to DNA damage lesions. We transiently depleted METTL14 in cells stably expressing GFP-METTL3 and transiently expressed GFP-METTL14 in ΔMETTL3 cells. We observed that both METTL3 and METTL14 recruit to DNA damage lesions without their interacting partner (Figure 9 A-B top), arguing that each methyltransferase recruitments independent of their interacting partner. Interestingly, GFP-METTL14 recruitment was slightly increased in ΔMETTL3 cells (Figure 9B). The efficiency of siRNA-mediated depletion was tested using Western blotting 48 h after transfection (Figure 9 A-B bottom), the time at which cells were used in microirradiation experiments.

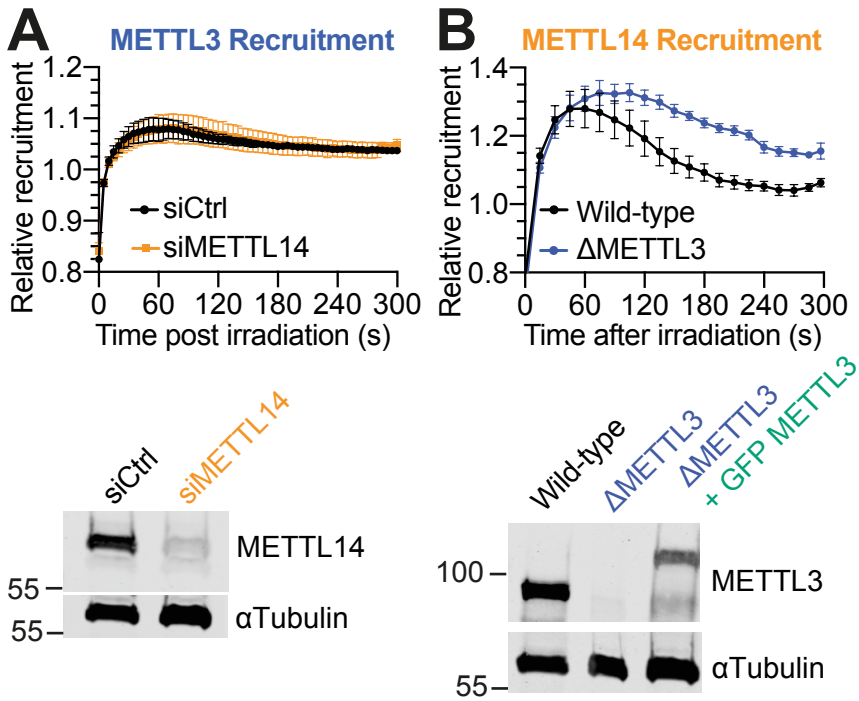

Figure 9. METTL3 and METTL14 recruit to DNA lesions independently of each other. Recruitment kinetics of (**A**) Recruitment kinetics of GFP-METTL3 in METTL14 knockdown cells. (**B**) Recruitment kinetics of GFP-METTL14 in METTL3 knockout cells to 355-nm microirradiation sites. (**A-B**) Data are presented as mean ± SEM, with more than 60 cells per condition were analyzed across three independent experiments. The bottom panels show Western blots verifying the depletion of target proteins and the expression of GFP-METTL3. Blots represent a single, representative experiment, with similar depletion levels observed across replicates.

3.1.5 The methyltransferase domain is sufficient for METTL3 recruitment

To understand what domains of METTL3 drive the recruitment of the protein to DNA damage sites, we generated constructs expressing truncated versions of METTL3 fused to GFP. The truncations were designed based on the functional domains annotated for this protein (Meiser et al., 2020), with the N- construct containing the WTAP-interacting regions, the MID construct containing the two zinc finger domains, and the C- construct containing the methyltransferase domain (Figure 10 A). All GFP-fused products were observed inside the nuclei of cells, although a cytoplasmic GFP signal was also observed for the MID and C- constructs (Figure 10 B). Interestingly, only the C- construct was recruited to DNA lesions (Figure 10 B-C), indicating that the methyltransferase domain is sufficient to recruit of METTL3.

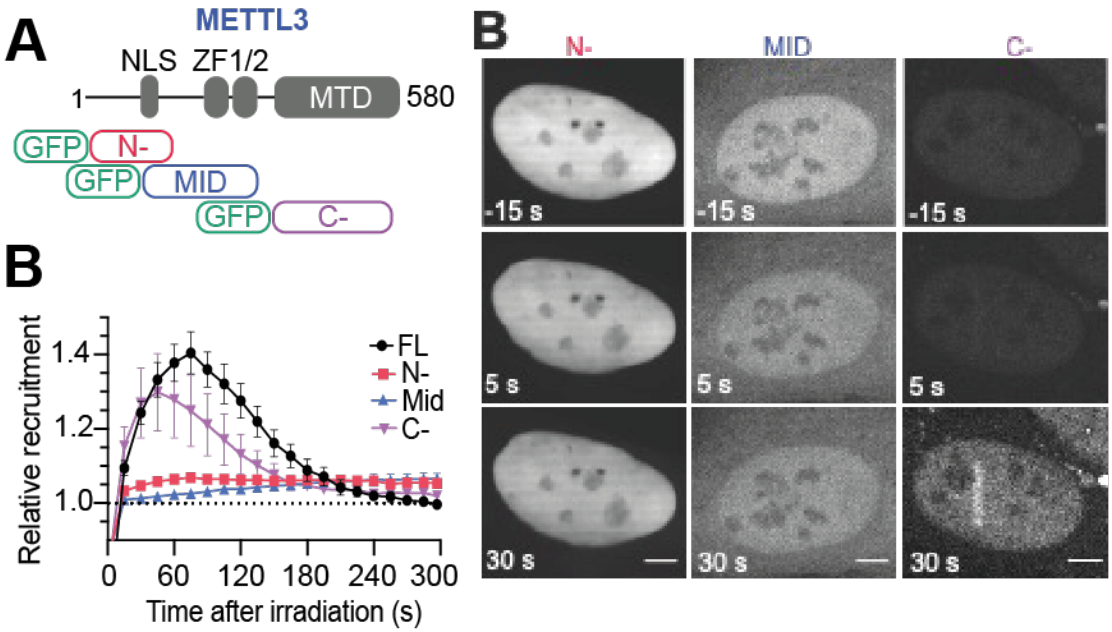

Figure 10. The methyltransferase domain of METTL3 is sufficient for recruitment to microirradiation sites. (**A**). Diagram illustrating the constructs generated to study the domains necessary for METTL3 recruitment to microirradiation sites, adapted from (Meiser et al., 2020). (**B**). Representative images showing the localization and expression of each construct. (**C**). Quantification of microirradiation assays using these constructs, with full-length GFP-METTL3 (FL) as control. More than 40 cells per condition were analyzed across three independent experiments. Data are presented as mean ± SEM.

3.2 Accumulation of METTL3/14 and m6A at DNA lesions depends on PAR dynamics

3.2.1 PAR dynamics modulate m6A accumulation

The rapid and transient accumulation of m6A and recruitment of the METTL3/14 complex resembles the kinetics of PARylation, a critical post-translational modification that guides the early DNA damage response (Blessing et al., 2020). In agreement with previous reports (Svobodová Kovaříková et al., 2020; Xiang et al., 2017), treatment with the olaparib abrogated the enrichment of m6A at UV-induced DNA damage lesions (Figure 11). We further validated the correlation between PAR levels and m6A accumulation by looking at methylation levels in PARP1 knockout cells (ΔPARP1). Interestingly, low yet stable levels of m6A were detected in ΔPARP1 (Figure 11), which could be attributed to the contribution of other poly-ADPribose polymerases, namely PARP2, or unspecific binding of the m6A antibody to adenosines, as previously reported (Bringmann & Lührmann, 1987). Together, these observations suggest a direct correlation between PARP1 catalytic activity and the accumulation of m6A at DNA lesions

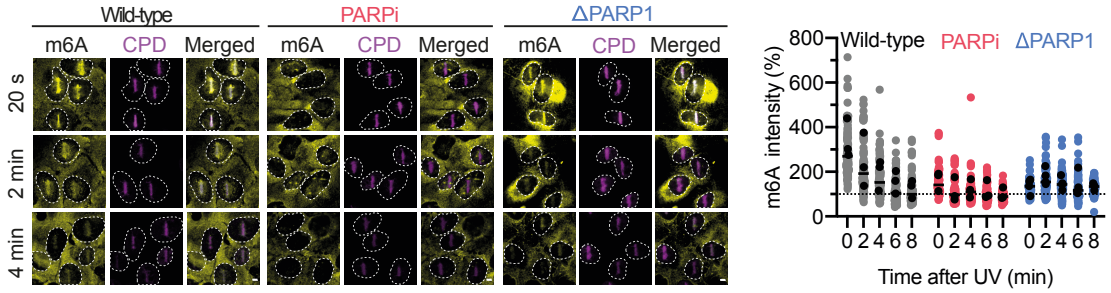

Figure 11. m6A accumulation in PARPi-treated and PARP1 deficient cells. (Left) Representative images showing m6A immunofluorescent signal at 355-nm microirradiation sites in PARPi and ΔPARP cells. (Right) Quantification of m6A immunofluorescent signal at microirradiation sites in PARPi and ΔPARP1 cells. More than 100 cells per condition were analyzed. Each nucleus from three biological replicates is depicted as individual data points. The black points represent the mean of each independent experiment, with the bar indicating the median of all points. The scale bar represents 5 µm.

3.2.2 METTL3 and METTL14 recruitment is sensitive to PAR dynamics

Using our live-cell imaging approach, we monitored the kinetics of GFP-METTL3 and GFP-METTL14 recruitment while modulating PAR levels using PARPi and poly-ADPribose glycohydrolase inhibitor (PARGi). After inhibition of PAR synthesis through PARPi, neither METTL3 (Figure 12 A) nor METTL14 (Figure 12 C) were recruited to DNA lesions. Preventing PAR degradation using PARGi, thereby increasing nuclear PAR levels after damage, increased METTL3 recruitment 30 s and 5 min after irradiation (Figure 12B). Interestingly, PARGi did not significantly affect the recruitment 30 s after microirradiation of METTL14 (Figure 12 D left), whereas increased METTL14 signal was observed 5 min after irradiation (Figure 12 D right).

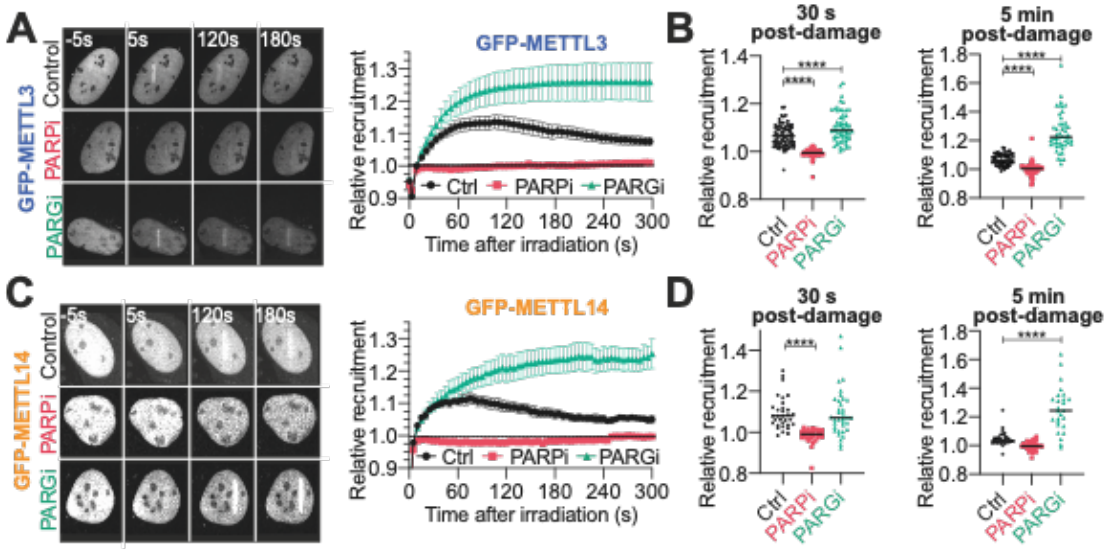

Figure 12. PAR dynamics regulate GFP-METTL3 and GFP-METTL14 recruitment. **(A)** Representative images and quantification of GFP-METTL3 recruitment to microirradiation sites after treatment with PARPi or PARGi. The recruitment kinetics of GFP-METTL3 to DNA damage sites were measured over 5 min in the presence or absence of PARPi or PARGi. More than 30 nuclei per condition were analyzed across three biological replicates. Data are presented as the mean ± SEM. The GFP signal is normalized to the pre-damage intensity at the microirradiation sites. (**B**) Relative GFP-METTL3 recruitment at 30s- and 5-min post-irradiation. Each data point represents a single cell. (**C**) Representative images and quantification of GFP-METTL14 recruitment to microirradiation sites after treatment with PARPi or PARGi. Recruitment kinetics were measured over 5 min in the presence or absence of PARPi or PARGi. More than 30 nuclei per condition were analyzed across three independent replicates. Data are shown as the mean ± SEM, normalized to the pre-damage GFP intensity at microirradiation sites. (**D**) Relative GFP-METTL14 recruitment at 30 s and 5 min post-irradiation. Each data point represents a single cell. Statistical comparisons were made using one-way ANOVA, with Dunnett's post-hoc test to compare each treatment to the control; **** $p<0.0001$.

The effect of PARPi and PARGi on the overall nuclear PAR intensity 10 min after H_2O_2 treatment served as a control for the impact of these inhibitors on PAR levels after damage, confirming the reduction of PAR after PARPi treatment and increased PAR signal after PARGi treatment (Figure 13). These observations correlate PAR levels with the recruitment of both methyltransferases, albeit both proteins recruit with slightly different kinetics.

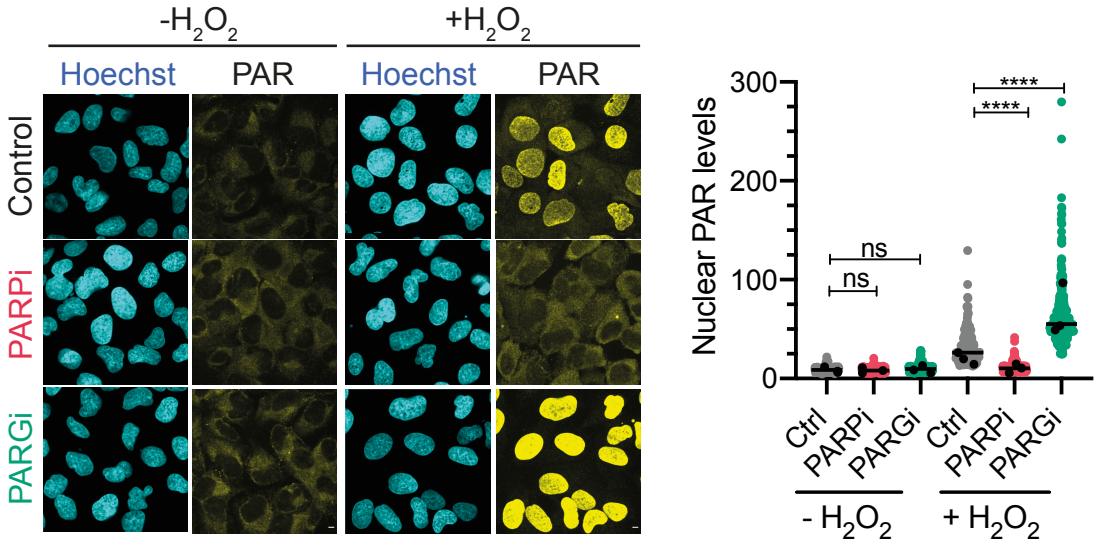

Figure 13. PAR levels in PARPi- and PARGi-treated cells. (Left). Representative images showing PAR immunofluorescent signal 10 min after H_2O_2 treatment, using 10H immunostaining. (Right) Quantification of nuclear PAR signal in cells treated with PARPi and PARGi, 10 min after H_2O_2 exposure. More than 100 cells per condition were analyzed. All nuclei from three biological replicates are shown as individual data points, with the means of each replicated represented as a black point and the bar representing the median across experiments. Statistical comparisons were made using one-way ANOVA, with Turkey's post-hoc test to compare each treatment to the control group. Significance levels: ns $p> 0.05$; **** $p<0.0001$.

Consistent with our previous observations, the recruitment kinetics of GFP-FTO and GFP-WTAP were not significantly affected by PARGi treatment (Figure 14). This

supports our hypothesis that these proteins do not recruit to DNA damage sites in response to PARylation.

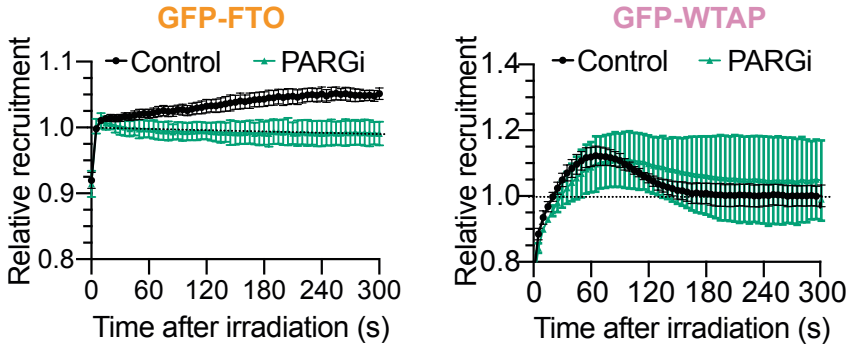

Figure 14. PARGi treatment does not influence the recruitment kinetics of FTO or WTAP after microirradiation. The recruitment dynamics of GFP-FTO (left) and GFP-WTAP (right) to DNA damage sites were measured over 5 min following microirradiation. More than 30 cells per condition were analyzed across three replicates. Data are presented as mean ± SEM, and the GFP signal is normalized to the intensity at the microirradiation pre-damage.

3.2.3 METTL3 and METTL14 recruitment can be rescued in PARP1-deficient cells

We further validated the specificity of PAR-driven recruitment of GFP-METTL3/14 by monitoring their kinetics in ΔPARP1 cells. Without PARP1, neither METTL3 nor METTL14 were recruited to DNA lesions (Figure 15). Reintroduction of PARP1 WT via transient transfection rescued the recruitment of both methyltransferases to microirradiation sites. Transfection of ΔPARP1 cells with PARP1 E988K, a mutant polymerase characterized by its inability to elongate initial mono (ADP-ribose) modifications (Marsischky et al., 1995; Rolli et al., 1997), failed to rescue the recruitment of METTL3 nor METTL14 (Figure 15). These findings confirm that the catalytic activity of PARP1, and thereby PAR levels, drive the recruitment of METTL3/14 after microirradiation.

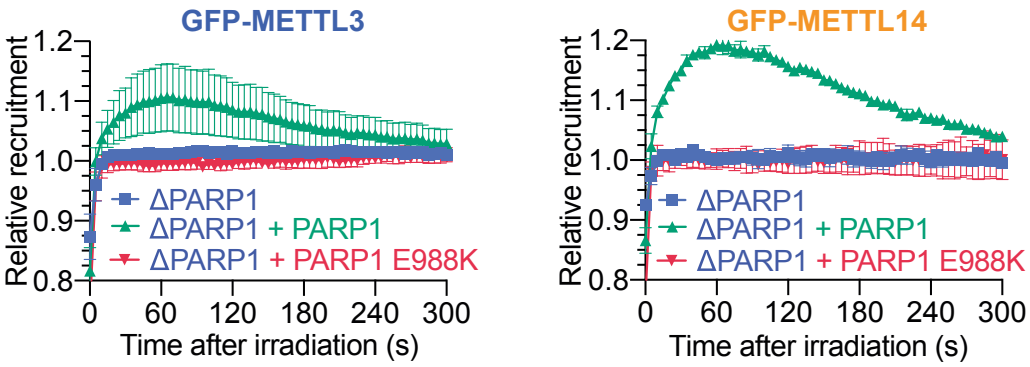

Figure 15. The catalytic activity of PARP1 is required for METTL3 and METTL14 recruitment. The recruitment dynamics of GFP-METTL3 (left) and GFP-METTL14 (right) were measured in ΔPARP1 cells and ΔPARP1 cells transfected with either PARP1

WT or the PARP1 E988K catalytic mutant over a 5 min window following microirradiation. More than 30 cells per condition were analyzed across three replicates. The data are presented as mean ± SEM, and the GFP signal is normalized to the intensity at the microirradiation site before damage.

One of the downstream effects of PARylation is chromatin decompaction driven by the negative electrostatic charge of the PAR chains and enhanced by the recruitment of ATP-dependent chromatin remodelers, some of which directly interact with PAR, such as CHD1L/ALC1 (Gottschalk et al., 2009; Sellou et al., 2016), and some that passively recruit to relaxed chromatin, such as CHD3 and CHD4 (Smith et al., 2018). Therefore, the observed METTL3/14 recruitment may be an effect of the changes in the chromatin state after DNA damage instead of a direct interaction with PAR. To explore this hypothesis, we tested the recruitment of GFP-METTL3 in cells treated with trichostatin A, an inhibitor of histone acetylases and deacetylases (HDAC) that induces reversible decondensation of chromatin (Tóth et al., 2004). Treatment with HDACi did not affect the initial recruitment of GPF-METTL3 to microirradiation sites (Figure 16), implying that the chromatin state does not drive the initial recruitment.

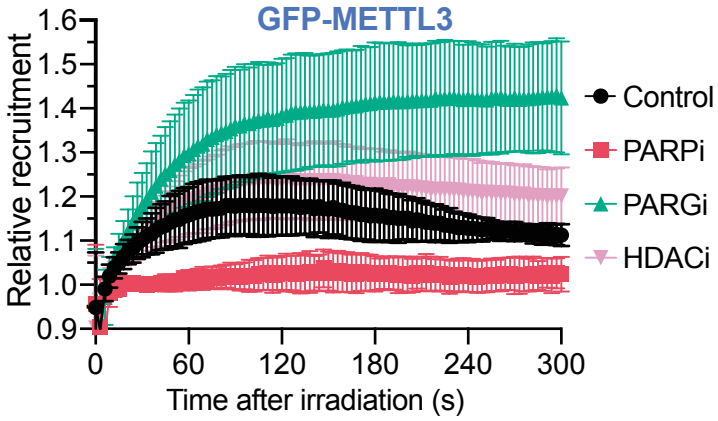

Figure 16. Early GFP-METTL3 recruitment is not affected by HDAC. The recruitment dynamics of GFP-METTL3 to 355-nm microirradiation sites were analyzed following treatment with olaparib (PARPi), PARGi, or the HDAC inhibitor trichostatin A (HDACi). Data are presented as mean ± SD; with 12 cells per condition analyzed across two biological replicates.

An alternative approach to assess whether METTL3 recruitment is driven by PARP1 activity or downstream chromatin rearrangement is to examine the methyltransferase recruitment in cells deficient in the PAR-dependent chromatin remodeler ALC1. In these cells, which preserve active PARP1, we did not observe a difference in the initial recruitment of METTL3 to irradiation sites, represented by the overlapped recruitment of METTL3 in wild-type cells and ALC1 deficient cells at 60s (Figure 17). However, METTL3 accumulation in the lesions was reduced in ALC1 deficient cells compared to the parental control after 240 s. In contrast, no recruitment of METTL3 was observed in PARP1-

deficient cells. Although no clear conclusions can be drawn due to the reduced sample size of these experiments, the effect of HDAC inhibitor and ALC1 deficiency in the recruitment of METTL3 led us to hypothesize that the initial recruitment of the methyltransferase is driven by the burst of PARylation after DNA damage. At the same time, the chromatin state contributes to METTL3 levels shortly after.

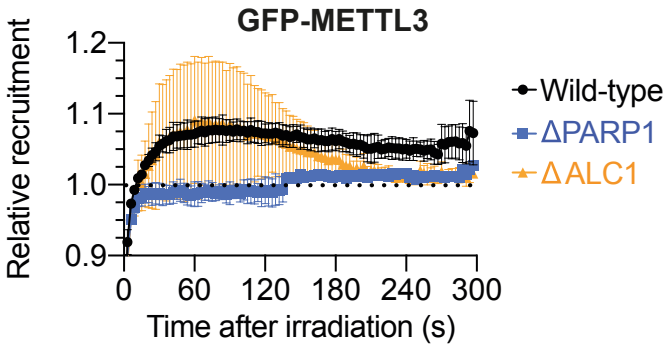

Figure 17. Early GFP-METTL3 recruitment is not affected by ALC1 deficiency. The recruitment dynamics of GFP-METTL3 to 355-nm microirradiation sites in PARP1- and ALC1-deficient cells. Data are presented as mean ± SD; with 12 cells per condition analyzed across two biological replicates.

3.2.4 METTL3 recruitment does not depend on TonEBP

Previous reports have suggested that the tonicity-responsive enhancer binding protein (TonEBP) recruits to microirradiation driven by PAR dynamics (Ye et al., 2021) and is required for METTL3-mediated methylation of DNA-RNA hybrids (Ye et al., 2021). Therefore, we tested whether TonEBP mediates the recruitment of METTL3 to microirradiation sites using our live-cell imaging approach. We used siRNA-mediated depletion of TonEBP and compared the recruitment of METTL3 against cells transfected with a control siRNA. In our hands, METTL3 still recruits to microirradiation sites independent of TonEBP presence (Figure 18 A). The efficiency of siRNAs was tested using Western blotting 48 h after transfection (Figure 18 B), the time at which cells were used in microirradiation experiments.

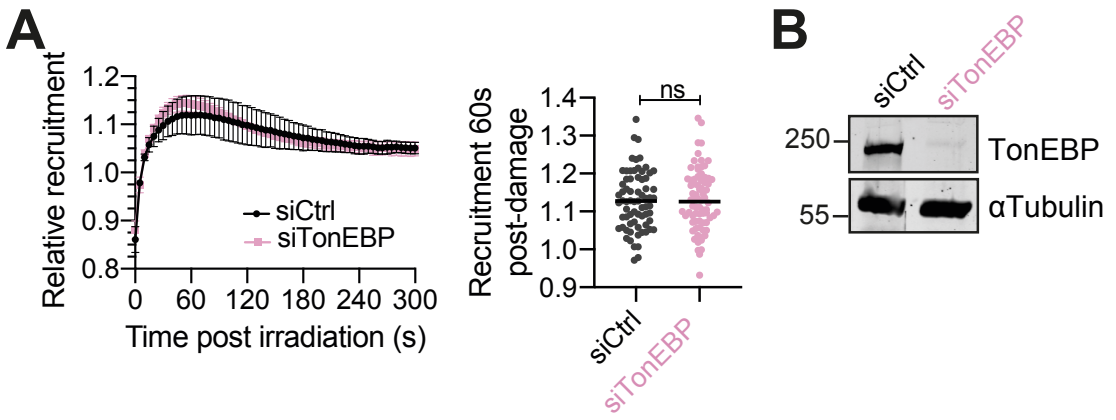

Figure 18. GFP-METTL3 recruitment to microirradiation sites is independent of TonEBP. (A). The recruitment dynamics of GFP-METTL3 to 355-nm microirradiation sites were analyzed in TonEBP knockdown cells. More than 60 cells per condition were analyzed across three biological replicates. Data are presented as mean ± SEM. (**B**) Western blot analysis confirming TonEBP depletion 48 h post-transfection. The images represent a representative experiment, with consistent depletion levels observed across replicates.

3.3 RNA contributes to the recruitment of METTL3/14 to DNA damage sites

3.3.1 RNA degradation reduces METTL3 recruitment to microirradiation sites

The METTL3/14 complex has been studied extensively concerning its mRNA methylation activity. Therefore, we explored whether RNA could contribute to recruiting these proteins to microirradiation sites. We performed live-cell imaging after microirradiation on cells permeabilized with 0.6% Tween-20 and treated with RNAse A, as described by Michelini and colleagues (Michelini et al., 2017). Changes in cell morphology under bright-field microscopy confirmed the cells' permeability. We used permeabilized cells supplemented with an equimolar concentration of acetylated BSA as a control. The permeability of cells resulted in a slight but not significant decrease in GFP-METTL3 recruitment to DNA lesions (Figure 19). Treating cells with RNAse A after permeabilization significantly reduced the recruitment of GFP-METTL3 after microirradiation (Figure 19). These observations indicate that the presence of RNA affects METTL3 recruitment kinetics.

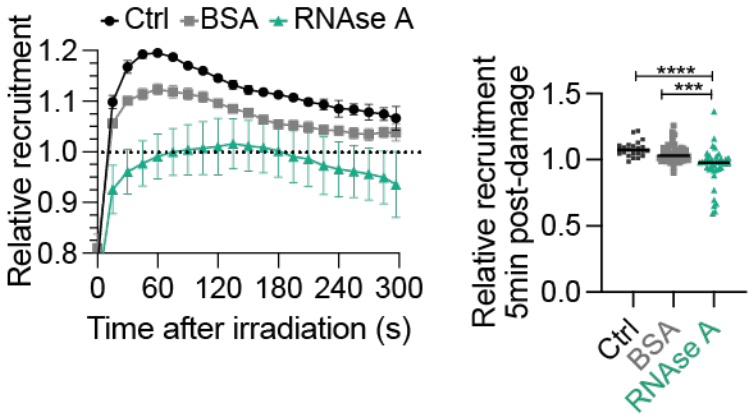

Figure 19. RNA degradation reduces GFP-METTL3 recruitment to DNA damage sites. (Left). Recruitment kinetics of GFP-METTL3 in permeabilized cells following microirradiation. Cells were treated with either BSA or RNAse A and observed for 5 min post-irradiation. More than 30 cells per condition were analyzed across three replicates. Data are presented as mean ± SEM, and the GFP signal is normalized to the intensity at microirradiation sites before irradiation. (Right). The relative enrichment of GFP-METTL3 5 minutes after irradiation. Each data point represents a single cell. Statistical comparisons were performed using one-way ANOVA with Turkey's post-hoc test to compare each treatment against control. Significance levels: ns $p>0.05$; *** $p< 0.0005$; **** $p<0.0001$.

3.3.2 Inhibition of RNA Pol II reduces METTL3 and METTL14 recruitment to microirradiation sites

Based on our findings, we aimed to understand the impact of RNA on the recruitment of GFP-METTL3 and GFP-METTL14. We used the transcription inhibitors α-Amanitin (aAM) and actinomycin D (ActD) to achieve this. These inhibitors act through distinct mechanisms: aAM binds to the largest subunit of RNA Pol II, RBP1, causing its degradation and preventing transcription initiation (Nguyen, 1996). Meanwhile, ActD disrupts the elongation of growing RNA chains by intercalating into DNA (Sobell, 1985). Using this approach, we can interrogate the impact of stalling RNA transcription at the initiation and elongation stages on the recruitment of the methyltransferases.

Treatment with aAM reduced GFP-METTL3 recruitment to DNA lesions (Figure 20 A), 60 s and 5 min after damage (Figure 20 B). Interestingly, treatment with ActD abrogated the recruitment of GFP-METTL3 to DNA lesions. Similarly, treatment with aAM decreased the recruitment of GFP-METTL14 to DNA damage lesions (Figure 20 C). However, this difference was not present at the initial recruitment (60 s) but 5 min after damage (Figure 20 D). These observations confirmed that nascent RNA assists the recruitment of METTL3 and METTL14 to microirradiation sites.

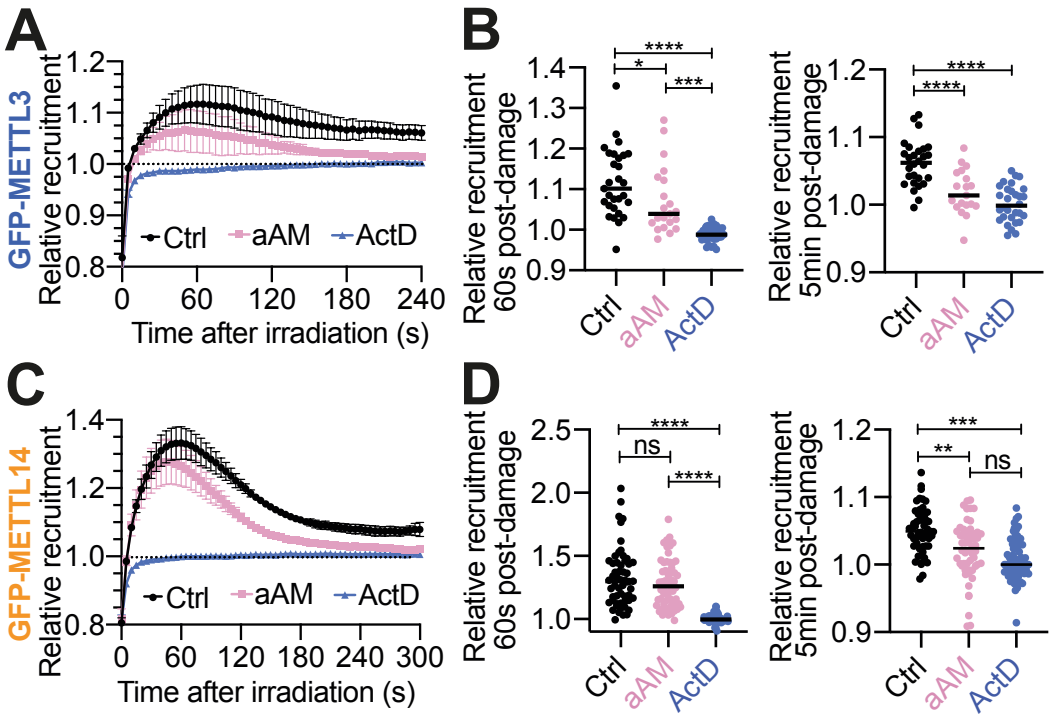

Figure 20. RNA Pol II inhibition reduces METTL3 and METTL14 recruitment to DNA damage sites. The recruitment dynamics of (**A**) GFP-METTL3 and (**C**) GFP-METTL14 to DNA lesions were analyzed in the presence of α-Amanitin (aAM; 2 μg/mL) or actinomycin D (ActD; 0.5 μg/mL) over 5 minutes. More than 20 cells per condition were analyzed across three replicates. Data are presented as mean ± SEM, and the GFP signal is normalized to the pre-damage intensity at microirradiation sites. (**B**,**D**) The relative recruitment of GFP-METTL3 and GFP-METTL14 at 60 s or 5 min post-damage. Each data point represents a single cell. Statistical comparisons were performed using one-way ANOVA with Turkey's post-hoc test to compare treatments against each other. Significance levels: ns $p > 0.05$; * $p < 0.05$; **$p<0.005$; *** $p< 0.0005$; **** $p<0.0001$.

3.3.3 Actinomycin D reduces the mobility of METTL3 and METTL14

From our microirradiation data, we observed a slight delay in the recovery of fluorescent signals at the microirradiation site. GFP-METTL3 fluorescent signal recovered to pre-irradiation levels after approximately 60 s, while GFP-METTL14 recovered after 30 s (Figures 20 A and C). As ActD stalls engaged RNA Pol II and mRNA m6A methylation occurs co-transcriptionally (H. Huang et al., 2019; Knuckles et al., 2017; Slobodin et al., 2017; W. Xu et al., 2022), we hypothesized that ActD could impact the mobility of the tagged proteins in the nucleus. This effect might occur, for example, by increasing the interaction of these proteins with chromatin or with other proteins.

To test this hypothesis, we used fluorescence recovery after photobleaching to monitor the movement of the tagged proteins to a photobleached region, thus obtaining information about their mobility. Treatment with aAM, which reduced GFP-METTL3 recruitment to microirradiation sites (Figure 21 A-B), did not affect the recovery kinetics of METTL3 after photobleaching (Figure 21 A). However, ActD treatment delayed recovery

of the GFP-METTL3 signal at the bleached region (Figure 21 A). This reduction in mobility is reflected as an increase in the immobile fraction upon ActD treatment, calculated as 1 minus the plateau of the normalized intensity, serving as a measure of the bleached fluorophores and the protein's mobility (Figure 21 A right). Consistent with our previous observations, ActD treatment also reduced the mobility of GFP-METTL14 (Figure 21 B).

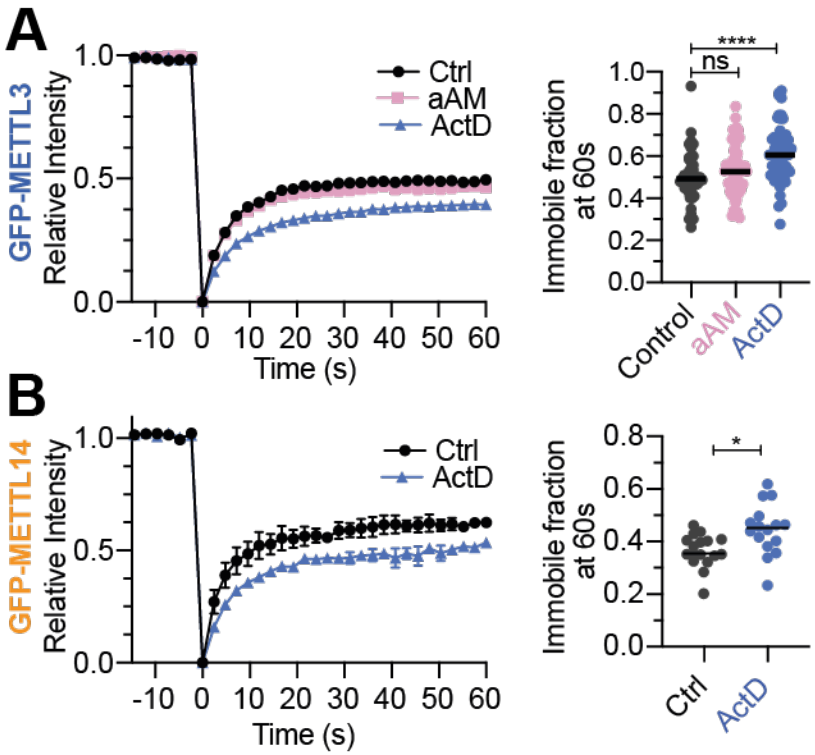

Figure 21. Actinomycin D reduces METTL3 and METTL14 mobility. Fluorescent recovery after photobleaching (FRAP) of (**A**) GFP-METL3 and (**B**) GFP-METTL14 in the presence or absence of α-Amanitin (aAM; 2µg/mL for 2 h) or actinomycin D (ActD; 0.5 µg/mL for 2 h), monitored over 1 min. More than 30 cells per condition were analyzed across three independent experiments. Data are presented as the mean ± SEM, and the GFP signal is normalized to the intensity before photobleaching. The left panels represent the immobilized fraction of (**A**) GFP-METTL3 and (**B**) GFP-METTL14. Each data point represents a single cell. Statistical comparisons were made using one-way ANOVA, with Dunnet's test to compare each treatment against the control group. Statistical levels: ns $p > 0.05$; * $p < 0.05$; ***$p<0.001$; *** $p< 0.0001$; **** $p<0.0001$.

3.3.4 METTL3 interacts with RNA Pol II

Previous studies have confirmed that ActD intercalation into DNA reduces transcription and diminishes RNA Pol II's mobility (Darzacq et al., 2007). Furthermore, m6A methylation of RNA by the METTL3/14 complex occurs co-transcriptionally (H. Huang et al., 2019; Knuckles et al., 2017; Slobodin et al., 2017; W. Xu et al., 2022). We hypothesized that METTL3/14 mobility reduction induced by ActD was driven by an increased interaction between the METTL3/14 complex and RNA Pol II. To investigate this, we performed

co-immunoprecipitation of GFP-METTL3 to examine its interaction with RBP1, the largest subunit of RNA Pol II. In alignment with Slobodin and colleagues (Slobodin et al., 2017), we observed a slight increase in the interaction between GFP-METTL3 and RBP1 in the presence of ActD. (Figure 22 A). The interaction with the elongating form of RNA Pol II phosphorylated RBP1 (RBP1 pS2) remained unaffected by ActD treatment. Additionally, treatment with RNAse A did not affect the coprecipitation of GFP-METTL3 and RBP1 (Figure 22 B), indicating that this interaction is not RNA-mediated. Further studies are required to characterize this potential protein-protein interaction between METTL3 and RBP1.

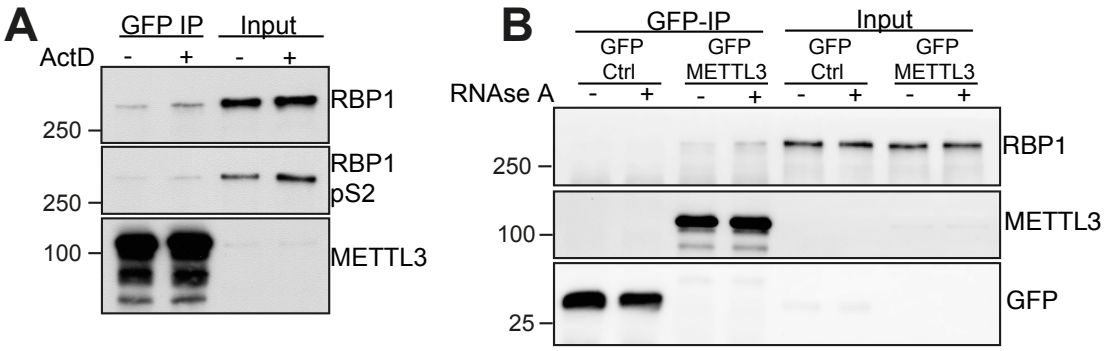

Figure 22. GFP-METTL3 interacts with the RBP1 subunit of RNA Pol II. (**A**). Co-immunoprecipitation of GFP-METTL3 in the presence or absence of actinomycin D (ActD; 0.5 µg/mL for 2 h). (**B**). Co-immunoprecipitation of GFP-METTL3 in the presence or absence of RNAse A (1µg/µL for 30 min) during lysis. Two biological replicates of each immunoprecipitation were performed, yielding similar results. Experiments performed by Jin Cai.

3.4 METTL3/14 binds to PAR chains *in vitro*

3.4.1 Recombinant METTL3/14 binds to PAR *in vitro*

As a polymer of ADP-ribose, PAR shares the same molecular components as RNA: the nucleobase adenine, ribose sugars, and phosphates. Our prior findings show that the recruitment of METTL3 and METTL14 is influenced by both PAR and RNA. While extensive research has characterized the affinity of the METTL3/14 complex for various RNA structures (Meiser et al., 2020; X. Wang et al., 2016) and DNA (Qi et al., 2022; Woodcock et al., 2019), it is not known if it can directly bind to PAR.

To explore this, we immobilized purified METTL3/14 onto a nitrocellulose membrane and then incubated with purified PAR chains. We used MacroH2A1.1, a known PAR-binder, as a positive control, and BSA as a negative control. Following extensive washing, we

probed the membrane for PAR signal. As expected, no PAR signal was observed where BSA was immobilized but detected at the locations where MacroH2A1.1 was immobilized, confirming the specificity of the test. Similarly, the PAR signal was detected at the sites where METTL3/14 was immobilized (Figure 23 A). Therefore, we confirmed that METTL3/14 can interact with PAR chains under these test conditions.

An alternative method to characterize protein-nucleic acid binding involves monitoring the change in the mobility of a substrate in the presence of its binding protein during electrophoretic separation in an electrophoretic mobility shift assay. Upon protein binding, the mobility of the nucleic acid is significantly reduced, manifesting as a change in the migration pattern of the substrate. We used this approach with an ADP-ribose 20-mer labelled with AlexaFluor™ 647, which the Leung's lab kindly provided, and an RNA probe containing 8 tandem repeats (40 nucleotides) of the DRACH motif labeled with Cy3. The concentration of the probes was calculated based on the molecular mass of one oligo. Increasing concentrations of METTL3/14 proteins were incubated with 10 µM of labeled RNA or PAR. In the absence of METTL3/14, two species of RNA can be seen running toward the end of the gel, corresponding to free single RNA and RNA dimers. Low concentrations of METTL3/14 (0.25 µM) induced a shift of the RNA probe, indicating the formation of an RNA-METTL3/14 species. This shift was further enhanced with increasing concentrations of METTL3/14 (Figure 23 B). Low concentrations of METTL3/14 lead to a change in the fluorescently-tagged PAR, indicating a direct binding of the complex to this polymer.

Interestingly, recombinant METTL3 alone exhibited very low affinity toward RNA, as evidenced by the low abundance of bound RNA-METTL3 compared with free RNA (Figure 23 C). This indicates that, despite having two zinc finger domains known to mediate RNA-target recognition (H. Huang et al., 2019; Śledź & Jinek, 2016), binding to RNA substrate requires the formation of the METTL3/14 heterodimer.

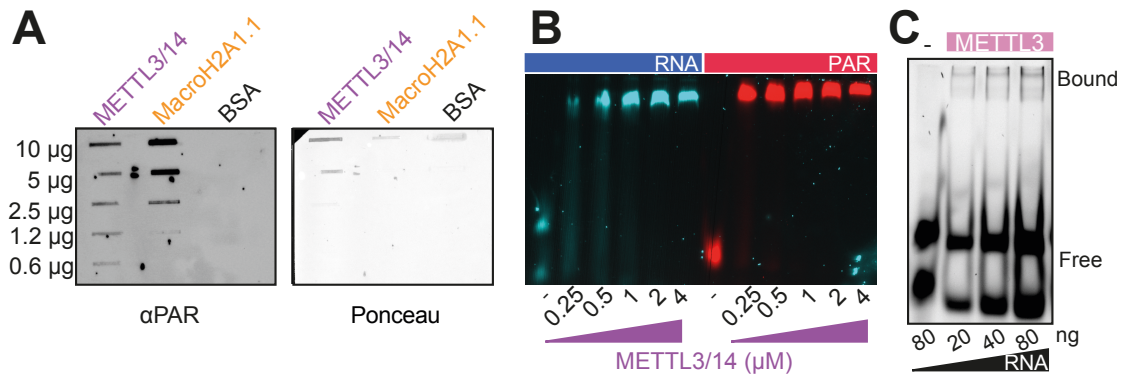

Figure 23. METTL3/14 interacts with PAR *in vitro*. (A). Purified METTL3/14 was blotted onto a membrane and incubated with purified PAR (0.5 μg/mL for 2 h). The membranes were washed and probed for PAR. MacroH2A1.1 and BSA served as positive and negative controls, respectively. Ponceau staining was used as a loading control. Two independent experiments of each membrane were performed, yielding similar results. (**B**) Electrophoretic mobility shift assay of METTL3/14 with 10 μM of an RNA probe containing 8 tandem repeats of the DRACH motif labeled with Cy3, or 20-mer of ADP-ribose labeled with Alexa Fluor™ 647. (**C**) Electrophoretic mobility shift assay of METTL3 (1 μg) with the Cy3-RNA probe.

Microscale thermophoresis (MST) is an orthogonal method for assessing protein-ligand interactions. By measuring changes in the mobility of molecules through a microscopic temperature gradient, this method can be used to approximate binding affinities in immobilization-free media using low volumes of reagents. We used the previously described Cy3-RNA or Alexa Fluor™ 647-PAR probes, together with recombinant increasing concentrations of METTL3/14.

To optimize probe concentration, we assessed the fluorescent signal using 20% excitation power and determined that 100 nM of labeled probes provided a signal between 1200 and 2000 A.U., as recommended by the manufacturer. MST traces were recorded using 80% MST power on a Monolith NT.115 (NanoTemper). Subsequently, we measured the thermophoresis signal of increasing METTL3/14 concentrations with 100 nM of labeled probe. An example of a raw thermophoresis signal is shown in Figure 24 A.

Data analysis was conducted using the NT Analysis software to calculate the bound and unbound ligand fractions. These values were used to generate a dose-response curve, and binding affinities (K_D) were determined by fitting a Hill slope model using GraphPad Prism8. The accuracy of the fitting model is reported as an R^2 value for each condition (Figure 24 B). As positive controls, we assessed the binding affinity of METTL3/14 to RNA, obtaining a calculated K_D of 0.7 μM (R^2= 0.96), and the binding of MacroH2A1/H2B to PAR resulting in a K_D of 0.5 μM (R^2= 0.93). The calculated affinity of METTL3/14 to PAR is 1.1 μM (R^2= 0.88). Our data indicate that the METTL3/14 complex can directly bind PAR *in vitro*, demonstrating a similar affinity compared to its canonical ligand, RNA, and akin to other PAR-binders such as the macrodomain of MacroH2A1.1.

In line with our prior electrophoretic mobility shift assay observations, no clear binding between RNA and recombinant METTL3 was detected under the tested conditions (Figure 24 C).

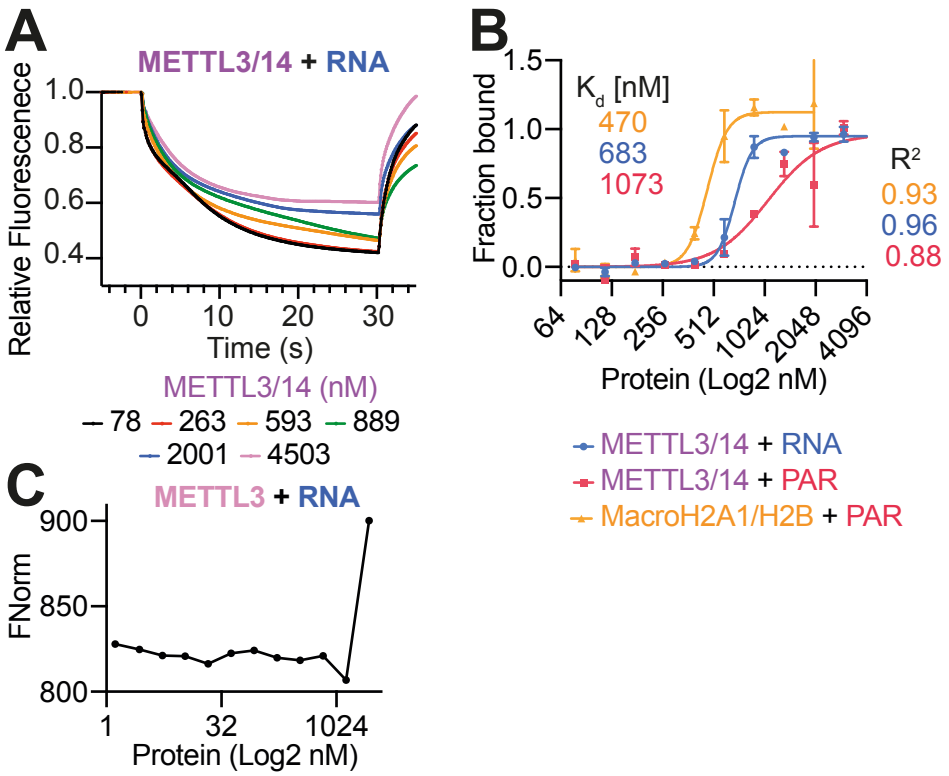

Figure 24. Microscale thermophoresis confirmed the binding of METTL3/14 to RNA and PAR. (A). Representative raw traces of fluorescent thermophoresis signal over time of Cy3-RNA with increasing concentrations of unlabeled recombinant METTL3/14. Time zero represents the point at which the MST laser is turned on. (**B**). Thermophoresis assays of METTL3/14 with Cy3-RNA or AlexaFluor™ 647-PAR, and MacroH2A1/H2B with AlexaFluor™ 647-PAR. Data are presented as the mean of 2-4 replicates ± SEM. The dissociation constant (K_D) was estimated by fitting a Hill slope model, and R^2 values indicate the goodness of the fit. (**C**). Representative thermophoretic experiment of Cy3-RNA with recombinant unlabeled METTL3. Data are presented as normalized fluorescence (FNorm) against METTL3 concentration. No clear binding was observed under the tested conditions.

3.4.2 Binding to PAR confers thermal stability to the METTL3/14 complex

The binding of ligands induces structural rearrangements to the bound protein, exposing or protecting amino acids that were previously unexposed. These changes can affect the thermal stability of proteins, manifested as a ligand-dependent shift in the melting temperature (T_m), which is the temperature at which 50% of the protein population unfolds. Amino acids such as tryptophan and tyrosine, with strong intrinsic fluorescence at 330-350 nm, enable the assessment of ligand binding by observing the changes in the fluorescence properties of the target protein. We used nano-differential scanning fluorimetry (nanoDSF) to evaluate the thermal stability, indicated by changes in the fluorescent properties, of recombinant METTL3/14 in the presence of a 20 nucleotide RNA and purified PAR. A dilution series of these two probes was generated, and a constant concentration

of protein was added. The values were then compared against METTL3/14 without ligand (Apo).

In the presence of RNA, the METTL3/14 complex showed a modest and concentration-independent increase of the ΔT_m of circa 1.0 °C (Figure 25 A left). In contrast, when METTL3/14 was incubated with PAR, a concentration-dependent increase in T_m of up to more than 2.0 °C was observed (Figure 25 A center), suggesting PAR-driven protein stabilization indicative of PAR binding. We used purified macroH2A1.1-H2B histone dimers as a control for PAR binding, obtaining a dose-dependent increase in T_m (Figure 25 A right). The normalized first derivative fluorescent traces of one representative experiment are illustrated in Figure 25 B, where the increase in T_m is observed as a shift of the curve toward higher temperature.

A

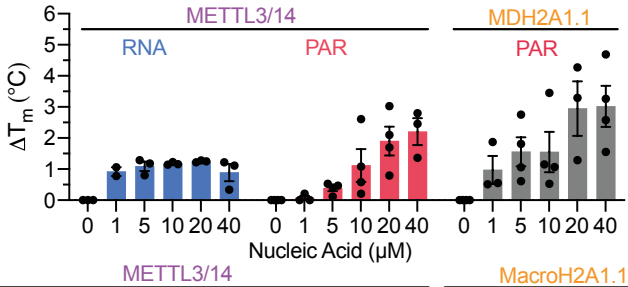

METTL3/14				MacroH2A1.1	
RNA (μM)	**Mean T_m (°C) ±SEM**	**PAR (μM)**	**Mean T_m (°C) ±SEM**	**PAR (μM)**	**Mean T_m (°C) ±SEM**
Apo	**49.6** ± 0.7	**Apo**	**49.6** ± 0.7	**Apo**	**49.6** ± 0.7
1	**51.2** ± 1.7	**1**	**49.8** ± 0.8	**1**	**49.8** ± 0.8
5	**50.9** ± 1.1	**5**	**50.0** ± 0.6	**5**	**50.0** ± 0.6
10	**51.0** ± 1.0	**10**	**50.7** ± 0.6	**10**	**50.7** ± 0.6
20	**51.1** ± 1.0	**20**	**51.5** ± 0.4	**20**	**51.5** ± 0.4
40	**50.7** ± 0.7	**40**	**52.0** ± 1.3	**40**	**52.0** ± 1.3

B

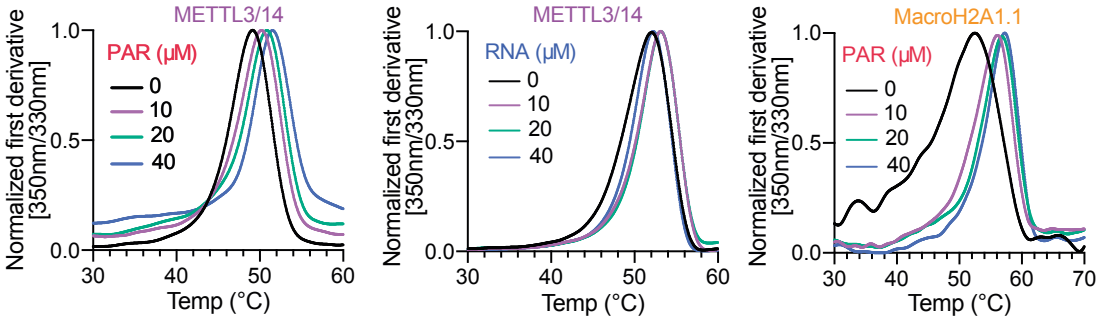

Figure 25. PAR induces thermal stabilization of METTL3/14 *in vitro*. (A) Change in melting temperature (ΔT_m) after incubating METTL3/14 with increasing concentrations of PAR or RNA and Macro H2A1.1 with PAR. The mean ΔT_m from 3-4 independent experiments is shown ± SEM (top), and the mean T_m at different ligand concentrations (bottom). ΔT_m is calculated as the difference between the T_m at a given concentration and the Apo form. **(B)** Normalized fluorescent emission of METTL3/14 in the presence of PAR and RNA and MDH2A1.1 in the presence of PAR (insert). The normalized first derivative of the ratio of the fluorescent signal emitted at 350 nm and 330 nm, with inflection

points representing protein melting. Traces correspond to the mean values from one representative experiment with two technical replicates.

Consistent with our earlier findings, METTL3 alone demonstrates inefficient interaction with RNA or PAR, as stabilization of the recombinant protein only occurs at high nucleic acid concentration (45 µM, Figure 26 A-B). It is noteworthy that the thermal profile of METTL3 exhibits two inflection points, a feature not observed in the METTL3/14 complex. We hypothesized this could be driven by the GST-tag in the recombinant METTL3. To investigate this, we conducted a thermal shift assay with recombinant GST-6His, generously provided by Maren Heimhalt. Indeed, we observed that GST unfolds above 60°C and remains unaffected by the presence of PAR (Figure 26 C). This observation may correlate with the second inflection point observed in the thermal shift profiles of GST-METTL3 (Figure 26 A-B).

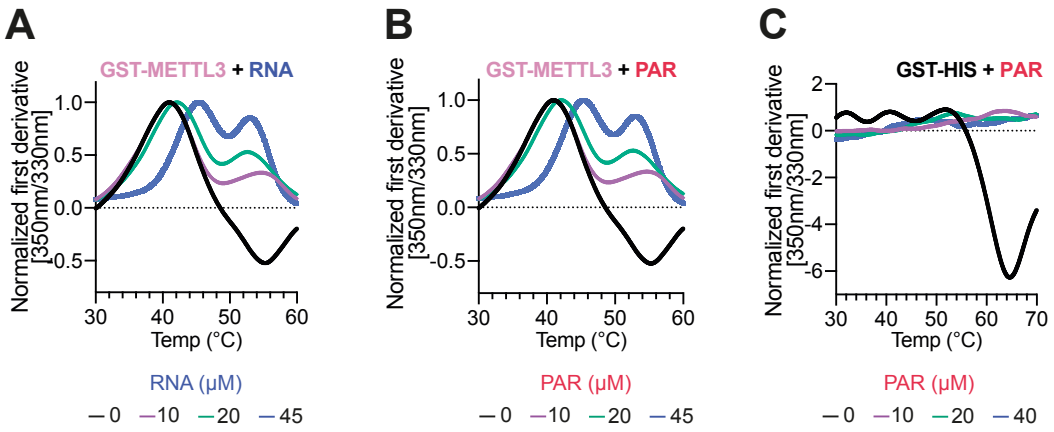

Figure 26. Recombinant METTL3 does not interact efficiently with nucleic acids *in vitro*. Thermal shift assay of (**A**) GST-METTL3 with RNA, (**B**) GST-METTL3 with PAR, and (**C**) GST-His with PAR. Thermal stabilization of METTL3 was observed at 45 µM of nucleic acid. Data were normalized to the maximum values of the first derivative of the 350 nm / 330 nm ratio and are presented as the mean of three independent experiments (**A**-**B**) and two independent experiments (**C**).

3.4.3 METTL3/14 simultaneously binds PAR and RNA *in vitro*.

Our electrophoretic mobility assays (EMSA) revealed the *in vitro* binding of METTL3/14 to both RNA and PAR, even at low enzyme concentrations. To further characterize the nature of the interaction between METTL3/14 and both nucleic acids, we conducted competitive EMSAs. We incubated 2 µM of METTL3/14 with 10 nM of the first nucleic acid probe for 15 min. Subsequently, we incubated this mix with varying molar ratios (1:1 to 1:50) of the second competitor probe.

First, we assessed the ability of PAR to outcompete RNA-METTL3/14 binding. In line with our previous results, the addition of METTL3/14 complex to Cy3-RNA resulted in a reduction in the mobility of the RNA probe, manifested as the formation of a species running at a higher position on the gel, labeled as “a” in Figure 27 A. When PAR was added in a 1:1 ratio, a second protein-nucleic acid species emerged, appearing as a band running higher than the METTL3/14-RNA species, marked as “b” in Figure 27 A. With excess PAR (molar ratio 1:10), a super-shift of the METTL3/14-PAR species occurred, along with the partial displacement of RNA from the METTL3/14 complex, labeled as species “c” (Figure 27 A). This phenomenon was exacerbated with increasing concentrations of PAR (ratios 1:20 to 1:100). Notably, RNA signal persisted in the METTL3/14 species even at high PAR concentrations, suggesting that while PAR can displace RNA, it does not entirely outcompete RNA binding.

Conversely, when RNA was employed to outcompete PAR-METTL3 complexes (“a” in Figure 27 B), a METTL3/14-RNA species appeared (“b” in Figure 27 B). Unlike PAR, excess of RNA did not displace PAR, as no free PAR was observed under these conditions. These data collectively suggest that METTL3/14 can recognize both nucleic acids concomitantly. Moreover, the difference in the mobility observed when METTL3/14 is exposed to RNA first versus PAR argues for differences in how the complex interacts with these nucleic acids. While RNA has been described to bind at the interphase of METTL3 with METTL14 (X. Wang et al., 2016), PAR may interact with the exposed surface of METTL3/14, potentially through electrostatic interactions, serving as a platform for METTL3/14. Further studies are needed to characterize how METTL3/14 engages with PAR structurally and biochemically.

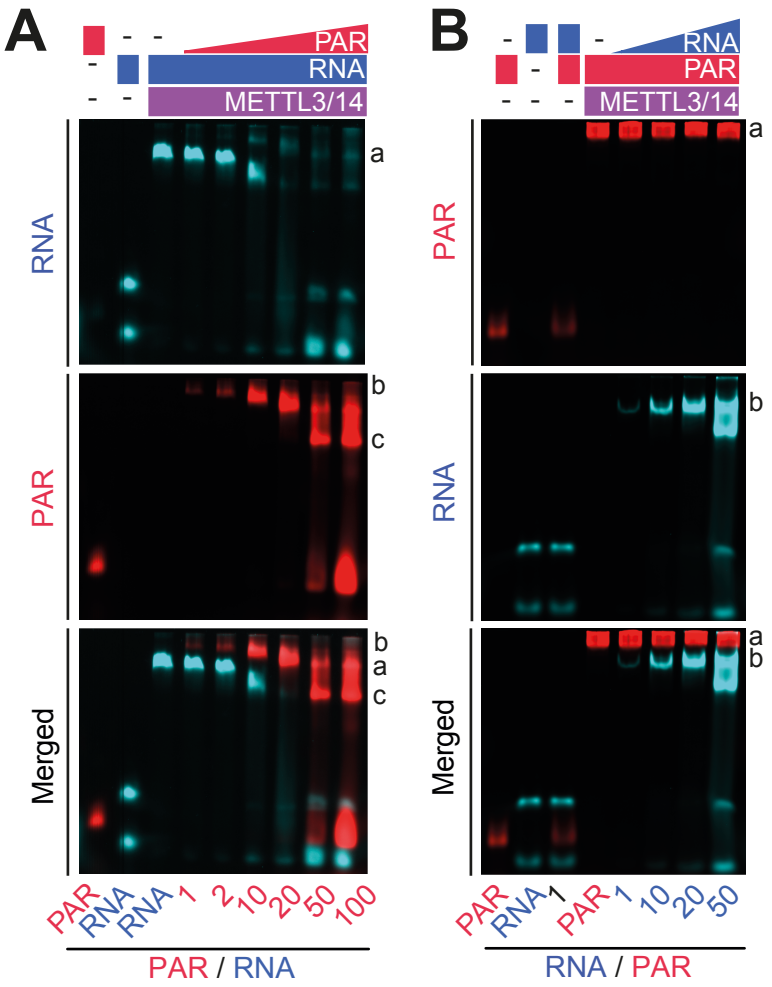

Figure 27. RNA and PAR cannot outcompete each other's binding to METTL3/14 *in vitro*. Competitive EMSA analysis of METTL3/14 binding to RNA (cyan) or PAR (red). In (**A**), 2 μM METTL3/14 is incubated with 10 nM of RNA first, followed by the addition of increasing concentrations of PAR. In (**B**), 2 μM METTL3/14 is incubated with 10 nM PAR first, followed by the addition of increasing concentrations of RNA. Representative images of two replicates with similar results are shown. Experiment performed by Jin Cai.

3.4.4 PAR binding does not affect the catalytic activity of METTL3/14

By our previous findings, METTL3/14 can interact simultaneously with both RNA and PAR. Subsequently, we explored whether PAR's presence could influence the catalytic activity of the methyltransferase complex *in vitro*. To assess this, we used the MTase-Flo™ Methyltransferase Assay by Promega, a bioluminescence-based assay relying on the production of S-adenosylhomocysteine (SAH), a byproduct of the methylation reaction. SAH is then converted into ADP and subsequently into ATP, which can be through a luciferase reaction.

To establish the range of the assay, we performed a standard curve of SAH following the guidelines of the manufacturer. The luminescent signal exhibited linearity at the highest concentration tested (1 μM), and our equipment demonstrated sensitivity to the low concentrations recommended by the manufacturer (Figure 28 A). We then optimized enzyme and substrate concentrations to find appropriate conditions for the assay. For this, we carried a methylation reaction for 1 h with increasing concentrations of METTL3/14 with 10 μM RNA (Figure 28 B) and titration of RNA in the presence of 62.5 nM METTL3/14 (Figure 28 C). Based on these tests, we identified 62.5 nM METTL3/14 and 5 μM RNA as optimal concentrations for our assays.

Next, we assessed the activity of METTL3/14 in the presence of RNA and PAR. We incubated METTL3/14 with RNA while introducing different concentrations of PAR (molar ratios from 1:05 to 1:10). As controls, we used RNA only (RNA +), a negative RNA probe that consisted of four tandem repeats of the DRACH motif with uracil instead of adenosine (RNA -) and the different PAR concentrations used in the RNA+PAR reactions. The RNA negative control showed a low background luminescent signal, similar to the signal observed in reactions containing PAR (Figure 28 D). At low PAR concentrations, a modest increase in luminescent signal was detected; however, higher PAR concentrations failed to significantly affect the activity of the methyltransferase complex (Figure 28 D). Consequently, we conclude that there is no clear evidence of PAR affecting the catalytic activity of the METTL3/14 complex.

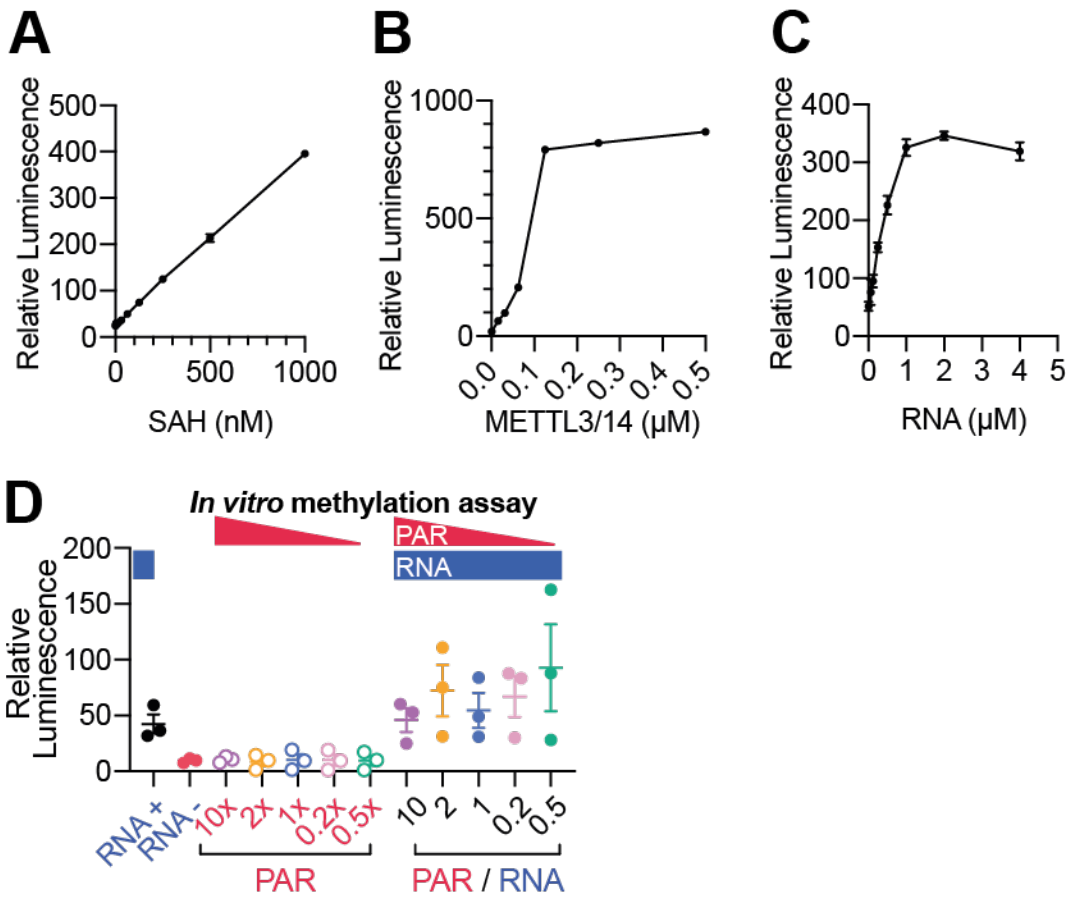

Figure 28. PAR does not affect the catalytic activity of METTL3/14 *in vitro*. (A). SAH titration was performed to assess the specificity of the assay and equipment, with sensitivity falling within the parameters recommended by the manufacturer. (**B**, **C**) Titration of the METTL3/14 complex (**B**) and RNA probe (**C**) was conducted to determine the optimal concentrations for the assay. Data are presented as the mean of two technical replicates ± SD. (**D**) Methylation reaction results of positive control (RNA +), negative control (RNA -), PAR + RNA (PAR/RNA) at different molar ratios, and PAR at the concentrations used for PAR/RNA reactions. The addition of PAR did not significantly affect methylation. Data are shown as the mean of three independent replicates ± SEM. All reactions were measured after 1 h.

3.4.5 METTL14 interacts with PAR *in cellulo*

Our previous findings indicate that METTL3/14 can interact with PAR *in vitro*. Consequently, we investigated whether this interaction can occur *in cellulo*. We used a modified Lac operator (LacO) colocalization imaging assay (Janicki et al., 2004). We linked the macrodomain of MacroH2A1.1 to the Lac repressor (LacR), effectively tethering this PAR-binding domain to the LacO array integrated into U2OS 263 cells (Figure 29 A).

Cells were sensitized overnight with BrdU and treated with 1 µM PARGi one hour before inducing PARylation through microirradiation with a 355-nm laser. As a proof of concept, we monitored the accumulation of GFP-PARP1. Consistent with previous reports (Blessing et al., 2022), we observed an accumulation of PARP1 at the MacroH2A1.1 foci upon

microirradiation (Figure 29 B, left). This accumulation was quantified as a ratio of the fluorescent signal at the macrodomain foci over the nuclear signal. A ratio above 1, as observed for GFP-PARP1, indicates accumulation above the nuclear signal (Figure 29 B, right).

Under these conditions, we did not observe a convincing accumulation of GFP-METTL3, but we did observe a low yet consistent accumulation of GFP-METTL14 at the tethered macrodomain (means 120 s after irradiation = 1.09 ± 0.02 SEM, and 1.14 ± 0.002 SEM, respectively; Figure 29 B). These findings imply that METTL14 interacts with PAR or PARylated proteins within the cellular context.

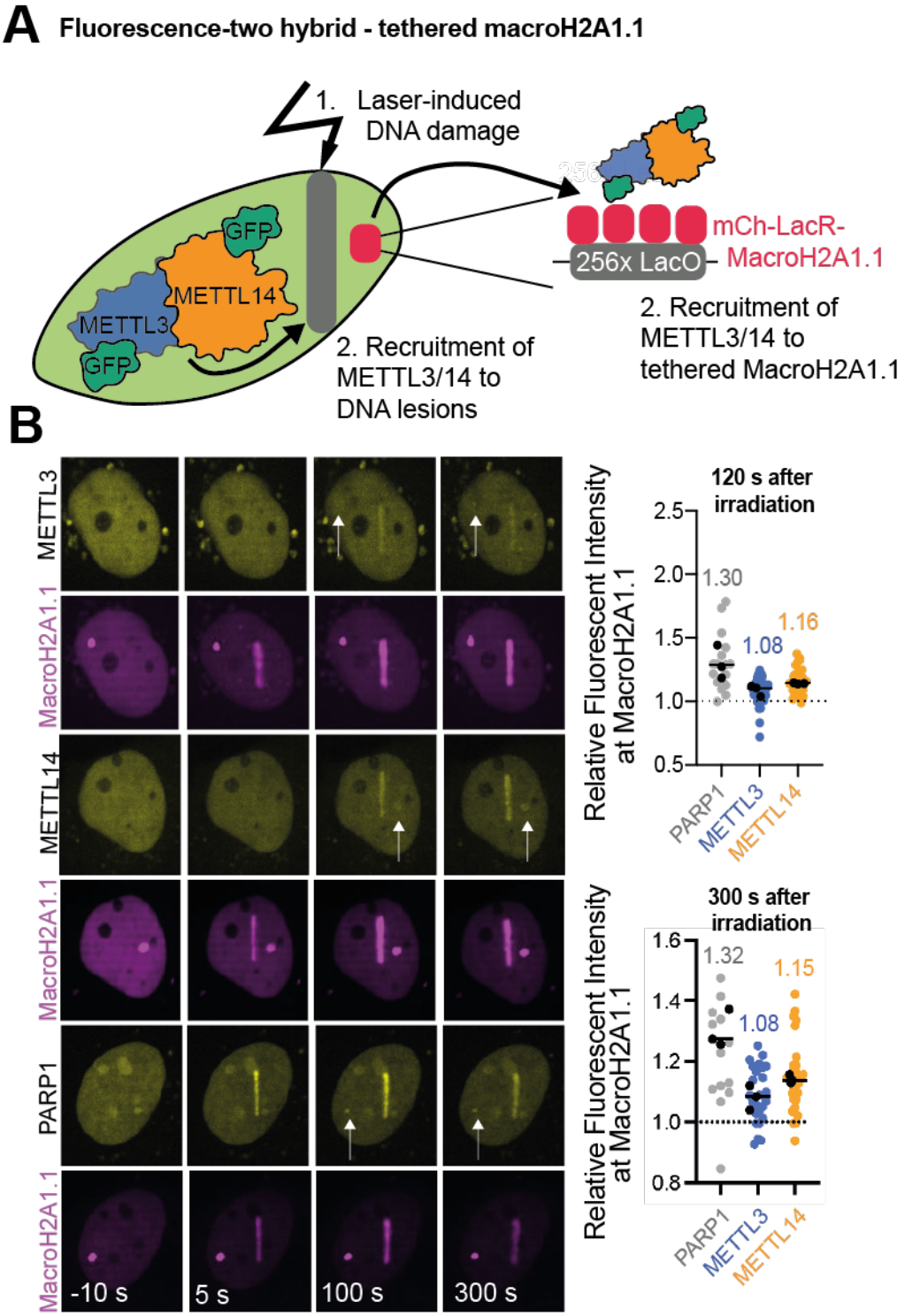

Figure 29. METTL14 interacts with PAR/PARylated proteins *in cellulo*. (A). U2OS cells with genomic-integrated Lac operator (LacO) repeats were co-transfected with mCherry-MacroH2A1.1 fused to the Lac repressor (LacR) and GFP-PARP1, -METTL3 or -METTL14. The accumulation of these proteins at MacroH2A1.1 foci was monitored after photomanipulation using a 355-nm laser. (**B**) Representative images of the LacO/LacR assay (left) and quantification of GFP-PARP1, -METTL3, and -METTL14 at MacroH2A1.1 foci (right). Foci are indicated by white arrows. More than 30 cells were analyzed across three biological replicates. Each nucleus is represented by a data point with the mean of each experiment shown as a black point. The line indicates the median value across all data points. The means for each condition are indicated. Experiments performed by Julia Preißer.

3.4.6 METTL3 and METTL14 are not PARylated

As a post-translational modification, PAR is covalently attached to target proteins. Since our data indicate that METTL3 and METTL14 interact with PARP1 and PAR, we explored whether METTL3 and METTL14 are directly poly-ADPribosylated. To investigate this, we performed co-immunoprecipitation experiments on cells transfected with GFP-METTL3 or GFP-METTL14 after UV irradiation. As controls, we used cells transfected with GFP-PARP1 WT and GFP-PARP1 E988K, a catalytic mutant that conserves its capacity to mono-ADPribosylate (Marsischky et al., 1995; Rolli et al., 1997). Following immunoprecipitation, we used high-salt buffer wash to reduce protein-protein interactions of the pulled GFP-tagged proteins, performed Western blotting to separate proteins, and detected PAR using the α pan-ADPribose antibody, which binds to mono- and poly-ADPribose.

As expected, a reduction of PAR signal was observed in the catalytic mutant GFP-PARP1 E998K compared to GFP-PARP1 WT for both recombinant and endogenous PARP1 (Figure 30, marked as * and ** respectively). However, under these conditions, no PAR signal was detected on the GFP-pulled METTL3 or METTL14 (Figure 30), indicating that neither of these proteins is a target of the poly-ADPribose polymerases.

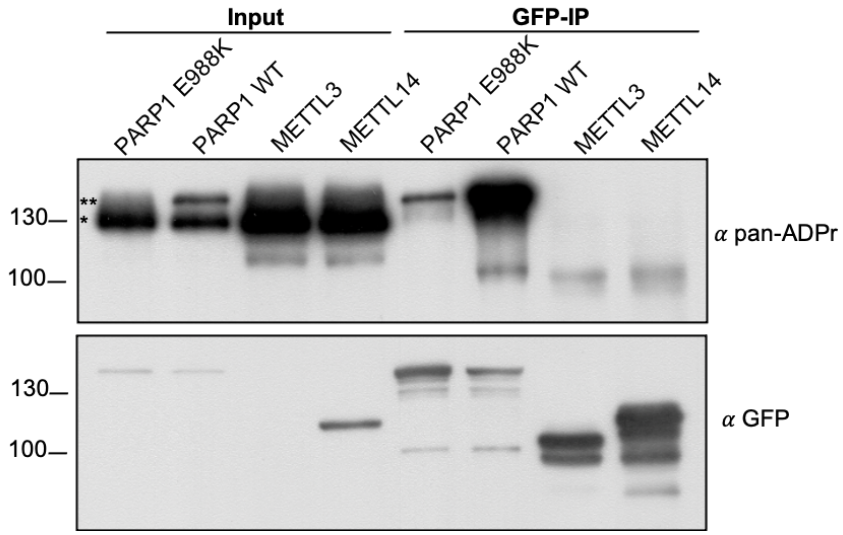

Figure 30. METTL3 and METTL14 are not PARylated. High-salt immunoprecipitation was performed on HEK293T cells transfected with GFP-METTL3, -METTL14, -PARP1 WT, or GFP-PARP1 E988K after UV irradiation. A reduced PAR signal was observed in the PARP1 E988K cells compared to PARP1 WT. However, no PAR signal was detected in METTL3 or METTL14 samples. The representative blot shown is from one of the two independent experiments performed, both yielding similar results. Experiment performed by Jin Cai.

3.5 METTL3 deficiency delays the DNA damage response

3.5.1 METTL3 deficiency increases sensitivity toward UV

As a second aim of my project, we sought to investigate the effect of METTL3/14 recruitment and m6A accumulation at DNA lesions on the DNA damage response (DDR). We mainly focused on the impact of METTL3, as it is the catalytic core of the heterodimer. We conducted clonogenic cell survival assays to assess cell sensitivity in the absence of METTL3, evaluating proliferation capacity when cells are exposed to different DNA damage sources. Consistent with prior reports (Xiang et al., 2017), we observed that ΔMETTL3 cells are sensitive to UV in the presence of BrdU (Figure 31 A left). This sensitivity can be rescued by reintroducing METTL3 WT to the deficient cells (ΔMETTL3 + METTL3 wt), but not with the catalytic mutant METTL3 D395A (ΔMETTL3 + METTL3 mut, Figure 31 A left). This suggests that UV sensitivity in the presence of BrdU depends on the catalytic activity of METTL3. Intriguingly, cells without BrdU pretreatment did not exhibit UV-sensitivity, yet the reintroduction of METTL3 WT conferred protection against UV (Figure 31 A right).

Considering that the presence of BrdU promotes double-strand break formation after UV (Limoli & Ward, 1993), and that METTL3/14 can methylate double-stranded DNA *in vitro* (D. Yu et al., 2021), we hypothesized that ΔMETTL3 cells might be sensitive to X-ray radiation (IR), as it induces double-strand DNA breaks. However, our results indicate that under the tested conditions, ΔMETTL3 cells are not sensitive to IR (Figure 31 B). The reintroduction of METTL3 WT, on the other hand, conferred resistance against high IR doses (Figure 31 B).

These observations contradict previous reports where shRNA-mediated depletion resulted in sensitivity against IR and cisplatin (C. Zhang et al., 2020). Additionally, the lack of sensitivity against IR and UV without BrdU, along with the apparent resistance conferred by the reintroduction of METTL3 WT, could be attributed to potential residual METTL3 activity in the apparent ΔMETTL3 cells, as previously reported in the literature (Poh et al., 2022). It is plausible that our cell system does not constitute a complete knockout, thus explaining the absence of DDR phenotypes are observed without pre-sensitization.

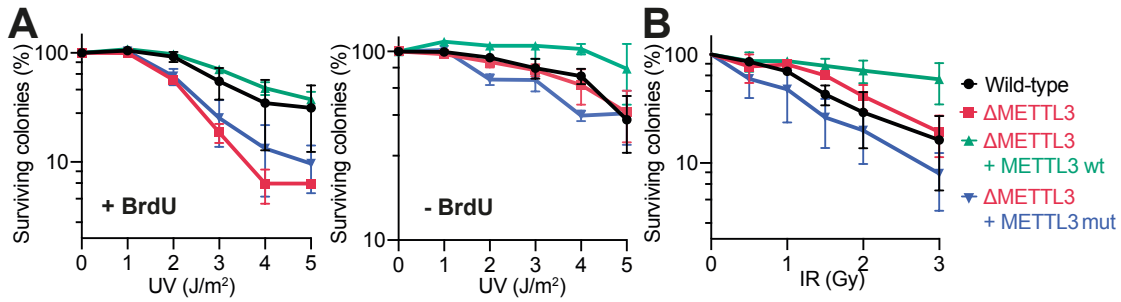

Figure 31. METTL3 deficient U2OS cells are sensitive to UV in the presence of BrdU. (A). Clonogenic survival cell survival assay depicting the sensitivity of wild-type, ΔMETTL3, ΔMETTL3 + METTL3 wt, and ΔMETTL3 + METTL3 D395A (ΔMETTL3 + METTL3 mut) U2OS cells to UV-irradiation. The assay was performed with (left) or without (right) BrdU. (**B**). Clonocegic survival assay illustrating the response of cells to X-ray irradiation (IR). Data are presented as the mean of three biological replicates ± SEM.

3.5.2 METTL3 deficiency delays photolesion repair

The energy emitted during UV irradiation is absorbed by DNA, leading to the formation of cyclobutene pyrimidine dimers (CPD) or 6-4 photoproducts (6-4PPs). These lesions cause distortions to the DNA helix, impairing vital biological processes such as DNA replication and RNA transcription (Lans & Vermeulen, 2011; G. Wang & Vasquez, 2017). Repairing of these lesions is crucial for maintaining genome integrity and cellular homeostasis. We investigated the role of METTL3 in the repair of CPDs and 6-4PPs by monitoring the resolution of these photolesions following UV treatment.

Consistent with previous reports, we observed that the depletion of METTL3 results in increased levels of CPDs compared to the control (Figure 32 A), indicating impaired UV repair (Xiang et al., 2017). Similarly, elevated levels of 6-4PP levels were observed in ΔMETTL3 cells (Figure 32 B). Furthermore, the resolution of 6-4PP could be restored after reintroducing METTL3 wt (ΔMETTL3 + METTL3 wt) but not with the catalytic mutant METTL3 D395A (ΔMETTL3 + METTL3 mut; Figure 32 B). Considering the kinetics of lesion repair (Matsumoto et al., 2007), our observations suggest that METTL3 deficiency affects both early (6-4PP) and late (CPD) stages of UV-damage repair.

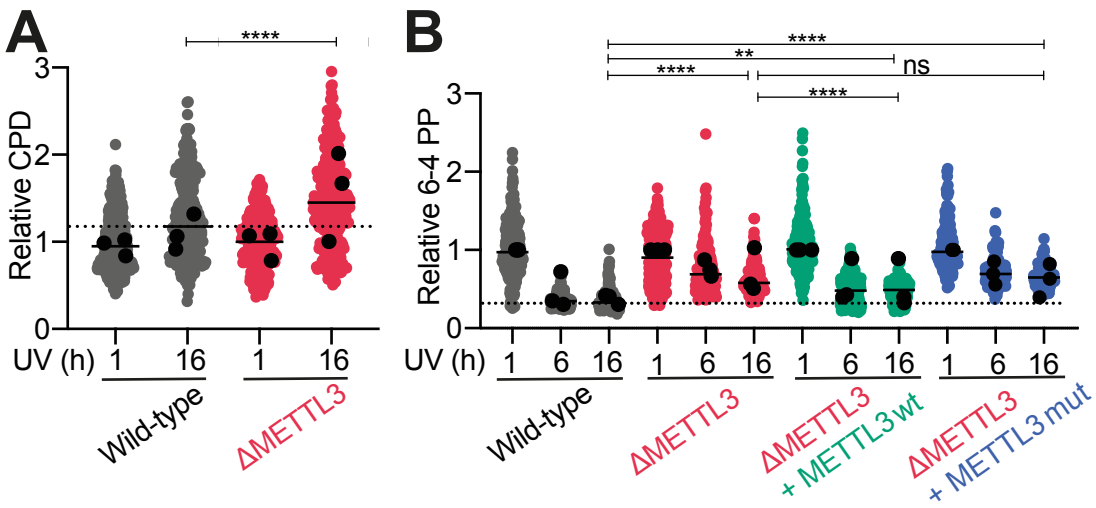

Figure 32. **METTL3 deficiency delays photolesion repair.** Quantification of nuclear immunofluorescence signal of (**A**) cyclobutene pyrimidine dimers (CPD) and (**B**) 6-4 photoproducts (6-4PP), normalized to signal 1 h after irradiation. All nuclei from three independent experiments are shown as individual points, more than 100 cells were analyzed per condition. Black points represent the means of three biological replicates, and the bar indicates the median of all points. Statistical comparisons were performed conditions were using one-way ANOVA with Tukey's post-hoc test to compare treatments against wild-type 16h. Significance levels: ns p> 0.05, **p<0.002, **** p<0.0001.

Importantly, no differences in cell cycle profiles were observed between METTL3 deficient cells and their parental cell line after UV irradiation in the presence of BrdU (Figure 33). Therefore, the delay in photolesion repair and UV-sensitivity are uncoupled from cell cycle progression.

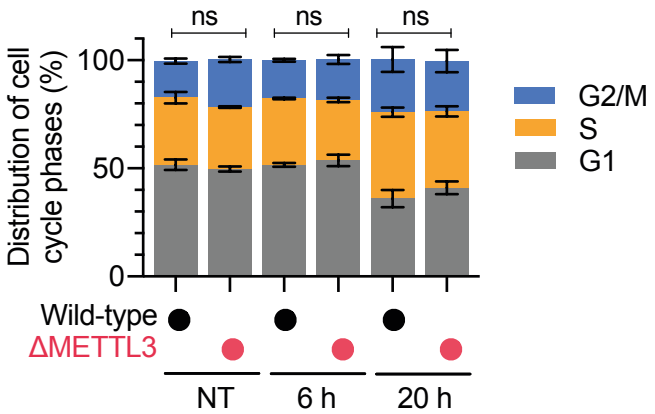

Figure 33. Cell cycle analysis of METTL3 deficient cells and wild-type cells after UV irradiation. Cell cycle analysis by flow cytometry was performed using propidium iodine staining of cells without UV-irradiation (NT), 6 h or 20 h after treatment. Data shown for three biological replicates, with more than 3,000 cells were analyzed per condition per replicate. Statistical comparisons were performed using two-way ANOVA with Tukey's post-hoc test to compare each treatment against wild-type at the corresponding time point. Significance levels: ns p> 0.05, **p<0.002, **** p<0.0001.

3.5.3 METTL3 deficiency delays transcription-related processes

The nucleotide excision repair pathway (NER) is one of the key pathways employed by the cells to repair UV-induced DNA lesions faithfully. This pathway can be initiated by directly recognizing photolesions (global genome-NER; GG-NER) or identifying the stalled RNA polymerase at the lesion site (transcription coupled-NER; TC-NER). Given our previous findings demonstrating the impact of METTL3 deficiency on photolesion repair (Figure 32) and the interaction of METTL3 with RNA Pol II (Figure 22), we investigated whether METTL3 plays a role in TC-NER.

To address this question, we initially examined the sensitivity of ΔMETTL3 cells to Illudin S, a compound known to induce lesions repaired through transcription- and replication-coupled pathways (Jaspers et al., 2002). Cell viability was measured using the CellTiter-Glo® bioluminescent assay, which quantifies ATP production. We found that ΔMETTL3 cells are sensitive to Illudin S, a phenotype rescued by the reintroducing METTL3 wt, but not METTL3 mut (Figure 34 A). Moreover, at low concentrations of Illudin S, transient depletion of METTL3 through siRNA, but not METTL14, decreased cell viability compared to cells transfected with a control siRNA (Figure 34 B). Nonetheless, this sensitivity disappeared at higher concentrations of Illudin S. XPA depletion, a key component of the NER machinery and served as a positive control for this assay.

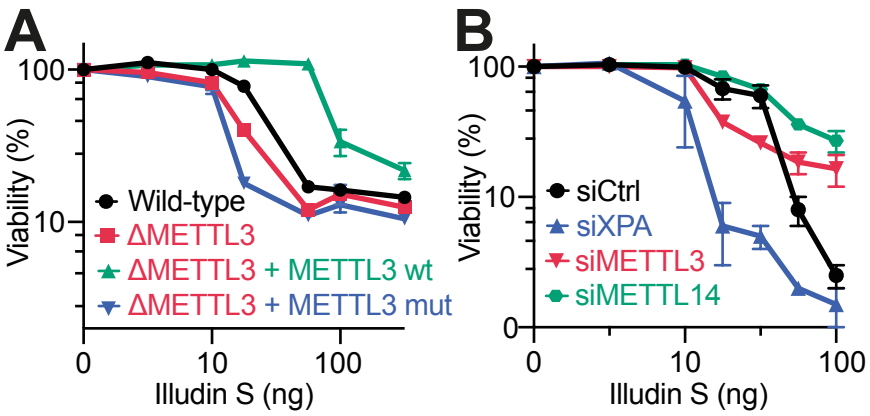

Figure 34. METTL3 deficient cells are sensitive to Illudin S. (**A**) Viability assay of wild-type, ΔMETTL3, and rescue (METTL3 wt, and METTL3 mut) cell lines exposed to Illudin S. (**B**) Viability assay of siRNA-depleted cells exposed to Illudin S. XPA depletion served as a positive control. Viability was measured using CellTiter-Glo®. Data are presented as the mean of three independent experiments ± SEM.

As a protective measure to maintain genome integrity, UV-irradiated cells undergo a significant reduction in RNA synthesis, which is later restored after the resolution of the DNA lesions (Mayne & Lehmann, 1982). Therefore, the restart of RNA synthesis can serve as

an indicator of cellular fitness following UV irradiation. In line with previous reports (Xiang et al., 2017), depletion of METTL3, and to a lesser extent METTL14, hindered transcription restart after UV, as evidenced by reduced 5-Ethynyl Uridine (EU) incorporation 20 h after UV-irradiation (Figure 35 A left). As positive controls, siRNAs targeting CSB and XPA, key proteins in TC-NER and GG-NER pathways, respectively, were used. The efficiency of the depletion was confirmed by Western blot (Figure 35 A right).

Similarly, ΔMETTL3 cells exhibited diminished RNA synthesis compared to the parental cell line 16 h after UV-treatment (Figure 35 B). Moreover, rescue with METTL3 wt restored RNA synthesis at this time point (ΔMETTL3 + METTL3 wt; Figure 35 B). A limitation of this dataset is the absence of EU incorporation 1 h after UV treatment. Therefore, confirmation of an appropriate shutdown of transcription is not available. Despite this limitation, the trends observed in these cells align with the observations made when using siRNA depletion (Figure 35 A); thereby supporting the argument that METTL3 deficiency impairs transcription restart after UV-damage.

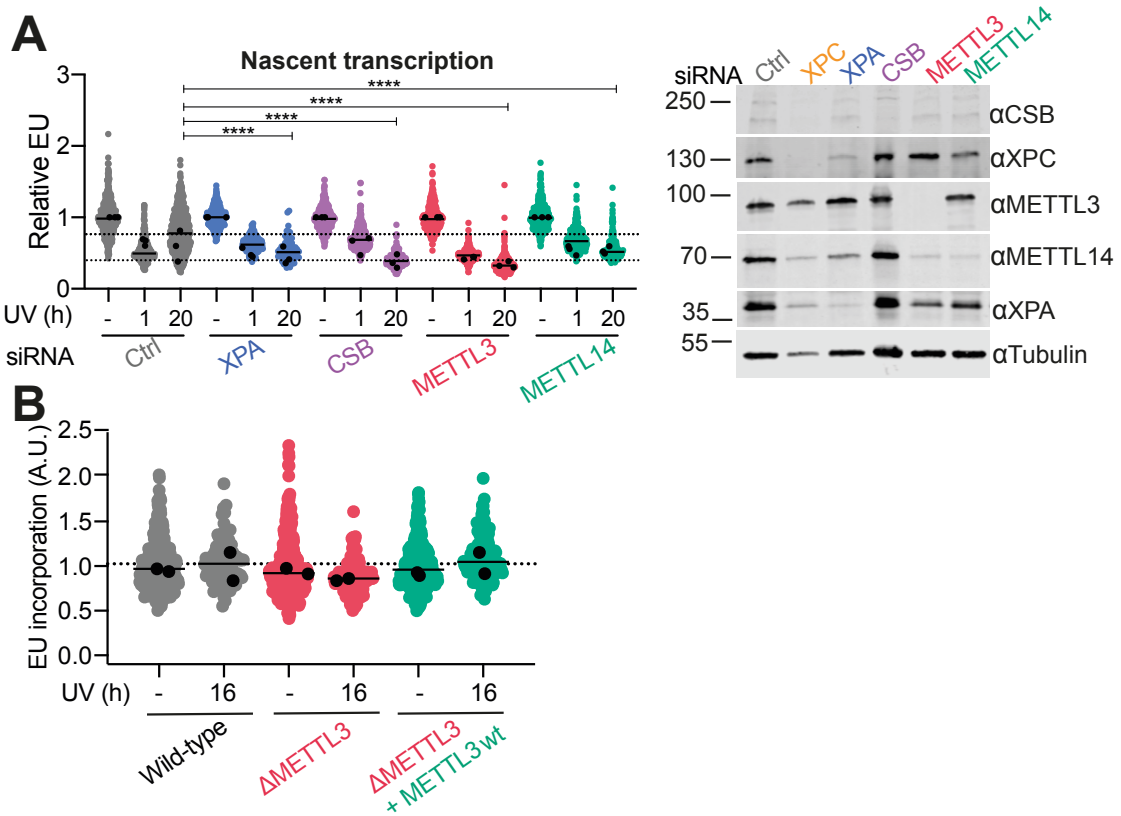

Figure 35. METTL3 deficiency delays transcription restart after UV-damage. (A). EU incorporation assay 1 h and 20 h after UV-irradiation in cells depleted of METTL3, METTL14, CSB, or XPA, with corresponding Western blot confirming protein depletion. (**B**) EU incorporation assay 16 h after UV-irradiation in parental, ΔMETTL3, and ΔMETTL3 + METTL3 wt rescue cells. All nuclei from three (**A**) or two (**B**) biological replicates are shown as individual points. More than 30 cells were analyzed per condition per replicate. Black points represent the means of each biological replicate, and the bar

shows the median of all points. For (**A**) Statistical comparisons were performed using one-way ANOVA with Tukey's post-hoc test to compare each treatment against siCtrl 20h; **** $p<0.0001$.

3.5.4 METTL3 deficient cells have increased ATF3 levels

The activating transcription factor 3 (ATF3) is a transcriptional repressor that is rapidly and transiently induced upon stress, including the DNA damage caused by agents, such as UV, IR, or MMS (Fan et al., 2002). Accumulation of ATF3 leads to transcriptional arrest, and sustained high levels can impact cell proliferation. The removal of ATF3 is guided by the TC-NER proteins CSA and CSB through the assembly of the ubiquitin/proteasome complex (Epanchintsev et al., 2017). Therefore, ATF3 levels after UV damage are correlated with TC-NER efficiency. We assessed ATF3 levels after UV-irradiation using immunofluorescence and observed persistent and elevated nuclear ATF3 signal in ΔMETTL3 cells compared to the parental control (Figure 36 A). Interestingly, the reintroduction of both METTL3 wt and METTL3 mut reduced ATF3 levels after 26 h (Figure 36 A), suggesting a role of METTL3 independent of its catalytic activity. Similar observations were confirmed using western blot on whole cell lysate (Figure 36 B).

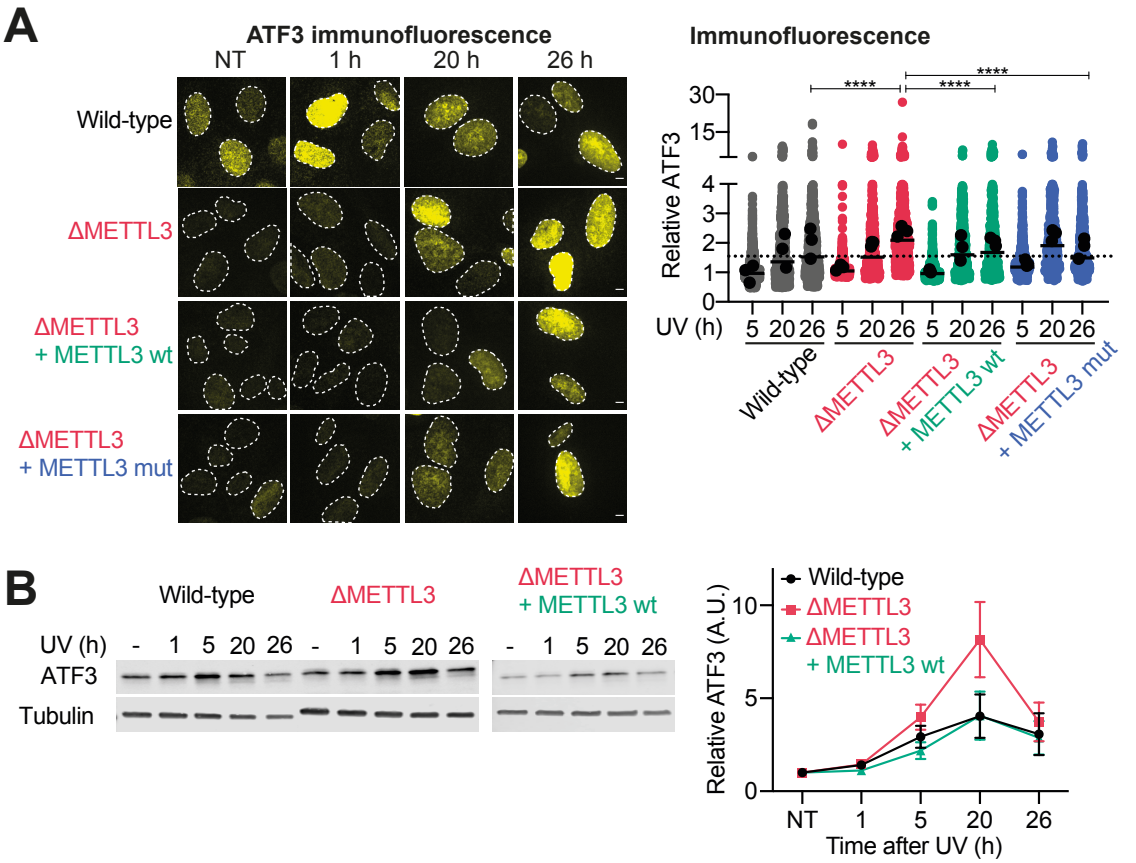

Figure 36. High levels of the transcription repressor ATF3 are sustained in METTL3 deficient cells. (**A**) Representative microscope images of the nuclear immunofluorescent signal (left) and quantification (right) of ATF3 in wild-type, ΔMETTL3, and rescue (ΔMETTL3 + METTL3 wt and ΔMETTL3 + METTL3 mut) cell lines. ATF3 signal was normalized to signal 1 h after irradiation. All nuclei are shown as individual points, more than 30 cells were analyzed per condition per replicate. Black points represent the means of three biological replicates, and the bar shows the median of all points. Statistical comparison was performed using one-way ANOVA with Tukey's post-hoc test to compare each treatment against wild-type 26h. (**B**) Western blot analysis of cell whole lysate testing the abundance of ATF3 in wild-type, ΔMETTL3 and ΔMETTL3 + METTL3 wt cells at different points after UV treatment. The images represent a single representative experiment (left), and the quantification of three biological replicates is shown on the right. The data were normalized to tubulin control and to ATF3 signal before irradiation. Data are presented as the mean of three biological replicates ± SEM.

Our observations indicate that METTL3 plays a role in NER, as evidenced by the impaired CPD and 6-4PP repair, and potentially in TC-NER. However, the subtle effects of the observed phenotypes (Figure 31-36), along with the protective effect against UV without BrdU presensitization and IR-irradiation observed after reintroducing METTL3 wt in the clonogenic survival assays (Figure 31), suggest potential residual activity of METTL3 in the cell model used. Furthermore, the consequences of DNA replication stress and transcription block cannot be disentangled in the cells we used, as the time required to restart transcription overlaps with the doubling time of the U2OS cells. The

limitations of our data prevent us from drawing a conclusive answer to whether METTL3 plays a role in TC-NER.

To address these limitations, we collaborated with the Luijsterberg lab at Leiden University to investigate the impact of METTL3 in TC-NER. They employed RPE1-iCas9 cells, which stably express inducible Cas9 and are deficient in *TP53*. Additionally, these cells were further engineered to knockout XPC, making the survival of cells to DNA damage depend on TC-NER proficiency. Furthermore, the absence of *TP53,* combined with the slow cell cycle kinetics of RPE1 cells, enables the uncoupling of defects arising from DNA replication stress from those related to the transcriptional block. In this cells system, METTL3 was depleted using shRNA before performing TC-NER assays such as viability studies in the presence of Illudin S, EU and EdU incorporation assays after UV-irradiation, and measurements of double-strand breaks after trabectedin treatment as an indicator of TC-NER efficiency. The collective findings from these experiments strongly suggest a role of METTL3 in TC-NER. The detailed results of the Luijsterberg lab are included in the manuscript published in Nucleic Acid Research in 2025 (see List of Publications).

3.6 Combination of PARPi and METTL3i decreases proliferation of different cancer cell models

In the clinic, PARPi are approved for treating several solid tumors, including breast, prostate, and ovarian cancer, and are also being investigated preclinically in hematological malignancies, reviewed in (Padella et al., 2022). Their therapeutic approach represents the first synthetic lethal targeted therapy, particularly effective in cells with BRCA1 or BRCA2 mutations, deficient in homologous recombination and particularly sensitive to PARPi.

On the other hand, METTL3 has emerged as a crucial player in specific cancers, notably in acute myeloid leukemia (AML) (Barbieri et al., 2017). This has led to the development of METTL3 inhibitors, some currently undergoing Phase 1 clinical trials (Identifier: NCT05584111). Given the identified interaction between METTL3 and PARP1, along with the evidence suggesting a role of METTL3 in DNA repair through homologous recombination (E. Li et al., 2022; C. Zhang et al., 2020) and NER (our data), we hypothesized that combining METTL3 and PARP inhibitors could enhance their effectiveness in treating cancer cells.

We first used an acute myeloid leukemia model, MOLM-13 cells, to explore this hypothesis. We assessed the growth inhibition of MOLM-13 cells treated with the METTL3i STM2457, the PARPi olaparib, or a combination of both. After 72 hours of continuous treatment, cell viability was measured using a luminescent-ATP-based assay. As previously reported (Yankova et al., 2021), MOLM-13 cells exhibited higher sensitivity to METTL3 inhibition (Figure 37 A left) compared to unrelated cell types (MDA-MB-231 and SUM149PT). Notably, combining METTL3i with PARPi in MOLM-13 cells resulted in a significant increase in inhibitory potency, as indicated by shifts in the dose-response curves (Figure 37, right curves).

Furthermore, we investigated the impact of this combination on the BRCA1/2 proficient triple-negative MDA-MB-231 cell line and the BRCA1-mutant triple-negative SUM149PT cell line. Similar to MOLM-13, the combination of PARPi with METTL3i enhanced proliferation inhibition to levels where complete inhibition of cellular growth was observed (Figure 37 B-C). These findings highlight the potential of combination therapies in various cancer contexts.

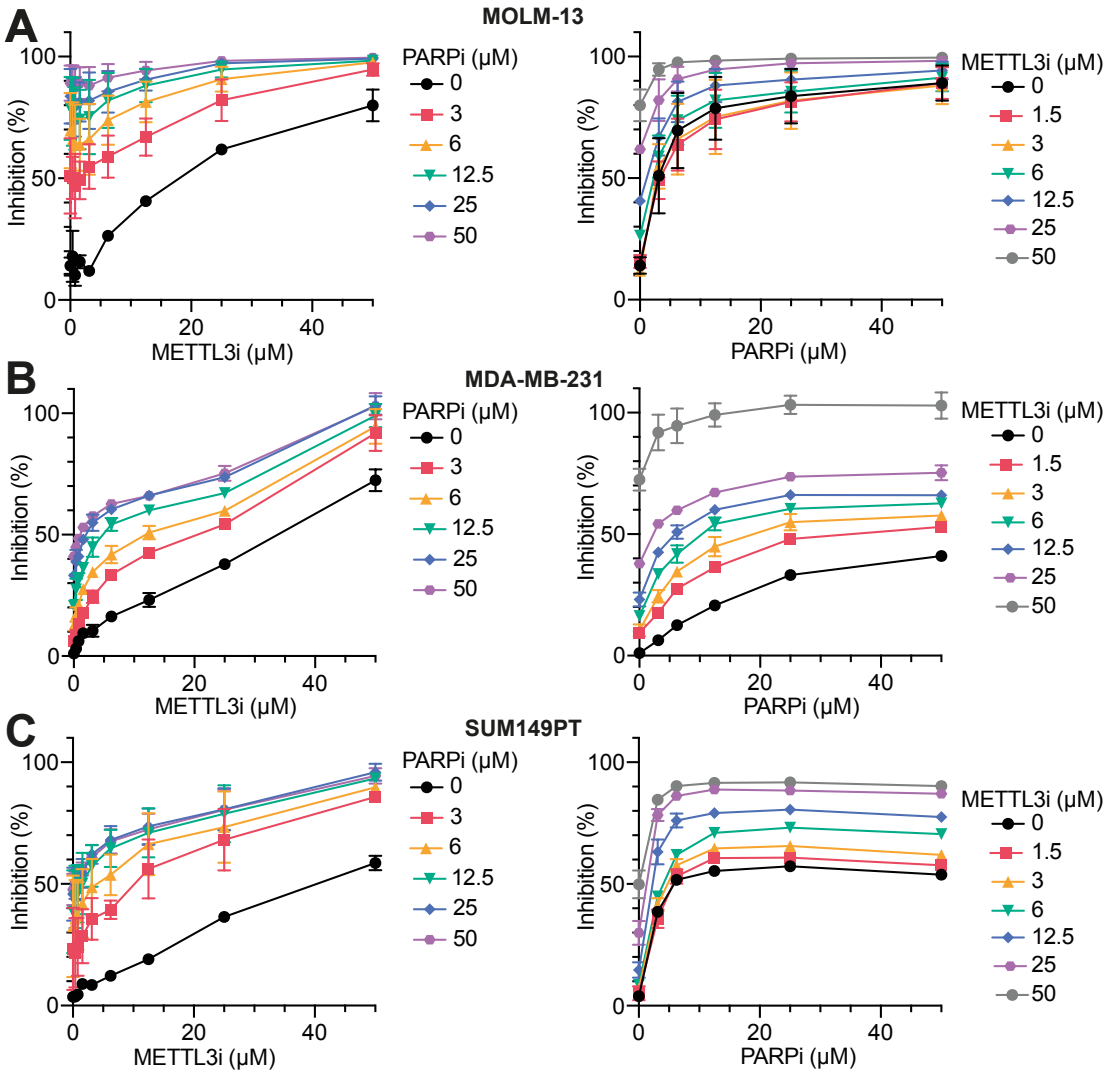

Figure 37. Combination of METTL3 and PARP inhibitors hinders the proliferation of cancer cells.
Viability of MOLM-13 acute myeloid leukemia cells (**A**), MDA-MB-231 BRCA-proficient triple negative breast cancer cells (**B**) and (**C**) SUM149PT BRCA1-mutant triple negative breast cancer cells after treatment with the PARPi olaparib and/or METTL3i STM2457 at different concentrations. Data are depicted as the mean of three biological replicates, each containing two technical replicates ± SEM. Viability was measured using CellTiter-Glo® and percentage inhibition as the inverse ratio of the luminescence of the sample and a live control, corrected for background signal.

4. Discussion

One of the earlier steps in the DNA damage response is the recognition of DNA lesions by PARP1, which triggers a rapid and transient burst of PARylation. PAR dynamics are crucial in DDR, aiding chromatin rearrangement, recruiting DDR proteins, modulating their activity via post-translational modification, and serving as a scaffold for the ensemble of DDR factories. However, the role of this post-translational modification extends beyond DNA repair as it is key in chromatin organization, modulation of gene expression, and RNA biology. PAR versatility relies on the number of proteins interacting with this dynamic polymer. Growing evidence highlights the overlap between RNA-binding and PAR-interacting proteins (Gagné et al., 2008, 2012; Kalesh et al., 2019). Some of these findings have clinical implications (Lee et al., 2021; Rhine et al., 2022). This thesis focused on one example of these RNA-binding PAR-interacting proteins, the METTL3/14 methyltransferase complex.

In this thesis, we built on previous reports (Xiang et al., 2017) to characterize the dynamics of METTL3/14 recruitment to microirradiation sites. Our findings dissect the role of PAR and the contribution of RNA towards the METTL3/14 kinetics of recruitment. Moreover, we identified METTL3/14 as a direct PAR-binder, using *in vitro* biochemical assays. We further characterized the role of METTL3 in DDR and found that METTL3 deficiency impaired TC-NER. Lastly, we explored the therapeutic potential of METTL3 and PARP inhibitors using a combination approach in a leukemia cancer cell line and triple-negative breast cancer models.

Collectively, our findings contribute to understanding the complex interplay between DNA repair, RNA biology, and PARylation and provide insights into the roles of METTL3/14 in these processes. The identified therapeutic opportunities pave the way for further investigation into the clinical applications of METTL3 and PARP inhibitors. This study lays the foundation for future research exploring the broader implications of these molecular interactions in health and disease.

4.1 PARP1-mediated PARylation mediates m6A accumulation and METTL3/14 recruitment to DNA photolesions.

This study investigated the dynamics of m6A and recruitment of the METTL3/14 complex to microirradiation sites. Similar to previous reports, we observed m6A accumulation at

microirradiation sites in BrdU-sensitized cells (Svobodová Kovaříková et al., 2020; Xiang et al., 2017). However, as the m6A signal was also observed in METTL3 deficient cells, we opted to use an antibody-independent approach to validate our observations. Therefore, we used live-cell imaging coupled with laser microirradiation to provide a detailed characterization of m6A writer complex METTL3/14 recruitment to DNA damage sites. Using this approach, we observed rapid and transient accumulation of METTL3 and METTL14 in the DNA lesions. Moreover, the recruitment of both proteins depended on PAR dynamics, as manipulating PAR levels through PARPi and PARGi either abolished or retained METTL3/14 at the damage sites, consistent with PAR-driven recruitment. Our rescue experiments in PARP1-deficient cells further validated the dependency of METTL3/14 recruitment on active PARylation at DNA lesions. Intriguingly, we observed that the early recruitment of METTL3 differs slightly from that of METTL14, with METTL3 accumulating more at DNA lesions. This difference in kinetics could allude to the two methyltransferases recruited independently from each other, as confirmed by our recruitment assays in METTL3 deficient cells or METTL14 depleted cells. While laser microirradiation can cause DNA breaks and METTL3/14 can methylate DNA in vitro (D. Yu et al., 2021), our data suggest that DNA breaks alone are insufficient for METTL3/14 recruitment and that METTL3/14 recruitment to micro-irradiation sites is regulated by PAR synthesis.

One of the downstream effects of active PARylation is chromatin decompaction, which is driven by the negative charge of this polymer and the recruitment of chromatin remodelers to PARylation sites. Chromatin remodelers such as CHD3 and CHD4 have been shown to accumulate at sites of PARylation as an indirect effect of PARylation instead of directly interacting with PAR (Smith et al., 2018). We excluded this possibility by comparing METTL3 recruitment in the presence of the HDAC inhibitor trichostatin A, which leads to an open chromatin state. This treatment did not affect the early recruitment of METTL3 to irradiation sites, although a slight increase was observed at later stages. This suggests that METTL3 recruitment is mainly driven by PAR synthesis and that the general chromatin state has a minor effect on the methyltransferase recruitment. Consistently, early recruitment of METTL3 was not affected in the absence of ALC1, a chromatin remodeler involved in PAR-driven chromatin decompaction.

Interestingly, WTAP, an accessory protein to the m6A writing protein, faintly and transiently accumulates at DNA damage sites but does not react to PAR dynamics. Furthermore, the demethylase FTO was not recruited to microirradiation sites. Thus, the PAR-

driven recruitment of the m6A machinery is specific to METTL3/14, although not all m6A-related proteins were tested.

4.2 Transcription affects METTL3/14 recruitment to DNA damage sites

As the core biological role of METTL3/14 is to methylate RNA, we investigated the role of this polymer in the recruitment kinetics of the METTL3/14 complex to the microirradiation sites. We found that treatment with RNase and inhibition of RNA synthesis using αAm and ActD reduced the recruitment of the methyltransferase dimer. Moreover, FRAP assays suggested that the treatment with ActD decreased the mobility of METTL3 and METTL14. As METTL3 co-immunoprecipitated with the RNAPII subunit RBP1 in an RNA-independent manner, we hypothesized that treatment with ActD would reduce METTL3 mobility by increasing the fraction of protein bound to RBP1. Although we observe interaction with RBP1, we did not observe increased interaction with elongating RNA Polymerase (phospho-RBP1). Future studies are essential to further dissect the intricate interplay between PAR and RNA at DNA damage sites and whether this interaction occurs in a homeostatic context, such as at active transcription sites.

4.3 METTL3/14 binds to RNA and PAR *in vitro*

Increasing evidence suggests an overlap between RNA-binding proteins and the PAR interactome. For instance, proteomic analysis has revealed significant enrichment of RNA-binding proteins among PAR binders (Dasovich et al., 2021). RBPs such as FUS, EWS, and DHX9 38 (Altmeyer et al., 2015; Cristini et al., 2018) are recruited to microirradiation sites in a PAR-dependent manner. However, the biochemical similarities between PAR and RNA raise questions about the specificity of these interactions and the mechanisms of selective interaction between RBPs and PAR or RNA.

Our *in vitro* data are consistent with the direct binding of METTL3/14 to PAR polymers, with high PAR concentrations partially displacing RNA binding but not outcompeting it. Conversely, RNA did not displace PAR. Interestingly, we observed no difference in the catalytic activity of METTL3/14 in the presence of PAR, suggesting that PAR and RNA do not compete for METTL3/14 binding. Instead, PAR can serve as a scaffold guide for METTL3/14 to specific nuclear locations, targeting its enzymatic activity at these sites.

Consistent with this idea, we observed the enrichment of METTL14 in chromatin-tethered PAR-binding macrodomains.

4.4 METTL3 affects Transcription-Coupled Nucleotide Excision Repair

Previous studies have suggested the role of UV-induced DNA damage repair. However, the precise pathway involved in m6A-mediated remained unknown. Based on this knowledge, we investigated the role of METTL3 in DNA repair. We observed that METTL3 deficiency in U2OS cells led to UV sensitivity and impaired photolesion clearance at both early (64PP) and late (CPD) DNA repair stages. Furthermore, the absence of METTL3 or transient depletion of this protein resulted in sensitivity to Illudin S, a mutagenic agent whose lesions can be repaired only through Transcription-Coupled Nucleotide Excision Repair. By these observations, METTL3 deficient cells exhibit a delay in transcription restart after UV damage and increased levels of the transcription repressor ATF3. Taken together, our data argues for a role of METTL3 in TC-NER.

It is important to note that some of these phenotypes were previously described by Xiang et al. (Xiang et al., 2017); e.g., sensitivity to UV radiation, delayed CPD repair, delayed transcription restart). Our work independently validated and expanded the characterization of the role of METTL3 in UV-induced DNA damage repair, highlighting the role of METTL3 and m6A in the transcriptional-dependent response to DNA damage. However, the subtlety of the phenotypes described, as well as the fact that they can only be observed in the presence of BrdU pre-sensitization, suggest that either the effect of METTL3 in DNA damage repair is either subtle or that it is masked by redundancy of multiple pathways, for instance, by compensating activity of other methyltransferases, or by potential residual catalytic activity of METTL3 as has been reported for some METTL3 knockout cell models (Poh et al., 2022). Moreover, using U2OS cells as the basis for our studies limits the interpretation of our results, as the doubling time of these cells limits the dissection of the DDR signaling induced after DNA replication stress or as a consequence of transcriptional blockade. Therefore, it was not possible to unequivocally delineate the role of METTL3 in TC-NER.

We collaborated with the Luijsterberg Lab at Leiden University. They engineered RPE1 cells, known for their extended doubling time, which allows the differentiation of DNA replication processes from transcriptional-related ones, with an inducible Cas9 system to acutely deplete XPC, thereby minimizing the contribution of GG-NER. Using shRNA in these cells, the Luijsterburg group confirmed the role of METTL3 in TC-NER. The detailed results generated in this collaboration are included in the manuscript published in Nucleic Acid Research in 2025 (see List of Publications in Appendix 4).

Our observations, together with the evidence provided by the Luijsterberg Lab, further validate previous genome-wide screening mapping genetic susceptibilities against DNA damage agents, where METTL3 depletion resulted in UV sensitivity while conferring resistance against trabectedin (Olivieri et al., 2020). Similar sensitivities have been reported for TC-NER factors, such as ELOF1 (Olivieri et al., 2020; Van Der Weegen et al., 2021).

4.5 Combination of METTL3i and PARPi additively inhibits the proliferation of diverse cancer cells.

Since the identification of METTL3 as a key oncogenic factor in AML (Barbieri et al., 2017; Vu et al., 2017), significant progress has been made in the development of METTL3 inhibitors (Yankova et al., 2021), with the first clinical trial currently underway. Given the clinical use of PARPi, we explored the potential of combining METTL3i and PARPi in cultured cancer cells. Our experiments showed an additive antiproliferative effect in cells derived from acute myeloid leukemia (MOLM-13) and triple-negative BRCA-proficient (MDA-MB-231) and BRCA-deficient (SUM194PT) breast cancers. Similar observations have recently been reported (Cesaro et al., 2023). These data support further efficacy analysis in different cancer models and suggest an additive effect independent of the BRCA proficiency status. Assuming that combining these two therapeutic agents does not exacerbate the established toxicity profiles of individual monotherapies, our results could pave the way for innovative combination treatments, potentially enabling the targeting of new cancer indications.

In summary, our work delineates the dependencies of METTL3/14 recruitment to DNA damage sites, highlighting the role of PAR and active transcription to colocalize the methyltransferase complex to microirradiation sites. We observed that the recruitment

kinetics follows DNA damage induced PARylation, and the recruitment of the METTL3/14 complex dependents on PAR dynamics. In this regard, we identified the MTAse domain of METTL3 as the structural domain that reacts to PAR stimuli. Furthermore, we provide biochemical evidence of the *in vitro* binding of METTL3/14 to PAR, where PAR can outcompete, yet not abolish, the binding of the heterodimer to RNA. As the catalytic activity of METTL3/14 is not affected by PAR, we propose that the ADP-ribose polymer acts as a scaffold to direct the activity of METTL3/14 locally.

In the second part of this work, we focused on the cellular role of METTL3 in the DNA damage response. We observed that the absence of METTL3 results in cell sensitivity towards UV irradiation. Consistent with this observation, the lack of METTL3 impairs the resolution of 6-4PP and CPD photolesions, highlighting the role of METTL3 in GG-NER repair at early and later time points. Furthermore, METTL3 deficiency resulted in sensitivity towards Illudin S, delayed transcription restart after DNA damage, and increased levels of the transcriptional repressor ATF, observations that are consistent with the role of METTL3 in TC-NER. This role was later confirmed in collaboration with the Luijsterburg lab, published in Nucleic Acid Research in 2025. Lastly, we provide evidence of an additive antiproliferative effect when METTL3 and PARP inhibitors are combined in different cancer models. Interestingly, this effect is independent of the BRCA status of the cells, thus providing a rationale to explore the use of these small molecules in combination.

5. Future directions

5.1 Cellular and biochemical characterization of the interaction between METTL3/14 with PAR and RNA

In light of our *in vitro* results, further characterization of the METTL3/14 complex domains that interact with the two nucleic acids would be desired. For this, a mutational approach followed by characterization of PAR and RNA binding is needed, as described in this work. However, it is likely that RNA-interacting surfaces are also involved in the interaction with PAR. Our live-cell microirradiation experiment of the METTL3 truncation mutants highlights this caveat, as the MTAse domain of the methyltransferase, which contains the catalytic site for RNA methylation, is recruited to the DNA damage sites.

Our findings raise the question of whether the interaction between PAR-RNA and the METTL3/14 complex occurs *in cellulo* and whether it occurs in cellular contexts beyond DNA repair. For instance, PAR is known to play a role in the heat shock response in *Drosophila* (Tulin & Spradling, 2003) and humans (Fujimoto et al., 2018) through chromatin rearrangements that facilitate transcription and recruitment of other proteins. At a transcriptional level, m6A is deposited to heat shock transcripts, enhancing translation (Zhou et al., 2015b). As m6A-mRNA methylation occurs co-transcriptionally, it is plausible that heat shock-induced PARylation assists recruiting METTL3/14 to the heat-shock loci. In this way, PAR acts as a signal and scaffold to assemble a virtual factory where transcription and translation are seamlessly coupled, resulting in the efficient production of heat shock proteins. More broadly, exploring the m6A-PAR axis at gene enhancers would be interesting. Recent data from Nussenzweig's lab highlights the presence of PARP activity at neuronal enhancers (W. Wu et al., 2021). It is, therefore, plausible that METTL3/14 is recruited to these sites. Whether these regions are transcribed and m6A methylated remains to be studied.

Methodologically, these questions could be explored by using a combination of chromatin immunoprecipitation sequencing (ChIP-seq) and methylated RNA sequencing (e.g, ADPribose ChIP-seq and meRIP/m6A-seq). In addition, the cellular interplay of METTL3/14, PAR and RNA could be approached using fluorescent microscopy by performing a proximity ligation assay (PLA) targeting METTL3 and PAR with available antibodies while simultaneously labeling RNA with a nucleoside analog followed by click chemistry (e.g., EU). Colocalization of the PLA and EU signals would indicate interaction

sites between PAR, METTL3, and RNA. Extensive optimization is required to couple the two chemical reactions without increasing the background signal, optimize the time points for RNA labeling, and obtain appropriate time points to capture the PAR-METTL3 interaction. In our study, co-immunoprecipitation of METTL3 and PARP1 resulted in highly variable results (data not shown). Therefore, this interaction is likely transient and thus difficult to capture. As an alternative, PLA could be performed targeting METTL3 and RBP1 and co-staining with a PAR antibody. However, this approach would limit the observations to interrogate the presence of PAR at transcription sites.

5.2 Mechanistic insights into the role of METTL3 in Transcription-Coupled Nucleotide Excision repair and the therapeutic opportunities of METTL3 and PARP inhibitors.

Our work builds on previous observations and provides a deeper understanding of the role of METTL3 in UV-induced DNA damage repair, centering on m6A at the intersection between DNA repair, RNA biology, and ADP-ribosylation. In collaboration with the Luijsterburg group, we observed that METTL3-deficient cells exhibit impaired TC-NER. However, we did not explore the potential interdependency between METTL3 and PARylation in the context of TC-NER or the mechanistic role of METTL3 in this pathway. That is, what are the molecular steps involved in METTL3 contribution to TC-NER? Does PARP1 modulate the contribution of METTL3 in this pathway? Moreover, it is not known whether PARP1 directly affects TC-NER repair.

To address these questions, we could repeat the functional cellular assays reported in our publication in Nucleic Acid Research (2025) in RPE1-XPC deficient cells and RPE1-XPC-METTL3 deficient cells with and without PARP1 treatment. If PAR dynamics drive METTL3 role, we would not observe additive effects when treating RPE1-XPC-METTL3 deficient cells with PARPi, thereby confirming epistasis. If PAR plays a role in TC-NER, we expect to observe TC-NER repair impairment in RPE-XPC cells treated with PARPi. However, PARP inhibitors are known to have effects beyond the catalytic activity of PARP1, for instance, by trapping the enzyme in chromatin (Murai et al., 2012); unpublished data from our lab). Therefore, it would be ideal to develop RPE-XPC-METTL3-PARP1 deficient cells. However, the engineering of cells and their viability can impose technical difficulties in this approach.

To address the question of the molecular steps guiding the contribution of METTL3 to TC-NER, we could perform a series of co-immunoprecipitation experiments to examine the changes in METTL3 and METTL14 interactions in the presence and absence of agents inducing TC-NER lesions, such as Illudin S. For instance, we could pull down GFP-METTL3 or GFP-METTL14 and probe for different TC-NER proteins. Enrichment of protein-protein interactions in the presence of Illudin S would highlight the steps in which the METTL3/14 complex intervenes. Based on our previous observations, these experiments should be performed in RPE1-XPC deficient cells to minimize the effects of DNA replication stress and the contribution of GG-NER.

Similarly, we do not fully understand the mechanisms underlying the additive effects observed when using METTL3 and PARP inhibitors in combination therapy. We hypothesize that the observed antiproliferative effects arise from the roles of these proteins outside of TC-NER, for instance, by modulating transcription and participating in other DDR pathways. However, it is needed to further characterize the effects and implications of this combination therapy.

Finally, there are areas that were not explored in this work that could open new interesting research areas derived from this work. For instance, in the presence of PARGi, GFP-METTL and GFP-METTL14 were enriched in small foci that moved away from the microirradiation sites to other areas of the nuclei. What is the composition of these foci, what happens with them after their formation, and what are their biological repercussions are questions that grant further research.

Acknowledgements / Agradecimientos

We stand on the shore of an ocean of mysteries, the depths of which we can only begin to fathom.
Carl Sagan

I would like to thank Prof. Andreas Ladurner for the opportunity to work on a project that has been equally exciting, challenging, and gratifying. Thank you for the training opportunities and for providing me with a space where I could grow and become a better and stronger version of myself, personally and scientifically. I would also like to thank Dr. Carla Margulies for her contagious passion for science and drive to make this a more inclusive environment.

I am immensely grateful to all the Ladurner-Margulies team, present, and past members. Your advice and support have made this an unforgettable journey. To Andreas Wegerer, Julia Preisser and Jin Cai: Thank you for being my team when I needed it the most. Your support and trust energized me more than any amount of caffeine could ever do (but thank you for the caffeine as well). I would like to thank Magdalena Murawska and Maren Heimhalt for being valuable sources of knowledge and strength. To Matin, Ming, Hannah and Christiane, for all the discussions and laughs we shared. My gratitude goes to Charlotte, Imke, Haris and Flavia: you made my days in the lab brighter, even after our days in Munich. I was lucky to have you as colleagues, and happy to have you as my friends.

A heartfelt thank you goes to all the members of the Department of Physiological Chemistry, and my special appreciation goes to Christine Werner and Dr. Anton Eberharter. Thank you for caring so deeply for us. Through the ups and downs of bureaucracy and life, you made me feel supported and empowered. Thank you for giving me a space to be human, for making me feel valued and seen.

To my Thesis Advisory Committee Members Dr. Peter Becker and Dr. Kathrin Lang, for their critical and strategic advice on my research goals and professional progress during my PhD. I also would like to thank Prof. Yang Shi at Harvard University for providing U2OS wild-type, ΔMETTL3 and ΔFTO cells; to Prof. Anthony Leung at John Hopkins for providing 20-mer ADP-ribose and valuable insights through emails. I thank Prof. Gunter Meister and Eva Schöller at the University of Regensburg for hosting me and sharing their knowledge to perform methylation assays. To Prof. Martijn Luijsterburg and Bram at Leiden University, thank you for joining me on this journey and bringing together a fruitful collaboration. Your energy and passion for science gave me the last push before getting on to the last lap of this race.

My PhD experience was greatly shaped by the networks I had the luck to be part of: the International Max Planck Research School for Molecular Life Sciences, the MSCA-ITN aDDRess, and the IRTG 1309 for Chemical Biology. I am grateful for these opportunities, as they provided me with excellent training and the opportunity to meet great scientists

and friends. Special thanks to Dr. Hans Joerg Schaeffer, Dr. Ingrid Wolf, Dr. Maximiliane Reif and Dr. Martha Cipinska.

I am deeply thankful to my friends, especially Anne, Mariana, and Ana. Thank you for being my source of strength and light. You are beautiful souls and brilliant minds, and I feel so fortunate to have you in my life.

Esta lista no estaría completa sin las personas a las que mi corazón les habla en español. Gracias a mi familia, de sangre y electa, que me acompañan sin importar la distancia ni husos horarios. A mi gente en México, que a base de abrazos y comida recargan mi espíritu. A mis padres: su amor y fortaleza corren por mis venas. Gracias por no cortar mis alas y enseñarme a volar. Agradezco a mis abuelos, porque sus sacrificios son hoy ejemplo vivo en mi labranza.

A los que siempre están en mi esquina: Iris, Pável, Fran y Ray. Gracias por ser mis guías en situaciones inciertas y hacer la vida mucho más divertida con ustedes a mi lado. A Laura, Tere, Lucía, Arely, Martha y Lesli, por ser mis raíces y darme un espacio seguro para descubrir quién soy. A mi querido Fellowship, por darme fuerza, cariño y paz cuando la vida es caos.

Y a ti, Andrés, mi compañero de aventuras, desvelos y vida. Tu apoyo es mi motor y batería; haces que cada locura se haga realidad a través del tiempo y espacio. Contra todo pronóstico o estadística, ¡lo logramos! Gracias por siempre estar, sin importar si los tiempos son buenos, malos, felices o tristes.

I am happy to have shared this journey with you all, and I am certain our paths will keep crossing. The moments shared with you are now part of the mosaic that is my life. Until we see each other again. Auf Wiedersehen.

References

- Abakir, A., Giles, T. C., Cristini, A., Foster, J. M., Dai, N., Starczak, M., Rubio-Roldan, A., Li, M., Eleftheriou, M., Crutchley, J., Flatt, L., Young, L., Gaffney, D. J., Denning, C., Dalhus, B., Emes, R. D., Gackowski, D., Corrêa, I. R., Garcia-Perez, J. L., … Ruzov, A. (2020). N6-methyladenosine regulates the stability of RNA:DNA hybrids in human cells. *Nature Genetics*, *52*(1), 48–55. https://doi.org/10.1038/s41588-019-0549-x
- Ahel, D., Hořejší, Z., Wiechens, N., Polo, S. E., Garcia-Wilson, E., Ahel, I., Flynn, H., Skehel, M., West, S. C., Jackson, S. P., Owen-Hughes, T., & Boulton, S. J. (2009). Poly(ADP-ribose)–Dependent Regulation of DNA Repair by the Chromatin Remodeling Enzyme ALC1. *Science*, *325*(5945), 1240–1243. https://doi.org/10.1126/science.1177321
- Akiyama, T., Takasawa, S., Nata, K., Kobayashi, S., Abe, M., Shervani, N. J., Ikeda, T., Nakagawa, K., Unno, M., Matsuno, S., & Okamoto, H. (2001). Activation of *Reg* gene, a gene for insulin-producing β-cell regeneration: Poly(ADP-ribose) polymerase binds *Reg* promoter and regulates the transcription by autopoly(ADP-ribosyl)ation. *Proceedings of the National Academy of Sciences*, *98*(1), 48–53. https://doi.org/10.1073/pnas.98.1.48
- Alarcón, C. R., Goodarzi, H., Lee, H., Liu, X., Tavazoie, S., & Tavazoie, S. F. (2015). HNRNPA2B1 Is a Mediator of m6A-Dependent Nuclear RNA Processing Events. *Cell*, *162*(6), 1299–1308. https://doi.org/10.1016/j.cell.2015.08.011
- Alarcón, C. R., Lee, H., Goodarzi, H., Halberg, N., & Tavazoie, S. F. (2015). N6-methyladenosine marks primary microRNAs for processing. *Nature*, *519*(7544), 482–485. https://doi.org/10.1038/nature14281
- Alemasova, E. E., & Lavrik, O. I. (2017). At the Interface of Three Nucleic Acids: The Role of RNA-Binding Proteins and Poly(ADP-ribose) in DNA Repair. *Acta Naturae*, *9*(2), 4–16. https://doi.org/10.32607/20758251-2017-9-2-4-16
- Alemasova, E. E., Naumenko, K. N., Kurgina, T. A., Anarbaev, R. O., & Lavrik, O. I. (2018). The multifunctional protein YB-1 potentiates PARP1 activity and decreases the efficiency of PARP1 inhibitors. *Oncotarget*, *9*(34), 23349–23365. https://doi.org/10.18632/oncotarget.25158
- Ali, A. A. E., Timinszky, G., Arribas-Bosacoma, R., Kozlowski, M., Hassa, P. O., Hassler, M., Ladurner, A. G., Pearl, L. H., & Oliver, A. W. (2012). The zinc-finger domains of PARP1 cooperate to recognize DNA strand breaks. *Nature Structural & Molecular Biology*, *19*(7), 685–692. https://doi.org/10.1038/nsmb.2335
- Althaus, F. R. (2005). Poly(ADP-ribose): A co-regulator of DNA methylation? *Oncogene*, *24*(1), 11–12. https://doi.org/10.1038/sj.onc.1208382
- Altmeyer, M., Neelsen, K. J., Teloni, F., Pozdnyakova, I., Pellegrino, S., Grøfte, M., Rask, M.-B. D., Streicher, W., Jungmichel, S., Nielsen, M. L., & Lukas, J. (2015). Liquid demixing of intrinsically disordered proteins is seeded by poly(ADP-ribose). *Nature Communications*, *6*(1), 8088. https://doi.org/10.1038/ncomms9088
- Alvarez-Gonzalez, R., & Jacobson, M. K. (1987). Characterization of polymers of adenosine diphosphate ribose generated in vitro and in vivo. *Biochemistry*, *26*(11), 3218–3224. https://doi.org/10.1021/bi00385a042
- Bader, A. S., Hawley, B. R., Wilczynska, A., & Bushell, M. (2020). The roles of RNA in DNA double-strand break repair. *British Journal of Cancer*, *122*(5), 613–623. https://doi.org/10.1038/s41416-019-0624-1
- Banáth, J. P., & Olive, P. L. (2003). Expression of phosphorylated histone H2AX as a surrogate of cell killing by drugs that create DNA double-strand breaks. *Cancer Research*, *63*(15), 4347–4350.
- Barbieri, I., Tzelepis, K., Pandolfini, L., Shi, J., Millán-Zambrano, G., Robson, S. C., Aspris, D., Migliori, V., Bannister, A. J., Han, N., De Braekeleer, E., Ponstingl, H., Hendrick, A., Vakoc, C. R., Vassiliou, G. S., & Kouzarides, T. (2017). Promoter-bound METTL3 maintains myeloid leukaemia by m6A-dependent translation control. *Nature*, *552*(7683), 126–131. https://doi.org/10.1038/nature24678
- Barkauskaite, E., Jankevicius, G., Ladurner, A. G., Ahel, I., & Timinszky, G. (2013). The recognition and removal of cellular poly(ADP -ribose) signals. *The FEBS Journal*, *280*(15), 3491–3507. https://doi.org/10.1111/febs.12358
- Batista, P. J., Molinie, B., Wang, J., Qu, K., Zhang, J., Li, L., Bouley, D. M., Lujan, E., Haddad, B., Daneshvar, K., Carter, A. C., Flynn, R. A., Zhou, C., Lim, K.-S., Dedon, P., Wernig, M., Mullen, A. C., Xing, Y., Giallourakis, C. C., & Chang, H. Y. (2014). m6A RNA Modification Controls Cell Fate Transition in Mammalian Embryonic Stem Cells. *Cell Stem Cell*, *15*(6), 707–719. https://doi.org/10.1016/j.stem.2014.09.019
- Becherel, O. J., Yeo, A. J., Stellati, A., Heng, E. Y. H., Luff, J., Suraweera, A. M., Woods, R., Fleming, J., Carrie, D., McKinney, K., Xu, X., Deng, C., & Lavin, M. F. (2013). Senataxin

Plays an Essential Role with DNA Damage Response Proteins in Meiotic Recombination and Gene Silencing. *PLoS Genetics*, *9*(4), e1003435. https://doi.org/10.1371/journal.pgen.1003435

- Bedi, R. K., Huang, D., Eberle, S. A., Wiedmer, L., Śledź, P., & Caflisch, A. (2020). Small-Molecule Inhibitors of METTL3, the Major Human Epitranscriptomic Writer. *ChemMedChem*, *15*(9), 744–748. https://doi.org/10.1002/cmdc.202000011
- Bilokapic, S., Suskiewicz, M. J., Ahel, I., & Halic, M. (2020). Bridging of DNA breaks activates PARP2–HPF1 to modify chromatin. *Nature*, *585*(7826), 609–613. https://doi.org/10.1038/s41586-020-2725-7
- Blessing, C., Apelt, K., Van Den Heuvel, D., Gonzalez-Leal, C., Rother, M. B., Van Der Woude, M., González-Prieto, R., Yifrach, A., Parnas, A., Shah, R. G., Kuo, T. T., Boer, D. E. C., Cai, J., Kragten, A., Kim, H.-S., Schärer, O. D., Vertegaal, A. C. O., Shah, G. M., Adar, S., … Luijsterburg, M. S. (2022). XPC–PARP complexes engage the chromatin remodeler ALC1 to catalyze global genome DNA damage repair. *Nature Communications*, *13*(1), 4762. https://doi.org/10.1038/s41467-022-31820-4
- Blessing, C., Mandemaker, I. K., Gonzalez-Leal, C., Preisser, J., Schomburg, A., & Ladurner, A. G. (2020). The Oncogenic Helicase ALC1 Regulates PARP Inhibitor Potency by Trapping PARP2 at DNA Breaks. *Molecular Cell*, *80*(5), 862-875.e6. https://doi.org/10.1016/j.molcel.2020.10.009
- Bork, P., Hofmann, K., Bucher, P., Neuwald, A. F., Altschul, S. F., & Koonin, E. V. (1997). A superfamily of conserved domains in DNA damage- responsive cell cycle checkpoint proteins. *The FASEB Journal*, *11*(1), 68–76. https://doi.org/10.1096/fasebj.11.1.9034168
- Bringmann, P., & Lührmann, R. (1987). Antibodies specific for N^6-methyladenosine react with intact snRNPs U2 and U4/U6. *FEBS Letters*, *213*(2), 309–315. https://doi.org/10.1016/0014-5793(87)81512-0
- Britton, S., Dernoncourt, E., Delteil, C., Froment, C., Schiltz, O., Salles, B., Frit, P., & Calsou, P. (2014). DNA damage triggers SAF-A and RNA biogenesis factors exclusion from chromatin coupled to R-loops removal. *Nucleic Acids Research*, *42*(14), 9047–9062. https://doi.org/10.1093/nar/gku601
- Bryant, H. E., Schultz, N., Thomas, H. D., Parker, K. M., Flower, D., Lopez, E., Kyle, S., Meuth, M., Curtin, N. J., & Helleday, T. (2005). Specific killing of BRCA2-deficient tumours with inhibitors of poly(ADP-ribose) polymerase. *Nature*, *434*(7035), 913–917. https://doi.org/10.1038/nature03443
- Buki, K. G., & Kun, E. (1988). Polypeptide domains of ADP-ribosyltransferase obtained by digestion with plasmin. *Biochemistry*, *27*(16), 5990–5995. https://doi.org/10.1021/bi00416a024
- Bütepage, M., Preisinger, C., Von Kriegsheim, A., Scheufen, A., Lausberg, E., Li, J., Kappes, F., Feederle, R., Ernst, S., Eckei, L., Krieg, S., Müller-Newen, G., Rossetti, G., Feijs, K. L. H., Verheugd, P., & Lüscher, B. (2018). Nucleolar-nucleoplasmic shuttling of TARG1 and its control by DNA damage-induced poly-ADP-ribosylation and by nucleolar transcription. *Scientific Reports*, *8*(1), 6748. https://doi.org/10.1038/s41598-018-25137-w
- Caldecott, K. W., Aoufouchi, S., Johnson, P., & Shall, S. (1996). XRCC1 Polypeptide Interacts with DNA Polymerase and Possibly Poly (ADP-Ribose) Polymerase, and DNA Ligase III Is a Novel Molecular "Nick-Sensor" In Vitro. *Nucleic Acids Research*, *24*(22), 4387–4394. https://doi.org/10.1093/nar/24.22.4387
- Caldecott, K. W., Tucker, J. D., Stanker, L. H., & Thompson, L. H. (1995). Characterization of the XRCC1-DNA ligase III complex *in vitro* and its absence from mutant hamster cells. *Nucleic Acids Research*, *23*(23), 4836–4843. https://doi.org/10.1093/nar/23.23.4836
- Carter-O'Connell, I., Jin, H., Morgan, R. K., David, L. L., & Cohen, M. S. (2014). Engineering the Substrate Specificity of ADP-Ribosyltransferases for Identifying Direct Protein Targets. *Journal of the American Chemical Society*, *136*(14), 5201–5204. https://doi.org/10.1021/ja412897a
- Cesaro, B., Iaiza, A., Piscopo, F., Tarullo, M., Cesari, E., Rotili, D., Mai, A., Diana, A., Londero, M., Del Giacco, L., Masetti, R., Di Leone, A., Naro, C., Masciarelli, S., Fontemaggi, G., Sette, C., Fazi, F., & Fatica, A. (2023). Enhancing sensitivity of triple-negative breast cancer to DNA-damaging therapy through chemical inhibition of the m6A methyltransferase METTL3. *Cancer Communications*, cac2.12509. https://doi.org/10.1002/cac2.12509
- Chaitanya, G. V., Alexander, J. S., & Babu, P. P. (2010). PARP-1 cleavage fragments: Signatures of cell-death proteases in neurodegeneration. *Cell Communication and Signaling*, *8*(1), 31. https://doi.org/10.1186/1478-811X-8-31
- Chambon, P., Weill, J. D., Doly, J., Strosser, M. T., & Mandel, P. (1966). On the formation of a novel adenylic compound by enzymatic extracts of liver nuclei. *Biochemical and Biophysical Research Communications*, *25*(6), 638–643. https://doi.org/10.1016/0006-291X(66)90502-X

- Chambon, P., Weill, J. D., & Mandel, P. (1963). Nicotinamide mononucleotide activation of a new DNA-dependent polyadenylic acid synthesizing nuclear enzyme. *Biochemical and Biophysical Research Communications*, *11*(1), 39–43. https://doi.org/10.1016/0006-291X(63)90024-X
- Chen, C.-C., Kass, E. M., Yen, W.-F., Ludwig, T., Moynahan, M. E., Chaudhuri, J., & Jasin, M. (2017). ATM loss leads to synthetic lethality in BRCA1 BRCT mutant mice associated with exacerbated defects in homology-directed repair. *Proceedings of the National Academy of Sciences*, *114*(29), 7665–7670. https://doi.org/10.1073/pnas.1706392114
- Chen, J., Zhang, Y.-C., Huang, C., Shen, H., Sun, B., Cheng, X., Zhang, Y.-J., Yang, Y.-G., Shu, Q., Yang, Y., & Li, X. (2019). m6A Regulates Neurogenesis and Neuronal Development by Modulating Histone Methyltransferase Ezh2. *Genomics, Proteomics & Bioinformatics*, *17*(2), 154–168. https://doi.org/10.1016/j.gpb.2018.12.007
- Chen, M., Wei, L., Law, C., Tsang, F. H., Shen, J., Cheng, C. L., Tsang, L., Ho, D. W., Chiu, D. K., Lee, J. M., Wong, C. C., Ng, I. O., & Wong, C. (2018). RNA N6-methyladenosine methyltransferase-like 3 promotes liver cancer progression through YTHDF2-dependent post-transcriptional silencing of SOCS2. *Hepatology*, *67*(6), 2254–2270. https://doi.org/10.1002/hep.29683
- Cohen-Armon, M., Visochek, L., Rozensal, D., Kalal, A., Geistrikh, I., Klein, R., Bendetz-Nezer, S., Yao, Z., & Seger, R. (2007). DNA-Independent PARP-1 Activation by Phosphorylated ERK2 Increases Elk1 Activity: A Link to Histone Acetylation. *Molecular Cell*, *25*(2), 297–308. https://doi.org/10.1016/j.molcel.2006.12.012
- Cristini, A., Groh, M., Kristiansen, M. S., & Gromak, N. (2018). RNA/DNA Hybrid Interactome Identifies DXH9 as a Molecular Player in Transcriptional Termination and R-Loop-Associated DNA Damage. *Cell Reports*, *23*(6), 1891–1905. https://doi.org/10.1016/j.celrep.2018.04.025
- Cui, Q., Shi, H., Ye, P., Li, L., Qu, Q., Sun, G., Sun, G., Lu, Z., Huang, Y., Yang, C.-G., Riggs, A. D., He, C., & Shi, Y. (2017). M 6 A RNA Methylation Regulates the Self-Renewal and Tumorigenesis of Glioblastoma Stem Cells. *Cell Reports*, *18*(11), 2622–2634. https://doi.org/10.1016/j.celrep.2017.02.059
- Dai, Q., Moshitch-Moshkovitz, S., Han, D., Kol, N., Amariglio, N., Rechavi, G., Dominissini, D., & He, C. (2017). Nm-seq maps 2′-O-methylation sites in human mRNA with base precision. *Nature Methods*, *14*(7), 695–698. https://doi.org/10.1038/nmeth.4294
- D'Amours, D., Desnoyers, S., D'Silva, I., & Poirier, G. G. (1999). Poly(ADP-ribosyl)ation reactions in the regulation of nuclear functions. *The Biochemical Journal*, *342 (Pt 2)*(Pt 2), 249–268.
- Darzacq, X., Shav-Tal, Y., De Turris, V., Brody, Y., Shenoy, S. M., Phair, R. D., & Singer, R. H. (2007). In vivo dynamics of RNA polymerase II transcription. *Nature Structural & Molecular Biology*, *14*(9), 796–806. https://doi.org/10.1038/nsmb1280
- Das, B. B., Huang, S. N., Murai, J., Rehman, I., Amé, J.-C., Sengupta, S., Das, S. K., Majumdar, P., Zhang, H., Biard, D., Majumder, H. K., Schreiber, V., & Pommier, Y. (2014). PARP1–TDP1 coupling for the repair of topoisomerase I–induced DNA damage. *Nucleic Acids Research*, *42*(7), 4435–4449. https://doi.org/10.1093/nar/gku088
- Das, S. K., Rehman, I., Ghosh, A., Sengupta, S., Majumdar, P., Jana, B., & Das, B. B. (2016). Poly(ADP-ribose) polymers regulate DNA topoisomerase I (Top1) nuclear dynamics and camptothecin sensitivity in living cells. *Nucleic Acids Research*, *44*(17), 8363–8375. https://doi.org/10.1093/nar/gkw665
- Dasovich, M., Beckett, M. Q., Bailey, S., Ong, S.-E., Greenberg, M. M., & Leung, A. K. L. (2021). Identifying Poly(ADP-ribose)-Binding Proteins with Photoaffinity-Based Proteomics. *Journal of the American Chemical Society*, *143*(8), 3037–3042. https://doi.org/10.1021/jacs.0c12246
- Demin, A. A., Hirota, K., Tsuda, M., Adamowicz, M., Hailstone, R., Brazina, J., Gittens, W., Kalasova, I., Shao, Z., Zha, S., Sasanuma, H., Hanzlikova, H., Takeda, S., & Caldecott, K. W. (2021). XRCC1 prevents toxic PARP1 trapping during DNA base excision repair. *Molecular Cell*, *81*(14), 3018-3030.e5. https://doi.org/10.1016/j.molcel.2021.05.009
- Di Giammartino, D. C., Shi, Y., & Manley, J. L. (2013). PARP1 Represses PAP and Inhibits Polyadenylation during Heat Shock. *Molecular Cell*, *49*(1), 7–17. https://doi.org/10.1016/j.molcel.2012.11.005
- Dina, C., Meyre, D., Gallina, S., Durand, E., Körner, A., Jacobson, P., Carlsson, L. M. S., Kiess, W., Vatin, V., Lecoeur, C., Delplanque, J., Vaillant, E., Pattou, F., Ruiz, J., Weill, J., Levy-Marchal, C., Horber, F., Potoczna, N., Hercberg, S., … Froguel, P. (2007). Variation in FTO contributes to childhood obesity and severe adult obesity. *Nature Genetics*, *39*(6), 724–726. https://doi.org/10.1038/ng2048
- Domingo-Prim, J., Endara-Coll, M., Bonath, F., Jimeno, S., Prados-Carvajal, R., Friedländer, M. R., Huertas, P., & Visa, N. (2019). EXOSC10 is required for RPA assembly and

controlled DNA end resection at DNA double-strand breaks. *Nature Communications*, *10*(1), 2135. https://doi.org/10.1038/s41467-019-10153-9

- Dominissini, D., Moshitch-Moshkovitz, S., Schwartz, S., Salmon-Divon, M., Ungar, L., Osenberg, S., Cesarkas, K., Jacob-Hirsch, J., Amariglio, N., Kupiec, M., Sorek, R., & Rechavi, G. (2012). Topology of the human and mouse m6A RNA methylomes revealed by m6A-seq. *Nature*, *485*(7397), 201–206. https://doi.org/10.1038/nature11112
- Du, M., Zhang, Y., Mao, Y., Mou, J., Zhao, J., Xue, Q., Wang, D., Huang, J., Gao, S., & Gao, Y. (2017). MiR-33a suppresses proliferation of NSCLC cells via targeting METTL3 mRNA. *Biochemical and Biophysical Research Communications*, *482*(4), 582–589. https://doi.org/10.1016/j.bbrc.2016.11.077
- Du, W., Huang, Y., Chen, X., Deng, Y., Sun, Y., Yang, H., Shi, Q., Wu, F., Liu, G., Huang, H., Ding, J., Huang, X., & Xu, S. (2024). Discovery of a PROTAC degrader for METTL3-METTL14 complex. *Cell Chemical Biology*, *31*(1), 177-183.e17. https://doi.org/10.1016/j.chembiol.2023.12.009
- Du, Y., Yuan, Y., Xu, L., Zhao, F., Wang, W., Xu, Y., & Tian, X. (2022). Discovery of METTL3 Small Molecule Inhibitors by Virtual Screening of Natural Products. *Frontiers in Pharmacology*, *13*, 878135. https://doi.org/10.3389/fphar.2022.878135
- Duan, M., Liu, H., Xu, S., Yang, Z., Zhang, F., Wang, G., Wang, Y., Zhao, S., & Jiang, X. (2024). IGF2BPs as novel m6A readers: Diverse roles in regulating cancer cell biological functions, hypoxia adaptation, metabolism, and immunosuppressive tumor microenvironment. *Genes & Diseases*, *11*(2), 890–920. https://doi.org/10.1016/j.gendis.2023.06.017
- Duan, Y., Du, A., Gu, J., Duan, G., Wang, C., Gui, X., Ma, Z., Qian, B., Deng, X., Zhang, K., Sun, L., Tian, K., Zhang, Y., Jiang, H., Liu, C., & Fang, Y. (2019). PARylation regulates stress granule dynamics, phase separation, and neurotoxicity of disease-related RNA-binding proteins. *Cell Research*, *29*(3), 233–247. https://doi.org/10.1038/s41422-019-0141-z
- Durkacz, B. W., Irwin, J., & Shall, S. (1981). The Effect of Inhibition of (ADP-ribose) $_n$ Biosynthesis on DNA Repair Assayed by the Nucleoid Technique. *European Journal of Biochemistry*, *121*(1), 65–69. https://doi.org/10.1111/j.1432-1033.1981.tb06430.x
- Durkacz, B. W., Omidiji, O., Gray, D. A., & Shall, S. (1980). (ADP-ribose)n participates in DNA excision repair. *Nature*, *283*(5747), 593–596. https://doi.org/10.1038/283593a0
- El-Khamisy, S. F. (2003). A requirement for PARP-1 for the assembly or stability of XRCC1 nuclear foci at sites of oxidative DNA damage. *Nucleic Acids Research*, *31*(19), 5526–5533. https://doi.org/10.1093/nar/gkg761
- Epanchintsev, A., Costanzo, F., Rauschendorf, M.-A., Caputo, M., Ye, T., Donnio, L.-M., Proietti-de-Santis, L., Coin, F., Laugel, V., & Egly, J.-M. (2017). Cockayne's Syndrome A and B Proteins Regulate Transcription Arrest after Genotoxic Stress by Promoting ATF3 Degradation. *Molecular Cell*, *68*(6), 1054-1066.e6. https://doi.org/10.1016/j.molcel.2017.11.009
- Eustermann, S., Wu, W.-F., Langelier, M.-F., Yang, J.-C., Easton, L. E., Riccio, A. A., Pascal, J. M., & Neuhaus, D. (2015). Structural Basis of Detection and Signaling of DNA Single-Strand Breaks by Human PARP-1. *Molecular Cell*, *60*(5), 742–754. https://doi.org/10.1016/j.molcel.2015.10.032
- Fahrer, J., Kranaster, R., Altmeyer, M., Marx, A., & Bürkle, A. (2007). Quantitative analysis of the binding affinity of poly(ADP-ribose) to specific binding proteins as a function of chain length. *Nucleic Acids Research*, *35*(21), e143–e143. https://doi.org/10.1093/nar/gkm944
- Fan, F., Jin, S., Amundson, S. A., Tong, T., Fan, W., Zhao, H., Zhu, X., Mazzacurati, L., Li, X., Petrik, K. L., Fornace, A. J., Rajasekaran, B., & Zhan, Q. (2002). ATF3 induction following DNA damage is regulated by distinct signaling pathways and over-expression of ATF3 protein suppresses cells growth. *Oncogene*, *21*(49), 7488–7496. https://doi.org/10.1038/sj.onc.1205896
- Farmer, H., McCabe, N., Lord, C. J., Tutt, A. N. J., Johnson, D. A., Richardson, T. B., Santarosa, M., Dillon, K. J., Hickson, I., Knights, C., Martin, N. M. B., Jackson, S. P., Smith, G. C. M., & Ashworth, A. (2005). Targeting the DNA repair defect in BRCA mutant cells as a therapeutic strategy. *Nature*, *434*(7035), 917–921. https://doi.org/10.1038/nature03445
- Ferro, A. M., & Olivera, B. M. (1982). Poly(ADP-ribosylation) in vitro. Reaction parameters and enzyme mechanism. *The Journal of Biological Chemistry*, *257*(13), 7808–7813.
- Francia, S., Michelini, F., Saxena, A., Tang, D., De Hoon, M., Anelli, V., Mione, M., Carninci, P., & d'Adda Di Fagagna, F. (2012). Site-specific DICER and DROSHA RNA products control the DNA-damage response. *Nature*, *488*(7410), 231–235. https://doi.org/10.1038/nature11179
- Frayling, T. M., Timpson, N. J., Weedon, M. N., Zeggini, E., Freathy, R. M., Lindgren, C. M., Perry, J. R. B., Elliott, K. S., Lango, H., Rayner, N. W., Shields, B., Harries, L. W., Barrett, J. C., Ellard, S., Groves, C. J., Knight, B., Patch, A.-M., Ness, A. R., Ebrahim, S., … McCarthy, M. I. (2007). A Common Variant in the *FTO* Gene Is Associated with Body Mass Index and

Predisposes to Childhood and Adult Obesity. *Science*, *316*(5826), 889–894. https://doi.org/10.1126/science.1141634

- Fu, Y., Jia, G., Pang, X., Wang, R. N., Wang, X., Li, C. J., Smemo, S., Dai, Q., Bailey, K. A., Nobrega, M. A., Han, K.-L., Cui, Q., & He, C. (2013). FTO-mediated formation of N6-hydroxymethyladenosine and N6-formyladenosine in mammalian RNA. *Nature Communications*, *4*(1), 1798. https://doi.org/10.1038/ncomms2822
- Fujimoto, M., Takii, R., Katiyar, A., Srivastava, P., & Nakai, A. (2018). Poly(ADP-Ribose) Polymerase 1 Promotes the Human Heat Shock Response by Facilitating Heat Shock Transcription Factor 1 Binding to DNA. *Molecular and Cellular Biology*, *38*(13), e00051-18. https://doi.org/10.1128/MCB.00051-18
- Fujimura, S., Hasegawa, S., Shimizu, Y., & Sugimura, T. (1967). Polymerization of the adenosine 5′-diphosphate-ribose moiety of nicotinamide-adenine dinucleotide by nuclear enzyme. I. Enzymatic reactions. *Biochimica et Biophysica Acta (BBA) - Nucleic Acids and Protein Synthesis*, *145*(2), 247–259. https://doi.org/10.1016/0005-2787(67)90043-3
- Fujimura, S., Hasegawa, S., & Sugimura, T. (1967). Nicotinamide mononucleotide-dependent incorporation of ATP into acidinsoluble material in rat liver nuclei preparation. *Biochimica et Biophysica Acta (BBA) - Nucleic Acids and Protein Synthesis*, *134*(2), 496–499. https://doi.org/10.1016/0005-2787(67)90036-6
- Fustin, J.-M., Doi, M., Yamaguchi, Y., Hida, H., Nishimura, S., Yoshida, M., Isagawa, T., Morioka, M. S., Kakeya, H., Manabe, I., & Okamura, H. (2013). RNA-Methylation-Dependent RNA Processing Controls the Speed of the Circadian Clock. *Cell*, *155*(4), 793–806. https://doi.org/10.1016/j.cell.2013.10.026
- Gagné, J.-P., Hunter, J. M., Labrecque, B., Chabot, B., & Poirier, G. G. (2003). A proteomic approach to the identification of heterogeneous nuclear ribonucleoproteins as a new family of poly(ADP-ribose)-binding proteins. *Biochemical Journal*, *371*(2), 331–340. https://doi.org/10.1042/bj20021675
- Gagné, J.-P., Isabelle, M., Lo, K. S., Bourassa, S., Hendzel, M. J., Dawson, V. L., Dawson, T. M., & Poirier, G. G. (2008). Proteome-wide identification of poly(ADP-ribose) binding proteins and poly(ADP-ribose)-associated protein complexes. *Nucleic Acids Research*, *36*(22), 6959–6976. https://doi.org/10.1093/nar/gkn771
- Gagné, J.-P., Pic, É., Isabelle, M., Krietsch, J., Éthier, C., Paquet, É., Kelly, I., Boutin, M., Moon, K.-M., Foster, L. J., & Poirier, G. G. (2012). Quantitative proteomics profiling of the poly(ADP-ribose)-related response to genotoxic stress. *Nucleic Acids Research*, *40*(16), 7788–7805. https://doi.org/10.1093/nar/gks486
- Gibson, B. A., Zhang, Y., Jiang, H., Hussey, K. M., Shrimp, J. H., Lin, H., Schwede, F., Yu, Y., & Kraus, W. L. (2016). Chemical genetic discovery of PARP targets reveals a role for PARP-1 in transcription elongation. *Science*, *353*(6294), 45–50. https://doi.org/10.1126/science.aaf7865
- Gottschalk, A. J., Timinszky, G., Kong, S. E., Jin, J., Cai, Y., Swanson, S. K., Washburn, M. P., Florens, L., Ladurner, A. G., Conaway, J. W., & Conaway, R. C. (2009). Poly(ADP-ribosyl)ation directs recruitment and activation of an ATP-dependent chromatin remodeler. *Proceedings of the National Academy of Sciences*, *106*(33), 13770–13774. https://doi.org/10.1073/pnas.0906920106
- Gradwohl, G., Ménissier De Murcia, J. M., Molinete, M., Simonin, F., Koken, M., Hoeijmakers, J. H., & De Murcia, G. (1990). The second zinc-finger domain of poly(ADP-ribose) polymerase determines specificity for single-stranded breaks in DNA. *Proceedings of the National Academy of Sciences*, *87*(8), 2990–2994. https://doi.org/10.1073/pnas.87.8.2990
- Guastafierro, T., Cecchinelli, B., Zampieri, M., Reale, A., Riggio, G., Sthandier, O., Zupi, G., Calabrese, L., & Caiafa, P. (2008). CCCTC-binding Factor Activates PARP-1 Affecting DNA Methylation Machinery. *Journal of Biological Chemistry*, *283*(32), 21873–21880. https://doi.org/10.1074/jbc.M801170200
- Guetg, C., Scheifele, F., Rosenthal, F., Hottiger, M. O., & Santoro, R. (2012). Inheritance of Silent rDNA Chromatin Is Mediated by PARP1 via Noncoding RNA. *Molecular Cell*, *45*(6), 790–800. https://doi.org/10.1016/j.molcel.2012.01.024
- Gulati, P., Cheung, M. K., Antrobus, R., Church, C. D., Harding, H. P., Tung, Y.-C. L., Rimmington, D., Ma, M., Ron, D., Lehner, P. J., Ashcroft, F. M., Cox, R. D., Coll, A. P., O'Rahilly, S., & Yeo, G. S. H. (2013). Role for the obesity-related *FTO* gene in the cellular sensing of amino acids. *Proceedings of the National Academy of Sciences*, *110*(7), 2557–2562. https://doi.org/10.1073/pnas.1222796110
- Haince, J.-F., McDonald, D., Rodrigue, A., Déry, U., Masson, J.-Y., Hendzel, M. J., & Poirier, G. G. (2008). PARP1-dependent Kinetics of Recruitment of MRE11 and NBS1 Proteins to Multiple DNA Damage Sites. *Journal of Biological Chemistry*, *283*(2), 1197–1208. https://doi.org/10.1074/jbc.M706734200

- Hasegawa, S., Fujimura, S., Shimizu, Y., & Sugimura, R. (1967). The polymerization of adenosine 5'-diphosphate-ribose moiety of NAD by nuclear enzyme. II. Properties of the reaction product. *Biochimica Et Biophysica Acta*, *149*(2), 369–376.
- Hassa, P. O., & Hottiger, M. O. (2002). The functional role of poly(ADP-ribose)polymerase 1 as novel coactivator of NF-κB in inflammatory disorders. *Cellular and Molecular Life Sciences CMLS*, *59*(9), 1534–1553. https://doi.org/10.1007/s00018-002-8527-2
- Hegde, M. L., Hazra, T. K., & Mitra, S. (2008). Early steps in the DNA base excision/single-strand interruption repair pathway in mammalian cells. *Cell Research*, *18*(1), 27–47. https://doi.org/10.1038/cr.2008.8
- Hewitt, G., Borel, V., Segura-Bayona, S., Takaki, T., Ruis, P., Bellelli, R., Lehmann, L. C., Sommerova, L., Vancevska, A., Tomas-Loba, A., Zhu, K., Cooper, C., Fugger, K., Patel, H., Goldstone, R., Schneider-Luftman, D., Herbert, E., Stamp, G., Brough, R., … Boulton, S. J. (2021). Defective ALC1 nucleosome remodeling confers PARPi sensitization and synthetic lethality with HRD. *Molecular Cell*, *81*(4), 767-783.e11. https://doi.org/10.1016/j.molcel.2020.12.006
- Hoeijmakers, J. H. J. (2001). Genome maintenance mechanisms for preventing cancer. *Nature*, *411*(6835), 366–374. https://doi.org/10.1038/35077232
- Houles, T., Lavoie, G., Nourreddine, S., Cheung, W., Vaillancourt-Jean, É., Guérin, C. M., Bouttier, M., Grondin, B., Lin, S., Saba-El-Leil, M. K., Angers, S., Meloche, S., & Roux, P. P. (2022). CDK12 is hyperactivated and a synthetic-lethal target in BRAF-mutated melanoma. *Nature Communications*, *13*(1), 6457. https://doi.org/10.1038/s41467-022-34179-8
- Hu, L.-Y., Chang, C.-C., Huang, Y.-S., Chou, W.-C., Lin, Y.-M., Ho, C.-C., Chen, W.-T., Shih, H.-M., Hsiung, C.-N., Wu, P.-E., & Shen, C.-Y. (2018). SUMOylation of XRCC1 activated by poly (ADP-ribosyl)ation regulates DNA repair. *Human Molecular Genetics*, *27*(13), 2306–2317. https://doi.org/10.1093/hmg/ddy135
- Huambachano, O., Herrera, F., Rancourt, A., & Satoh, M. S. (2011). Double-stranded DNA binding domain of poly(ADP-ribose) polymerase-1 and molecular insight into the regulation of its activity. *The Journal of Biological Chemistry*, *286*(9), 7149–7160. https://doi.org/10.1074/jbc.M110.175190
- Huang, H., Weng, H., Sun, W., Qin, X., Shi, H., Wu, H., Zhao, B. S., Mesquita, A., Liu, C., Yuan, C. L., Hu, Y.-C., Hüttelmaier, S., Skibbe, J. R., Su, R., Deng, X., Dong, L., Sun, M., Li, C., Nachtergaele, S., … Chen, J. (2018). Recognition of RNA N6-methyladenosine by IGF2BP proteins enhances mRNA stability and translation. *Nature Cell Biology*, *20*(3), 285–295. https://doi.org/10.1038/s41556-018-0045-z
- Huang, H., Weng, H., Zhou, K., Wu, T., Zhao, B. S., Sun, M., Chen, Z., Deng, X., Xiao, G., Auer, F., Klemm, L., Wu, H., Zuo, Z., Qin, X., Dong, Y., Zhou, Y., Qin, H., Tao, S., Du, J., … Chen, J. (2019). Histone H3 trimethylation at lysine 36 guides m6A RNA modification co-transcriptionally. *Nature*, *567*(7748), 414–419. https://doi.org/10.1038/s41586-019-1016-7
- Huang, K., Tidyman, W. E., Le, K.-U. T., Kirsten, E., Kun, E., & Ordahl, C. P. (2004). Analysis of Nucleotide Sequence-Dependent DNA Binding of Poly(ADP-ribose) Polymerase in a Purified System. *Biochemistry*, *43*(1), 217–223. https://doi.org/10.1021/bi0301800
- Ikejima, M., & Gill, D. M. (1988). Poly(ADP-ribose) degradation by glycohydrolase starts with an endonucleolytic incision. *The Journal of Biological Chemistry*, *263*(23), 11037–11040.
- Illuzzi, G., Fouquerel, E., Amé, J.-C., Noll, A., Rehmet, K., Nasheuer, H.-P., Dantzer, F., & Schreiber, V. (2014). PARG is dispensable for recovery from transient replicative stress but required to prevent detrimental accumulation of poly(ADP-ribose) upon prolonged replicative stress. *Nucleic Acids Research*, *42*(12), 7776–7792. https://doi.org/10.1093/nar/gku505
- Isabelle, M., Gagné, J.-P., Gallouzi, I.-E., & Poirier, G. G. (2012). Quantitative proteomics and dynamic imaging reveal that G3BP-mediated stress granule assembly is poly(ADP-ribose)-dependent following exposure to MNNG-induced DNA alkylation. *Journal of Cell Science*, jcs.106963. https://doi.org/10.1242/jcs.106963
- Isabelle, M., Moreel, X., Gagné, J.-P., Rouleau, M., Ethier, C., Gagné, P., Hendzel, M. J., & Poirier, G. G. (2010). Investigation of PARP-1, PARP-2, and PARG interactomes by affinity-purification mass spectrometry. *Proteome Science*, *8*(1), 22. https://doi.org/10.1186/1477-5956-8-22
- Izhar, L., Adamson, B., Ciccia, A., Lewis, J., Pontano-Vaites, L., Leng, Y., Liang, A. C., Westbrook, T. F., Harper, J. W., & Elledge, S. J. (2015). A Systematic Analysis of Factors Localized to Damaged Chromatin Reveals PARP-Dependent Recruitment of Transcription Factors. *Cell Reports*, *11*(9), 1486–1500. https://doi.org/10.1016/j.celrep.2015.04.053
- Jain, A., Bacolla, A., Del Mundo, I. M., Zhao, J., Wang, G., & Vasquez, K. M. (2013). DHX9 helicase is involved in preventing genomic instability induced by alternatively structured DNA in human cells. *Nucleic Acids Research*, *41*(22), 10345–10357. https://doi.org/10.1093/nar/gkt804

- Jain, A. K. (2020). Emerging roles of long non-coding RNAs in the p53 network. *RNA Biology*, *17*(11), 1648–1656. https://doi.org/10.1080/15476286.2020.1770981
- Janicki, S. M., Tsukamoto, T., Salghetti, S. E., Tansey, W. P., Sachidanandam, R., Prasanth, K. V., Ried, T., Shav-Tal, Y., Bertrand, E., Singer, R. H., & Spector, D. L. (2004). From Silencing to Gene Expression. *Cell*, *116*(5), 683–698. https://doi.org/10.1016/S0092-8674(04)00171-0
- Ji, Y., & Tulin, A. V. (2009). Poly(ADP-ribosyl)ation of heterogeneous nuclear ribonucleoproteins modulates splicing. *Nucleic Acids Research*, *37*(11), 3501–3513. https://doi.org/10.1093/nar/gkp218
- Jia, G., Fu, Y., Zhao, X., Dai, Q., Zheng, G., Yang, Y., Yi, C., Lindahl, T., Pan, T., Yang, Y.-G., & He, C. (2011). N6-Methyladenosine in nuclear RNA is a major substrate of the obesity-associated FTO. *Nature Chemical Biology*, *7*(12), 885–887. https://doi.org/10.1038/nchembio.687
- Juarez-Salinas, H., Sims, J. L., & Jacobson, M. K. (1979). Poly(ADP-ribose) levels in carcinogen-treated cells. *Nature*, *282*(5740), 740–741. https://doi.org/10.1038/282740a0
- Juhász, S., Smith, R., Schauer, T., Spekhardt, D., Mamar, H., Zentout, S., Chapuis, C., Huet, S., & Timinszky, G. (2020). The chromatin remodeler ALC1 underlies resistance to PARP inhibitor treatment. *Science Advances*, *6*(51), eabb8626. https://doi.org/10.1126/sciadv.abb8626
- Jungmichel, S., Rosenthal, F., Altmeyer, M., Lukas, J., Hottiger, M. O., & Nielsen, M. L. (2013). Proteome-wide Identification of Poly(ADP-Ribosyl)ation Targets in Different Genotoxic Stress Responses. *Molecular Cell*, *52*(2), 272–285. https://doi.org/10.1016/j.molcel.2013.08.026
- Kalesh, K., Lukauskas, S., Borg, A. J., Snijders, A. P., Ayyappan, V., Leung, A. K. L., Haskard, D. O., & DiMaggio, P. A. (2019). An Integrated Chemical Proteomics Approach for Quantitative Profiling of Intracellular ADP-Ribosylation. *Scientific Reports*, *9*(1), 6655. https://doi.org/10.1038/s41598-019-43154-1
- Kang, H. J., Cheon, N. Y., Park, H., Jeong, G. W., Ye, B. J., Yoo, E. J., Lee, J. H., Hur, J.-H., Lee, E.-A., Kim, H., Lee, K., Choi, S. Y., Lee-Kwon, W., Myung, K., Lee, J. Y., & Kwon, H. M. (2021). TonEBP recognizes R-loops and initiates m6A RNA methylation for R-loop resolution. *Nucleic Acids Research*, *49*(1), 269–284. https://doi.org/10.1093/nar/gkaa1162
- Karras, G. I., Kustatscher, G., Buhecha, H. R., Allen, M. D., Pugieux, C., Sait, F., Bycroft, M., & Ladurner, A. G. (2005). The macro domain is an ADP-ribose binding module. *The EMBO Journal*, *24*(11), 1911–1920. https://doi.org/10.1038/sj.emboj.7600664
- Ke, Y., Han, Y., Guo, X., Wen, J., Wang, K., Jiang, X., Tian, X., Ba, X., Boldogh, I., & Zeng, X. (2017). PARP1 promotes gene expression at the post-transcriptional level by modulating the RNA-binding protein HuR. *Nature Communications*, *8*(1), 14632. https://doi.org/10.1038/ncomms14632
- Khurana, S., Kruhlak, M. J., Kim, J., Tran, A. D., Liu, J., Nyswaner, K., Shi, L., Jailwala, P., Sung, M.-H., Hakim, O., & Oberdoerffer, P. (2014). A Macrohistone Variant Links Dynamic Chromatin Compaction to BRCA1-Dependent Genome Maintenance. *Cell Reports*, *8*(4), 1049–1062. https://doi.org/10.1016/j.celrep.2014.07.024
- Kim, D.-S., Camacho, C. V., Nagari, A., Malladi, V. S., Challa, S., & Kraus, W. L. (2019). Activation of PARP-1 by snoRNAs Controls Ribosome Biogenesis and Cell Growth via the RNA Helicase DDX21. *Molecular Cell*, *75*(6), 1270-1285.e14. https://doi.org/10.1016/j.molcel.2019.06.020
- Knuckles, P., Carl, S. H., Musheev, M., Niehrs, C., Wenger, A., & Bühler, M. (2017). RNA fate determination through cotranscriptional adenosine methylation and microprocessor binding. *Nature Structural & Molecular Biology*, *24*(7), 561–569. https://doi.org/10.1038/nsmb.3419
- Knuckles, P., Lence, T., Haussmann, I. U., Jacob, D., Kreim, N., Carl, S. H., Masiello, I., Hares, T., Villaseñor, R., Hess, D., Andrade-Navarro, M. A., Biggiogera, M., Helm, M., Soller, M., Bühler, M., & Roignant, J.-Y. (2018). Zc3h13/Flacc is required for adenosine methylation by bridging the mRNA-binding factor Rbm15/Spenito to the m ^{6} A machinery component Wtap/Fl(2)d. *Genes & Development*, *32*(5–6), 415–429. https://doi.org/10.1101/gad.309146.117
- Kotake, Y., Kitagawa, K., Ohhata, T., Sakai, S., Uchida, C., Niida, H., Naemura, M., & Kitagawa, M. (2016). Long Non-coding RNA, PANDA, Contributes to the Stabilization of p53 Tumor Suppressor Protein. *Anticancer Research*, *36*(4), 1605–1611.
- Kotova, E., Jarnik, M., & Tulin, A. V. (2010). Uncoupling of the transactivation and transrepression functions of PARP1 protein. *Proceedings of the National Academy of Sciences*, *107*(14), 6406–6411. https://doi.org/10.1073/pnas.0914152107
- Kozaki, T., Komano, J., Kanbayashi, D., Takahama, M., Misawa, T., Satoh, T., Takeuchi, O., Kawai, T., Shimizu, S., Matsuura, Y., Akira, S., & Saitoh, T. (2017). Mitochondrial damage

elicits a TCDD-inducible poly(ADP-ribose) polymerase-mediated antiviral response. *Proceedings of the National Academy of Sciences*, *114*(10), 2681–2686. https://doi.org/10.1073/pnas.1621508114

- Kozlowski, M., Corujo, D., Hothorn, M., Guberovic, I., Mandemaker, I. K., Blessing, C., Sporn, J., Gutierrez-Triana, A., Smith, R., Portmann, T., Treier, M., Scheffzek, K., Huet, S., Timinszky, G., Buschbeck, M., & Ladurner, A. G. (2018). MacroH2A histone variants limit chromatin plasticity through two distinct mechanisms. *EMBO Reports*, *19*(10), e44445. https://doi.org/10.15252/embr.201744445
- Kraus, W. L. (2015). PARPs and ADP-Ribosylation: 50 Years … and Counting. *Molecular Cell*, *58*(6), 902–910. https://doi.org/10.1016/j.molcel.2015.06.006
- Krietsch, J., Caron, M.-C., Gagné, J.-P., Ethier, C., Vignard, J., Vincent, M., Rouleau, M., Hendzel, M. J., Poirier, G. G., & Masson, J.-Y. (2012). PARP activation regulates the RNA-binding protein NONO in the DNA damage response to DNA double-strand breaks. *Nucleic Acids Research*, *40*(20), 10287–10301. https://doi.org/10.1093/nar/gks798
- Krishnakumar, R., Gamble, M. J., Frizzell, K. M., Berrocal, J. G., Kininis, M., & Kraus, W. L. (2008). Reciprocal Binding of PARP-1 and Histone H1 at Promoters Specifies Transcriptional Outcomes. *Science*, *319*(5864), 819–821. https://doi.org/10.1126/science.1149250
- Krishnakumar, R., & Kraus, W. L. (2010). PARP-1 Regulates Chromatin Structure and Transcription through a KDM5B-Dependent Pathway. *Molecular Cell*, *39*(5), 736–749. https://doi.org/10.1016/j.molcel.2010.08.014
- Kubota, Y., Nash, R. A., Klungland, A., Schär, P., Barnes, D. E., & Lindahl, T. (1996). Reconstitution of DNA base excision-repair with purified human proteins: Interaction between DNA polymerase beta and the XRCC1 protein. *The EMBO Journal*, *15*(23), 6662–6670.
- Kurl, R. N., & Jacob, S. T. (1985). Characterization of a factor that can prevent random transcription of cloned rDNA and its probable relationship to poly(ADP-ribose) polymerase. *Nucleic Acids Research*, *13*(1), 89–101. https://doi.org/10.1093/nar/13.1.89
- Langelier, M.-F., Billur, R., Sverzhinsky, A., Black, B. E., & Pascal, J. M. (2021). HPF1 dynamically controls the PARP1/2 balance between initiating and elongating ADP-ribose modifications. *Nature Communications*, *12*(1), 6675. https://doi.org/10.1038/s41467-021-27043-8
- Langelier, M.-F., Eisemann, T., Riccio, A. A., & Pascal, J. M. (2018). PARP family enzymes: Regulation and catalysis of the poly(ADP-ribose) posttranslational modification. *Current Opinion in Structural Biology*, *53*, 187–198. https://doi.org/10.1016/j.sbi.2018.11.002
- Langelier, M.-F., & Pascal, J. M. (2013). PARP-1 mechanism for coupling DNA damage detection to poly(ADP-ribose) synthesis. *Current Opinion in Structural Biology*, *23*(1), 134–143. https://doi.org/10.1016/j.sbi.2013.01.003
- Langelier, M.-F., Planck, J. L., Roy, S., & Pascal, J. M. (2012). Structural Basis for DNA Damage–Dependent Poly(ADP-ribosyl)ation by Human PARP-1. *Science*, *336*(6082), 728–732. https://doi.org/10.1126/science.1216338
- Langelier, M.-F., Ruhl, D. D., Planck, J. L., Kraus, W. L., & Pascal, J. M. (2010). The Zn3 Domain of Human Poly(ADP-ribose) Polymerase-1 (PARP-1) Functions in Both DNA-dependent Poly(ADP-ribose) Synthesis Activity and Chromatin Compaction. *Journal of Biological Chemistry*, *285*(24), 18877–18887. https://doi.org/10.1074/jbc.M110.105668
- Lans, H., & Vermeulen, W. (2011). Nucleotide Excision Repair in *Caenorhabditis elegans*. *Molecular Biology International*, *2011*, 1–12. https://doi.org/10.4061/2011/542795
- Laspata, N., Kaur, P., Mersaoui, S. Y., Muoio, D., Liu, Z. S., Bannister, M. H., Nguyen, H. D., Curry, C., Pascal, J. M., Poirier, G. G., Wang, H., Masson, J.-Y., & Fouquerel, E. (2023). PARP1 associates with R-loops to promote their resolution and genome stability. *Nucleic Acids Research*, *51*(5), 2215–2237. https://doi.org/10.1093/nar/gkad066
- Lee, J.-H., Ryu, S. W., Ender, N. A., & Paull, T. T. (2021). Poly-ADP-ribosylation drives loss of protein homeostasis in ATM and Mre11 deficiency. *Molecular Cell*, *81*(7), 1515-1533.e5. https://doi.org/10.1016/j.molcel.2021.01.019
- Leung, A. K. L., Griffin, D. E., Bosch, J., & Fehr, A. R. (2022). The Conserved Macrodomain Is a Potential Therapeutic Target for Coronaviruses and Alphaviruses. *Pathogens*, *11*(1), 94. https://doi.org/10.3390/pathogens11010094
- Li, E., Xia, M., Du, Y., Long, K., Ji, F., Pan, F., He, L., Hu, Z., & Guo, Z. (2022). METTL3 promotes homologous recombination repair and modulates chemotherapeutic response in breast cancer by regulating the EGF/RAD51 axis. *eLife*, *11*, e75231. https://doi.org/10.7554/eLife.75231
- Li, F., Zhao, D., Wu, J., & Shi, Y. (2014). Structure of the YTH domain of human YTHDF2 in complex with an m6A mononucleotide reveals an aromatic cage for m6A recognition. *Cell Research*, *24*(12), 1490–1492. https://doi.org/10.1038/cr.2014.153
- Li, L., Monckton, E. A., & Godbout, R. (2008). A Role for DEAD Box 1 at DNA Double-Strand Breaks. *Molecular and Cellular Biology*, *28*(20), 6413–6425. https://doi.org/10.1128/MCB.01053-08

- Li, S., Wang, L., Wang, Y., Zhang, C., Hong, Z., & Han, Z. (2022). The synthetic lethality of targeting cell cycle checkpoints and PARPs in cancer treatment. *Journal of Hematology & Oncology*, *15*(1), 147. https://doi.org/10.1186/s13045-022-01360-x
- Li, X., & Heyer, W.-D. (2008). Homologous recombination in DNA repair and DNA damage tolerance. *Cell Research*, *18*(1), 99–113. https://doi.org/10.1038/cr.2008.1
- Li, Y., Cheng, X., Chen, Y., Zhou, T., Li, D., & Zheng, W. V. (2021). METTL3 facilitates the progression of hepatocellular carcinoma by modulating the m6A level of USP7. *American Journal of Translational Research*, *13*(12), 13423–13437.
- Lieber, M. R. (2010). The Mechanism of Double-Strand DNA Break Repair by the Nonhomologous DNA End-Joining Pathway. *Annual Review of Biochemistry*, *79*(1), 181–211. https://doi.org/10.1146/annurev.biochem.052308.093131
- Lima-Bessa, K. M. D., Armelini, M. G., Chiganças, V., Jacysyn, J. F., Amarante-Mendes, G. P., Sarasin, A., & Menck, C. F. M. (2008). CPDs and 6-4PPs play different roles in UV-induced cell death in normal and NER-deficient human cells. *DNA Repair*, *7*(2), 303–312. https://doi.org/10.1016/j.dnarep.2007.11.003
- Limoli, C. L., & Ward, J. F. (1993). A New Method for Introducing Double-Strand Breaks into Cellular DNA. *Radiation Research*, *134*(2), 160. https://doi.org/10.2307/3578455
- Lin, W.-L., Chen, J.-K., Wen, X., He, W., Zarceno, G. A., Chen, Y., Chen, S., Paull, T. T., & Liu, H. (2022). DDX18 prevents R-loop-induced DNA damage and genome instability via PARP-1. *Cell Reports*, *40*(3), 111089. https://doi.org/10.1016/j.celrep.2022.111089
- Lin, Z., Hsu, P. J., Xing, X., Fang, J., Lu, Z., Zou, Q., Zhang, K.-J., Zhang, X., Zhou, Y., Zhang, T., Zhang, Y., Song, W., Jia, G., Yang, X., He, C., & Tong, M.-H. (2017). Mettl3-/Mettl14-mediated mRNA N6-methyladenosine modulates murine spermatogenesis. *Cell Research*, *27*(10), 1216–1230. https://doi.org/10.1038/cr.2017.117
- Littlefield, J. W., & Dunn, D. B. (1958). Natural Occurrence of Thymine and Three Methylated Adenine Bases in Several Ribonucleic Acids. *Nature*, *181*(4604), 254–255. https://doi.org/10.1038/181254a0
- Liu, J., Li, K., Cai, J., Zhang, M., Zhang, X., Xiong, X., Meng, H., Xu, X., Huang, Z., Peng, J., Fan, J., & Yi, C. (2020). Landscape and Regulation of m6A and m6Am Methylome across Human and Mouse Tissues. *Molecular Cell*, *77*(2), 426-440.e6. https://doi.org/10.1016/j.molcel.2019.09.032
- Liu, J., Yue, Y., Han, D., Wang, X., Fu, Y., Zhang, L., Jia, G., Yu, M., Lu, Z., Deng, X., Dai, Q., Chen, W., & He, C. (2014). A METTL3–METTL14 complex mediates mammalian nuclear RNA N6-adenosine methylation. *Nature Chemical Biology*, *10*(2), 93–95. https://doi.org/10.1038/nchembio.1432
- Liu, X.-M., Mao, Y., Wang, S., Zhou, J., & Qian, S.-B. (2022). METTL3 modulates chromatin and transcription dynamics during cell fate transition. *Cellular and Molecular Life Sciences*, *79*(11), 559. https://doi.org/10.1007/s00018-022-04590-x
- Ljungman, M., & Zhang, F. (1996). Blockage of RNA polymerase as a possible trigger for u.v. Light-induced apoptosis. *Oncogene*, *13*(4), 823–831.
- Lord, C. J., & Ashworth, A. (2016). BRCAness revisited. *Nature Reviews Cancer*, *16*(2), 110–120. https://doi.org/10.1038/nrc.2015.21
- Lu, W.-T., Hawley, B. R., Skalka, G. L., Baldock, R. A., Smith, E. M., Bader, A. S., Malewicz, M., Watts, F. Z., Wilczynska, A., & Bushell, M. (2018). Drosha drives the formation of DNA:RNA hybrids around DNA break sites to facilitate DNA repair. *Nature Communications*, *9*(1), 532. https://doi.org/10.1038/s41467-018-02893-x
- Ludwig, A., Behnke, B., Holtlund, J., & Hilz, H. (1988). Immunoquantitation and size determination of intrinsic poly(ADP-ribose) polymerase from acid precipitates. An analysis of the in vivo status in mammalian species and in lower eukaryotes. *The Journal of Biological Chemistry*, *263*(15), 6993–6999.
- Luijsterburg, M. S., de Krijger, I., Wiegant, W. W., Shah, R. G., Smeenk, G., de Groot, A. J. L., Pines, A., Vertegaal, A. C. O., Jacobs, J. J. L., Shah, G. M., & van Attikum, H. (2016). PARP1 Links CHD2-Mediated Chromatin Expansion and H3.3 Deposition to DNA Repair by Non-homologous End-Joining. *Molecular Cell*, *61*(4), 547–562. https://doi.org/10.1016/j.molcel.2016.01.019
- Lupey-Green, L. N., Caruso, L. B., Madzo, J., Martin, K. A., Tan, Y., Hulse, M., & Tempera, I. (2018). PARP1 Stabilizes CTCF Binding and Chromatin Structure To Maintain Epstein-Barr Virus Latency Type. *Journal of Virology*, *92*(18), e00755-18. https://doi.org/10.1128/JVI.00755-18
- Lüscher, B., Bütepage, M., Eckei, L., Krieg, S., Verheugd, P., & Shilton, B. H. (2018). ADP-Ribosylation, a Multifaceted Posttranslational Modification Involved in the Control of Cell Physiology in Health and Disease. *Chemical Reviews*, *118*(3), 1092–1136. https://doi.org/10.1021/acs.chemrev.7b00122

- Mah, L.-J., El-Osta, A., & Karagiannis, T. C. (2010). γH2AX: A sensitive molecular marker of DNA damage and repair. *Leukemia*, *24*(4), 679–686. https://doi.org/10.1038/leu.2010.6
- Malanga, M., Czubaty, A., Girstun, A., Staron, K., & Althaus, F. R. (2008). Poly(ADP-ribose) Binds to the Splicing Factor ASF/SF2 and Regulates Its Phosphorylation by DNA Topoisomerase I. *Journal of Biological Chemistry*, *283*(29), 19991–19998. https://doi.org/10.1074/jbc.M709495200
- Mamontova, E. M., Clément, M.-J., Sukhanova, M. V., Joshi, V., Bouhss, A., Rengifo-Gonzalez, J. C., Desforges, B., Hamon, L., Lavrik, O. I., & Pastré, D. (2023). FUS RRM regulates poly(ADP-ribose) levels after transcriptional arrest and PARP-1 activation on DNA damage. *Cell Reports*, *42*(10), 113199. https://doi.org/10.1016/j.celrep.2023.113199
- Mandemaker, I. K., Zhou, D., Bruens, S. T., Dekkers, D. H., Verschure, P. J., Edupuganti, R. R., Meshorer, E., Demmers, J. A., & Marteijn, J. A. (2020). Histone H1 eviction by the histone chaperone SET reduces cell survival following DNA damage. *Journal of Cell Science*, jcs.235473. https://doi.org/10.1242/jcs.235473
- Marchand, V., Blanloeil-Oillo, F., Helm, M., & Motorin, Y. (2016). Illumina-based RiboMethSeq approach for mapping of 2′-O-Me residues in RNA. *Nucleic Acids Research*, *44*(16), e135–e135. https://doi.org/10.1093/nar/gkw547
- Marechal, A., & Zou, L. (2013). DNA Damage Sensing by the ATM and ATR Kinases. *Cold Spring Harbor Perspectives in Biology*, *5*(9), a012716–a012716. https://doi.org/10.1101/cshperspect.a012716
- Marin-Vicente, C., Domingo-Prim, J., Eberle, A. B., & Visa, N. (2015). RRP6/EXOSC10 is required for the repair of DNA double-strand breaks by homologous recombination. *Journal of Cell Science*, jcs.158733. https://doi.org/10.1242/jcs.158733
- Marsischky, G. T., Wilson, B. A., & Collier, R. J. (1995). Role of Glutamic Acid 988 of Human Poly-ADP-ribose Polymerase in Polymer Formation. *Journal of Biological Chemistry*, *270*(7), 3247–3254. https://doi.org/10.1074/jbc.270.7.3247
- Marteijn, J. A., Lans, H., Vermeulen, W., & Hoeijmakers, J. H. J. (2014). Understanding nucleotide excision repair and its roles in cancer and ageing. *Nature Reviews Molecular Cell Biology*, *15*(7), 465–481. https://doi.org/10.1038/nrm3822
- Masaoka, A., Gassman, N. R., Kedar, P. S., Prasad, R., Hou, E. W., Horton, J. K., Bustin, M., & Wilson, S. H. (2012). HMGN1 Protein Regulates Poly(ADP-ribose) Polymerase-1 (PARP-1) Self-PARylation in Mouse Fibroblasts. *Journal of Biological Chemistry*, *287*(33), 27648–27658. https://doi.org/10.1074/jbc.M112.370759
- Matsumoto, M., Yaginuma, K., Igarashi, A., Imura, M., Hasegawa, M., Iwabuchi, K., Date, T., Mori, T., Ishizaki, K., Yamashita, K., Inobe, M., & Matsunaga, T. (2007). Perturbed gap-filling synthesis in nucleotide excision repair causes histone H2AX phosphorylation in human quiescent cells. *Journal of Cell Science*, *120*(6), 1104–1112. https://doi.org/10.1242/jcs.03391
- Matveeva, E. A., Al-Tinawi, Q. M. H., Rouchka, E. C., & Fondufe-Mittendorf, Y. N. (2019). Coupling of PARP1-mediated chromatin structural changes to transcriptional RNA polymerase II elongation and cotranscriptional splicing. *Epigenetics & Chromatin*, *12*(1), 15. https://doi.org/10.1186/s13072-019-0261-1
- Matveeva, E., Maiorano, J., Zhang, Q., Eteleeb, A. M., Convertini, P., Chen, J., Infantino, V., Stamm, S., Wang, J., Rouchka, E. C., & Fondufe-Mittendorf, Y. N. (2016). Involvement of PARP1 in the regulation of alternative splicing. *Cell Discovery*, *2*(1), 15046. https://doi.org/10.1038/celldisc.2015.46
- Mayne, L. V., & Lehmann, A. R. (1982). Failure of RNA synthesis to recover after UV irradiation: An early defect in cells from individuals with Cockayne's syndrome and xeroderma pigmentosum. *Cancer Research*, *42*(4), 1473–1478.
- Meiser, N., Mench, N., & Hengesbach, M. (2020). RNA secondary structure dependence in METTL3–METTL14 mRNA methylation is modulated by the N-terminal domain of METTL3. *Biological Chemistry*, *402*(1), 89–98. https://doi.org/10.1515/hsz-2020-0265
- Meyer, K. D., Patil, D. P., Zhou, J., Zinoviev, A., Skabkin, M. A., Elemento, O., Pestova, T. V., Qian, S.-B., & Jaffrey, S. R. (2015). 5′ UTR m6A Promotes Cap-Independent Translation. *Cell*, *163*(4), 999–1010. https://doi.org/10.1016/j.cell.2015.10.012
- Meyer, K. D., Saletore, Y., Zumbo, P., Elemento, O., Mason, C. E., & Jaffrey, S. R. (2012). Comprehensive Analysis of mRNA Methylation Reveals Enrichment in 3′ UTRs and near Stop Codons. *Cell*, *149*(7), 1635–1646. https://doi.org/10.1016/j.cell.2012.05.003
- Michelini, F., Pitchiaya, S., Vitelli, V., Sharma, S., Gioia, U., Pessina, F., Cabrini, M., Wang, Y., Capozzo, I., Iannelli, F., Matti, V., Francia, S., Shivashankar, G. V., Walter, N. G., & d'Adda Di Fagagna, F. (2017). Damage-induced lncRNAs control the DNA damage response through interaction with DDRNAs at individual double-strand breaks. *Nature Cell Biology*, *19*(12), 1400–1411. https://doi.org/10.1038/ncb3643
- Min, W., Bruhn, C., Grigaravicius, P., Zhou, Z.-W., Li, F., Krüger, A., Siddeek, B., Greulich, K.-O., Popp, O., Meisezahl, C., Calkhoven, C. F., Bürkle, A., Xu, X., & Wang, Z.-Q. (2013).

Poly(ADP-ribose) binding to Chk1 at stalled replication forks is required for S-phase checkpoint activation. *Nature Communications*, *4*(1), 2993. https://doi.org/10.1038/ncomms3993
- Miranda, E. A., Dantzer, F., Ofarrell, M., Demurcia, G., & Demurcia, J. M. (1995). Characterization of a Gain-of-Function Mutant of Poly(ADP-Ribose) Polymerase. *Biochemical and Biophysical Research Communications*, *212*(2), 317–325. https://doi.org/10.1006/bbrc.1995.1972
- Miwa, M., Tanaka, M., Matsushima, T., & Sugimura, T. (1974). Purification and properties of glycohydrolase from calf thymus splitting ribose-ribose linkages of poly(adenosine diphosphate ribose). *The Journal of Biological Chemistry*, *249*(11), 3475–3482.
- Mortusewicz, O., Fouquerel, E., Amé, J.-C., Leonhardt, H., & Schreiber, V. (2011). PARG is recruited to DNA damage sites through poly(ADP-ribose)- and PCNA-dependent mechanisms. *Nucleic Acids Research*, *39*(12), 5045–5056. https://doi.org/10.1093/nar/gkr099
- Müller, S., Glaß, M., Singh, A. K., Haase, J., Bley, N., Fuchs, T., Lederer, M., Dahl, A., Huang, H., Chen, J., Posern, G., & Hüttelmaier, S. (2019). IGF2BP1 promotes SRF-dependent transcription in cancer in a m6A- and miRNA-dependent manner. *Nucleic Acids Research*, *47*(1), 375–390. https://doi.org/10.1093/nar/gky1012
- Munnur, D., Bartlett, E., Mikolčević, P., Kirby, I. T., Rack, J. G. M., Mikoč, A., Cohen, M. S., & Ahel, I. (2019). Reversible ADP-ribosylation of RNA. *Nucleic Acids Research*, *47*(11), 5658–5669. https://doi.org/10.1093/nar/gkz305
- Murai, J., Huang, S. N., Das, B. B., Renaud, A., Zhang, Y., Doroshow, J. H., Ji, J., Takeda, S., & Pommier, Y. (2012). Trapping of PARP1 and PARP2 by Clinical PARP Inhibitors. *Cancer Research*, *72*(21), 5588–5599. https://doi.org/10.1158/0008-5472.CAN-12-2753
- Nalabothula, N., Al-jumaily, T., Eteleeb, A. M., Flight, R. M., Xiaorong, S., Moseley, H., Rouchka, E. C., & Fondufe-Mittendorf, Y. N. (2015). Genome-Wide Profiling of PARP1 Reveals an Interplay with Gene Regulatory Regions and DNA Methylation. *PLOS ONE*, *10*(8), e0135410. https://doi.org/10.1371/journal.pone.0135410
- Nash, R. A., Caldecott, K. W., Barnes, D. E., & Lindahl, T. (1997). XRCC1 Protein Interacts with One of Two Distinct Forms of DNA Ligase III. *Biochemistry*, *36*(17), 5207–5211. https://doi.org/10.1021/bi962281m
- Naumenko, K. N., Sukhanova, M. V., Hamon, L., Kurgina, T. A., Alemasova, E. E., Kutuzov, M. M., Pastré, D., & Lavrik, O. I. (2020). Regulation of Poly(ADP-Ribose) Polymerase 1 Activity by Y-Box-Binding Protein 1. *Biomolecules*, *10*(9), 1325. https://doi.org/10.3390/biom10091325
- Naumenko, K. N., Sukhanova, M. V., Hamon, L., Kurgina, T. A., Anarbaev, R. O., Mangerich, A., Pastré, D., & Lavrik, O. I. (2022). The C-Terminal Domain of Y-Box Binding Protein 1 Exhibits Structure-Specific Binding to Poly(ADP-Ribose), Which Regulates PARP1 Activity. *Frontiers in Cell and Developmental Biology*, *10*, 831741. https://doi.org/10.3389/fcell.2022.831741
- Nguyen, V. (1996). In vivo degradation of RNA polymerase II largest subunit triggered by alpha-amanitin. *Nucleic Acids Research*, *24*(15), 2924–2929. https://doi.org/10.1093/nar/24.15.2924
- Nishizuka, Y., Ueda, K., Nakazawa, K., & Hayaishi, O. (1967). Studies on the polymer of adenosine diphosphate ribose. I. Enzymic formation from nicotinamide adenine dinuclotide in mammalian nuclei. *The Journal of Biological Chemistry*, *242*(13), 3164–3171.
- Nusinow, D. A., Hernández-Muñoz, I., Fazzio, T. G., Shah, G. M., Kraus, W. L., & Panning, B. (2007). Poly(ADP-ribose) Polymerase 1 Is Inhibited by a Histone H2A Variant, MacroH2A, and Contributes to Silencing of the Inactive X Chromosome. *Journal of Biological Chemistry*, *282*(17), 12851–12859. https://doi.org/10.1074/jbc.M610502200
- Ohnishi, T., Mori, E., & Takahashi, A. (2009). DNA double-strand breaks: Their production, recognition, and repair in eukaryotes. *Mutation Research/Fundamental and Molecular Mechanisms of Mutagenesis*, *669*(1–2), 8–12. https://doi.org/10.1016/j.mrfmmm.2009.06.010
- Okano, S., Lan, L., Caldecott, K. W., Mori, T., & Yasui, A. (2003). Spatial and Temporal Cellular Responses to Single-Strand Breaks in Human Cells. *Molecular and Cellular Biology*, *23*(11), 3974–3981. https://doi.org/10.1128/MCB.23.11.3974-3981.2003
- Olivieri, M., Cho, T., Álvarez-Quilón, A., Li, K., Schellenberg, M. J., Zimmermann, M., Hustedt, N., Rossi, S. E., Adam, S., Melo, H., Heijink, A. M., Sastre-Moreno, G., Moatti, N., Szilard, R. K., McEwan, A., Ling, A. K., Serrano-Benitez, A., Ubhi, T., Feng, S., … Durocher, D. (2020). A Genetic Map of the Response to DNA Damage in Human Cells. *Cell*, *182*(2), 481-496.e21. https://doi.org/10.1016/j.cell.2020.05.040
- Padella, A., Ghelli Luserna Di Rorà, A., Marconi, G., Ghetti, M., Martinelli, G., & Simonetti, G. (2022). Targeting PARP proteins in acute leukemia: DNA damage response inhibition and therapeutic strategies. *Journal of Hematology & Oncology*, *15*(1), 10. https://doi.org/10.1186/s13045-022-01228-0

- Palavalli Parsons, L. H., Challa, S., Gibson, B. A., Nandu, T., Stokes, M. S., Huang, D., Lea, J. S., & Kraus, W. L. (2021). Identification of PARP-7 substrates reveals a role for MARylation in microtubule control in ovarian cancer cells. *eLife*, *10*, e60481. https://doi.org/10.7554/eLife.60481
- Patil, D. P., Chen, C.-K., Pickering, B. F., Chow, A., Jackson, C., Guttman, M., & Jaffrey, S. R. (2016). m6A RNA methylation promotes XIST-mediated transcriptional repression. *Nature*, *537*(7620), 369–373. https://doi.org/10.1038/nature19342
- Pehrson, J. R., & Fried, V. A. (1992). MacroH2A, a Core Histone Containing a Large Nonhistone Region. *Science*, *257*(5075), 1398–1400. https://doi.org/10.1126/science.1529340
- Peng, C., Hu, W., Weng, X., Tong, R., Cheng, S., Ding, C., Xiao, H., Lv, Z., Xie, H., Zhou, L., Wu, J., & Zheng, S. (2017). Over Expression of Long Non-Coding RNA PANDA Promotes Hepatocellular Carcinoma by Inhibiting Senescence Associated Inflammatory Factor IL8. *Scientific Reports*, *7*(1), 4186. https://doi.org/10.1038/s41598-017-04045-5
- Perry, R. P., Kelley, D. E., Friderici, K., & Rottman, F. (1975). The methylated constituents of L cell messenger RNA: Evidence for an unusual cluster at the 5′ terminus. *Cell*, *4*(4), 387–394. https://doi.org/10.1016/0092-8674(75)90159-2
- Pessina, F., Giavazzi, F., Yin, Y., Gioia, U., Vitelli, V., Galbiati, A., Barozzi, S., Garre, M., Oldani, A., Flaus, A., Cerbino, R., Parazzoli, D., Rothenberg, E., & d'Adda Di Fagagna, F. (2019). Functional transcription promoters at DNA double-strand breaks mediate RNA-driven phase separation of damage-response factors. *Nature Cell Biology*, *21*(10), 1286–1299. https://doi.org/10.1038/s41556-019-0392-4
- Petermann, E., Lan, L., & Zou, L. (2022). Sources, resolution and physiological relevance of R-loops and RNA–DNA hybrids. *Nature Reviews Molecular Cell Biology*, *23*(8), 521–540. https://doi.org/10.1038/s41580-022-00474-x
- Petesch, S. J., & Lis, J. T. (2008). Rapid, Transcription-Independent Loss of Nucleosomes over a Large Chromatin Domain at Hsp70 Loci. *Cell*, *134*(1), 74–84. https://doi.org/10.1016/j.cell.2008.05.029
- Pines, A., Vrouwe, M. G., Marteijn, J. A., Typas, D., Luijsterburg, M. S., Cansoy, M., Hensbergen, P., Deelder, A., De Groot, A., Matsumoto, S., Sugasawa, K., Thoma, N., Vermeulen, W., Vrieling, H., & Mullenders, L. (2012). PARP1 promotes nucleotide excision repair through DDB2 stabilization and recruitment of ALC1. *Journal of Cell Biology*, *199*(2), 235–249. https://doi.org/10.1083/jcb.201112132
- Ping, X.-L., Sun, B.-F., Wang, L., Xiao, W., Yang, X., Wang, W.-J., Adhikari, S., Shi, Y., Lv, Y., Chen, Y.-S., Zhao, X., Li, A., Yang, Y., Dahal, U., Lou, X.-M., Liu, X., Huang, J., Yuan, W.-P., Zhu, X.-F., … Yang, Y.-G. (2014). Mammalian WTAP is a regulatory subunit of the RNA N6-methyladenosine methyltransferase. *Cell Research*, *24*(2), 177–189. https://doi.org/10.1038/cr.2014.3
- Pleschke, J. M., Kleczkowska, H. E., Strohm, M., & Althaus, F. R. (2000). Poly(ADP-ribose) Binds to Specific Domains in DNA Damage Checkpoint Proteins. *Journal of Biological Chemistry*, *275*(52), 40974–40980. https://doi.org/10.1074/jbc.M006520200
- Poh, H. X., Mirza, A. H., Pickering, B. F., & Jaffrey, S. R. (2022). Alternative splicing of METTL3 explains apparently METTL3-independent m6A modifications in mRNA. *PLOS Biology*, *20*(7), e3001683. https://doi.org/10.1371/journal.pbio.3001683
- Poirier, G. G., De Murcia, G., Jongstra-Bilen, J., Niedergang, C., & Mandel, P. (1982). Poly(ADP-ribosyl)ation of polynucleosomes causes relaxation of chromatin structure. *Proceedings of the National Academy of Sciences*, *79*(11), 3423–3427. https://doi.org/10.1073/pnas.79.11.3423
- Purnell, M. R., & Whish, W. J. (1980). Novel inhibitors of poly(ADP-ribose) synthetase. *Biochemical Journal*, *185*(3), 775–777. https://doi.org/10.1042/bj1850775
- Qi, S., Mota, J., Chan, S.-H., Villarreal, J., Dai, N., Arya, S., Hromas, R. A., Rao, M. K., Corrêa Jr, I. R., & Gupta, Y. K. (2022). RNA binding to human METTL3-METTL14 restricts N6-deoxyadenosine methylation of DNA in vitro. *eLife*, *11*, e67150. https://doi.org/10.7554/eLife.67150
- Rack, J. G. M., Palazzo, L., & Ahel, I. (2020). (ADP-ribosyl)hydrolases: Structure, function, and biology. *Genes & Development*, *34*(5–6), 263–284. https://doi.org/10.1101/gad.334631.119
- Rack, J. G. M., Perina, D., & Ahel, I. (2016). Macrodomains: Structure, Function, Evolution, and Catalytic Activities. *Annual Review of Biochemistry*, *85*(1), 431–454. https://doi.org/10.1146/annurev-biochem-060815-014935
- Rafalska, I., Zhang, Z., Benderska, N., Wolff, H., Hartmann, A. M., Brack-Werner, R., & Stamm, S. (2004). The intranuclear localization and function of YT521-B is regulated by tyrosine phosphorylation. *Human Molecular Genetics*, *13*(15), 1535–1549. https://doi.org/10.1093/hmg/ddh167

- Ragupathi, A., Singh, M., Perez, A. M., & Zhang, D. (2023). Targeting the BRCA1/2 deficient cancer with PARP inhibitors: Clinical outcomes and mechanistic insights. *Frontiers in Cell and Developmental Biology*, *11*, 1133472. https://doi.org/10.3389/fcell.2023.1133472
- Rastogi, R. P., Richa, Kumar, A., Tyagi, M. B., & Sinha, R. P. (2010). Molecular Mechanisms of Ultraviolet Radiation-Induced DNA Damage and Repair. *Journal of Nucleic Acids*, *2010*, 1–32. https://doi.org/10.4061/2010/592980
- Ray Chaudhuri, A., & Nussenzweig, A. (2017). The multifaceted roles of PARP1 in DNA repair and chromatin remodelling. *Nature Reviews Molecular Cell Biology*, *18*(10), 610–621. https://doi.org/10.1038/nrm.2017.53
- Reber, J. M., Božić-Petković, J., Lippmann, M., Mazzardo, M., Dilger, A., Warmers, R., Bürkle, A., & Mangerich, A. (2023). PARP1 and XRCC1 exhibit a reciprocal relationship in genotoxic stress response. *Cell Biology and Toxicology*, *39*(1), 345–364. https://doi.org/10.1007/s10565-022-09739-9
- Reeder, R. H., Ueda, K., Honjo, T., Nishizuka, Y., & Hayaishi, O. (1967). Studies on the polymer of adenosine diphosphate ribose. II. Characterization of the polymer. *The Journal of Biological Chemistry*, *242*(13), 3172–3179.
- Rhine, K., Dasovich, M., Yoniles, J., Badiee, M., Skanchy, S., Ganser, L. R., Ge, Y., Fare, C. M., Shorter, J., Leung, A. K. L., & Myong, S. (2022). Poly(ADP-ribose) drives condensation of FUS via a transient interaction. *Molecular Cell*, *82*(5), 969-985.e11. https://doi.org/10.1016/j.molcel.2022.01.018
- Robu, M., Shah, R. G., Petitclerc, N., Brind'Amour, J., Kandan-Kulangara, F., & Shah, G. M. (2013). Role of poly(ADP-ribose) polymerase-1 in the removal of UV-induced DNA lesions by nucleotide excision repair. *Proceedings of the National Academy of Sciences*, *110*(5), 1658–1663. https://doi.org/10.1073/pnas.1209507110
- Robu, M., Shah, R. G., Purohit, N. K., Zhou, P., Naegeli, H., & Shah, G. M. (2017). Poly(ADP-ribose) polymerase 1 escorts XPC to UV-induced DNA lesions during nucleotide excision repair. *Proceedings of the National Academy of Sciences*, *114*(33). https://doi.org/10.1073/pnas.1706981114
- Roitt, I. M. (1956). The inhibition of carbohydrate metabolism in ascites-tumour cells by ethyleneimines. *The Biochemical Journal*, *63*(2), 300–307. https://doi.org/10.1042/bj0630300
- Rolli, V., O'Farrell, M., Ménissier-de Murcia, J., & De Murcia, G. (1997). Random Mutagenesis of the Poly(ADP-ribose) Polymerase Catalytic Domain Reveals Amino Acids Involved in Polymer Branching. *Biochemistry*, *36*(40), 12147–12154. https://doi.org/10.1021/bi971055p
- Ruf, A., Rolli, V., De Murcia, G., & Schulz, G. E. (1998). The mechanism of the elongation and branching reaction of Poly(ADP-ribose) polymerase as derived from crystal structures and mutagenesis. *Journal of Molecular Biology*, *278*(1), 57–65. https://doi.org/10.1006/jmbi.1998.1673
- Rulten, S. L., Rotheray, A., Green, R. L., Grundy, G. J., Moore, D. A. Q., Gómez-Herreros, F., Hafezparast, M., & Caldecott, K. W. (2014). PARP-1 dependent recruitment of the amyotrophic lateral sclerosis-associated protein FUS/TLS to sites of oxidative DNA damage. *Nucleic Acids Research*, *42*(1), 307–314. https://doi.org/10.1093/nar/gkt835
- Satoh, M. S., & Lindahl, T. (1992). Role of poly(ADP-ribose) formation in DNA repair. *Nature*, *356*(6367), 356–358. https://doi.org/10.1038/356356a0
- Schibler, U., & Perry, R. P. (1977). The 5′-termini of heterogeneous nuclear RNA: A comparison among molecules of different sizes and ages. *Nucleic Acids Research*, *4*(12), 4133–4150. https://doi.org/10.1093/nar/4.12.4133
- Schwartz, S., & Ast, G. (2010). Chromatin density and splicing destiny: On the cross-talk between chromatin structure and splicing. *The EMBO Journal*, *29*(10), 1629–1636. https://doi.org/10.1038/emboj.2010.71
- Sellou, H., Lebeaupin, T., Chapuis, C., Smith, R., Hegele, A., Singh, H. R., Kozlowski, M., Bultmann, S., Ladurner, A. G., Timinszky, G., & Huet, S. (2016). The poly(ADP-ribose)-dependent chromatin remodeler Alc1 induces local chromatin relaxation upon DNA damage. *Molecular Biology of the Cell*, *27*(24), 3791–3799. https://doi.org/10.1091/mbc.E16-05-0269
- Shall, S. (1975). Proceedings: Experimental manipulation of the specific activity of poly(ADP-ribose) polymerase. *Journal of Biochemistry*, *77*(1?), 2p.
- Shi, H., Wang, X., Lu, Z., Zhao, B. S., Ma, H., Hsu, P. J., Liu, C., & He, C. (2017). YTHDF3 facilitates translation and decay of N6-methyladenosine-modified RNA. *Cell Research*, *27*(3), 315–328. https://doi.org/10.1038/cr.2017.15
- Shi, Y., Di Giammartino, D. C., Taylor, D., Sarkeshik, A., Rice, W. J., Yates, J. R., Frank, J., & Manley, J. L. (2009). Molecular Architecture of the Human Pre-mRNA 3′ Processing Complex. *Molecular Cell*, *33*(3), 365–376. https://doi.org/10.1016/j.molcel.2008.12.028
- Shi, Y., Zheng, C., Jin, Y., Bao, B., Wang, D., Hou, K., Feng, J., Tang, S., Qu, X., Liu, Y., Che, X., & Teng, Y. (2020). Reduced Expression of METTL3 Promotes Metastasis of Triple-

Negative Breast Cancer by m6A Methylation-Mediated COL3A1 Up-Regulation. *Frontiers in Oncology*, *10*, 1126. https://doi.org/10.3389/fonc.2020.01126

- Shieh, W. M., Amé, J.-C., Wilson, M. V., Wang, Z.-Q., Koh, D. W., Jacobson, M. K., & Jacobson, E. L. (1998). Poly(ADP-ribose) Polymerase Null Mouse Cells Synthesize ADP-ribose Polymers. *Journal of Biological Chemistry*, *273*(46), 30069–30072. https://doi.org/10.1074/jbc.273.46.30069
- Shiloh, Y. (2003). ATM and related protein kinases: Safeguarding genome integrity. *Nature Reviews Cancer*, *3*(3), 155–168. https://doi.org/10.1038/nrc1011
- Singatulina, A. S., Hamon, L., Sukhanova, M. V., Desforges, B., Joshi, V., Bouhss, A., Lavrik, O. I., & Pastré, D. (2019). PARP-1 Activation Directs FUS to DNA Damage Sites to Form PARG-Reversible Compartments Enriched in Damaged DNA. *Cell Reports*, *27*(6), 1809-1821.e5. https://doi.org/10.1016/j.celrep.2019.04.031
- Śledź, P., & Jinek, M. (2016). Structural insights into the molecular mechanism of the m6A writer complex. *eLife*, *5*, e18434. https://doi.org/10.7554/eLife.18434
- Slobodin, B., Han, R., Calderone, V., Vrielink, J. A. F. O., Loayza-Puch, F., Elkon, R., & Agami, R. (2017). Transcription Impacts the Efficiency of mRNA Translation via Co-transcriptional N6-adenosine Methylation. *Cell*, *169*(2), 326-337.e12. https://doi.org/10.1016/j.cell.2017.03.031
- Smeenk, G., Wiegant, W. W., Marteijn, J. A., Luijsterburg, M. S., Sroczynski, N., Costelloe, T., Romeijn, R. J., Pastink, A., Mailand, N., Vermeulen, W., & Van Attikum, H. (2012). Poly(ADP-ribosyl)ation links the chromatin remodeler SMARCA5/SNF2H to RNF168-dependent DNA damage signaling. *Journal of Cell Science*, jcs.109413. https://doi.org/10.1242/jcs.109413
- Smith, R., Lebeaupin, T., Juhász, S., Chapuis, C., D'Augustin, O., Dutertre, S., Burkovics, P., Biertümpfel, C., Timinszky, G., & Huet, S. (2019). Poly(ADP-ribose)-dependent chromatin unfolding facilitates the association of DNA-binding proteins with DNA at sites of damage. *Nucleic Acids Research*, *47*(21), 11250–11267. https://doi.org/10.1093/nar/gkz820
- Smith, R., Sellou, H., Chapuis, C., Huet, S., & Timinszky, G. (2018). CHD3 and CHD4 recruitment and chromatin remodeling activity at DNA breaks is promoted by early poly(ADP-ribose)-dependent chromatin relaxation. *Nucleic Acids Research*, *46*(12), 6087–6098. https://doi.org/10.1093/nar/gky334
- Sobell, H. M. (1985). Actinomycin and DNA transcription. *Proceedings of the National Academy of Sciences*, *82*(16), 5328–5331. https://doi.org/10.1073/pnas.82.16.5328
- Song, T., Lv, S., Li, N., Zhao, X., Ma, X., Yan, Y., Wang, W., & Sun, L. (2022). Versatile functions of RNA m6A machinery on chromatin. *Journal of Molecular Cell Biology*, *14*(3), mjac011. https://doi.org/10.1093/jmcb/mjac011
- Strumberg, D., Pilon, A. A., Smith, M., Hickey, R., Malkas, L., & Pommier, Y. (2000). Conversion of Topoisomerase I Cleavage Complexes on the Leading Strand of Ribosomal DNA into 5′-Phosphorylated DNA Double-Strand Breaks by Replication Runoff. *Molecular and Cellular Biology*, *20*(11), 3977–3987. https://doi.org/10.1128/MCB.20.11.3977-3987.2000
- Sugasawa, K. (2016). Molecular mechanisms of DNA damage recognition for mammalian nucleotide excision repair. *DNA Repair*, *44*, 110–117. https://doi.org/10.1016/j.dnarep.2016.05.015
- Sugimura, T., Fujimura, S., Hasegawa, S., & Kawamura, Y. (1967). Polymerization of the adenosine 5′-diphosphate ribose moiety of NAD by rat liver nuclear enzyme. *Biochimica et Biophysica Acta (BBA) - Nucleic Acids and Protein Synthesis*, *138*(2), 438–441. https://doi.org/10.1016/0005-2787(67)90507-2
- Sun, F.-H., Zhao, P., Zhang, N., Kong, L.-L., Wong, C. C. L., & Yun, C.-H. (2021). HPF1 remodels the active site of PARP1 to enable the serine ADP-ribosylation of histones. *Nature Communications*, *12*(1), 1028. https://doi.org/10.1038/s41467-021-21302-4
- Suskiewicz, M. J., Zobel, F., Ogden, T. E. H., Fontana, P., Ariza, A., Yang, J.-C., Zhu, K., Bracken, L., Hawthorne, W. J., Ahel, D., Neuhaus, D., & Ahel, I. (2020). HPF1 completes the PARP active site for DNA damage-induced ADP-ribosylation. *Nature*, *579*(7800), 598–602. https://doi.org/10.1038/s41586-020-2013-6
- Svobodová Kovaříková, A., Stixová, L., Kovařík, A., Komůrková, D., Legartová, S., Fagherazzi, P., & Bártová, E. (2020). N6-Adenosine Methylation in RNA and a Reduced m3G/TMG Level in Non-Coding RNAs Appear at Microirradiation-Induced DNA Lesions. *Cells*, *9*(2), 360. https://doi.org/10.3390/cells9020360
- Tang, C., Klukovich, R., Peng, H., Wang, Z., Yu, T., Zhang, Y., Zheng, H., Klungland, A., & Yan, W. (2018). ALKBH5-dependent m6A demethylation controls splicing and stability of long 3′-UTR mRNAs in male germ cells. *Proceedings of the National Academy of Sciences*, *115*(2). https://doi.org/10.1073/pnas.1717794115
- Teloni, F., & Altmeyer, M. (2016). Readers of poly(ADP-ribose): Designed to be fit for purpose. *Nucleic Acids Research*, *44*(3), 993–1006. https://doi.org/10.1093/nar/gkv1383

- Thevenaz, P., Ruttimann, U. E., & Unser, M. (1998). A pyramid approach to subpixel registration based on intensity. *IEEE Transactions on Image Processing*, *7*(1), 27–41. https://doi.org/10.1109/83.650848
- Thomas, C., Ji, Y., Wu, C., Datz, H., Boyle, C., MacLeod, B., Patel, S., Ampofo, M., Currie, M., Harbin, J., Pechenkina, K., Lodhi, N., Johnson, S. J., & Tulin, A. V. (2019). Hit and run versus long-term activation of PARP-1 by its different domains fine-tunes nuclear processes. *Proceedings of the National Academy of Sciences*, *116*(20), 9941–9946. https://doi.org/10.1073/pnas.1901183116
- Timinszky, G., Till, S., Hassa, P. O., Hothorn, M., Kustatscher, G., Nijmeijer, B., Colombelli, J., Altmeyer, M., Stelzer, E. H. K., Scheffzek, K., Hottiger, M. O., & Ladurner, A. G. (2009). A macrodomain-containing histone rearranges chromatin upon sensing PARP1 activation. *Nature Structural & Molecular Biology*, *16*(9), 923–929. https://doi.org/10.1038/nsmb.1664
- Toh, J. D. W., Crossley, S. W. M., Bruemmer, K. J., Ge, E. J., He, D., Iovan, D. A., & Chang, C. J. (2020). Distinct RNA *N*- demethylation pathways catalyzed by nonheme iron ALKBH5 and FTO enzymes enable regulation of formaldehyde release rates. *Proceedings of the National Academy of Sciences*, *117*(41), 25284–25292. https://doi.org/10.1073/pnas.2007349117
- Tóth, K. F., Knoch, T. A., Wachsmuth, M., Frank-Stöhr, M., Stöhr, M., Bacher, C. P., Müller, G., & Rippe, K. (2004). Trichostatin A-induced histone acetylation causes decondensation of interphase chromatin. *Journal of Cell Science*, *117*(18), 4277–4287. https://doi.org/10.1242/jcs.01293
- Tulin, A., & Spradling, A. (2003). Chromatin Loosening by Poly(ADP)-Ribose Polymerase (PARP) at *Drosophila* Puff Loci. *Science*, *299*(5606), 560–562. https://doi.org/10.1126/science.1078764
- Turner, N., Tutt, A., & Ashworth, A. (2004). Hallmarks of “BRCAness” in sporadic cancers. *Nature Reviews Cancer*, *4*(10), 814–819. https://doi.org/10.1038/nrc1457
- Van Beek, L., McClay, É., Patel, S., Schimpl, M., Spagnolo, L., & Maia De Oliveira, T. (2021). PARP Power: A Structural Perspective on PARP1, PARP2, and PARP3 in DNA Damage Repair and Nucleosome Remodelling. *International Journal of Molecular Sciences*, *22*(10), 5112. https://doi.org/10.3390/ijms22105112
- Van Den Heuvel, D., Van Der Weegen, Y., Boer, D. E. C., Ogi, T., & Luijsterburg, M. S. (2021). Transcription-Coupled DNA Repair: From Mechanism to Human Disorder. *Trends in Cell Biology*, *31*(5), 359–371. https://doi.org/10.1016/j.tcb.2021.02.007
- Van Der Weegen, Y., De Lint, K., Van Den Heuvel, D., Nakazawa, Y., Mevissen, T. E. T., Van Schie, J. J. M., San Martin Alonso, M., Boer, D. E. C., González-Prieto, R., Narayanan, I. V., Klaassen, N. H. M., Wondergem, A. P., Roohollahi, K., Dorsman, J. C., Hara, Y., Vertegaal, A. C. O., De Lange, J., Walter, J. C., Noordermeer, S. M., … Luijsterburg, M. S. (2021). ELOF1 is a transcription-coupled DNA repair factor that directs RNA polymerase II ubiquitylation. *Nature Cell Biology*, *23*(6), 595–607. https://doi.org/10.1038/s41556-021-00688-9
- Van Gent, D. C., Hoeijmakers, J. H. J., & Kanaar, R. (2001). Chromosomal stability and the DNA double-stranded break connection. *Nature Reviews Genetics*, *2*(3), 196–206. https://doi.org/10.1038/35056049
- Vidal, A. E. (2001). XRCC1 coordinates the initial and late stages of DNA abasic site repair through protein-protein interactions. *The EMBO Journal*, *20*(22), 6530–6539. https://doi.org/10.1093/emboj/20.22.6530
- Visvanathan, A., Patil, V., Arora, A., Hegde, A. S., Arivazhagan, A., Santosh, V., & Somasundaram, K. (2018). Essential role of METTL3-mediated m6A modification in glioma stem-like cells maintenance and radioresistance. *Oncogene*, *37*(4), 522–533. https://doi.org/10.1038/onc.2017.351
- Vu, L. P., Pickering, B. F., Cheng, Y., Zaccara, S., Nguyen, D., Minuesa, G., Chou, T., Chow, A., Saletore, Y., MacKay, M., Schulman, J., Famulare, C., Patel, M., Klimek, V. M., Garrett-Bakelman, F. E., Melnick, A., Carroll, M., Mason, C. E., Jaffrey, S. R., & Kharas, M. G. (2017). The N6-methyladenosine (m6A)-forming enzyme METTL3 controls myeloid differentiation of normal hematopoietic and leukemia cells. *Nature Medicine*, *23*(11), 1369–1376. https://doi.org/10.1038/nm.4416
- Vujovic, P., Stamenkovic, S., Jasnic, N., Lakic, I., Djurasevic, S. F., Cvijic, G., & Djordjevic, J. (2013). Fasting Induced Cytoplasmic Fto expression in Some Neurons of Rat Hypothalamus. *PLoS ONE*, *8*(5), e63694. https://doi.org/10.1371/journal.pone.0063694
- Wang, G., & Vasquez, K. (2017). Effects of Replication and Transcription on DNA Structure-Related Genetic Instability. *Genes*, *8*(1), 17. https://doi.org/10.3390/genes8010017
- Wang, M., Wu, W., Wu, W., Rosidi, B., Zhang, L., Wang, H., & Iliakis, G. (2006). PARP-1 and Ku compete for repair of DNA double strand breaks by distinct NHEJ pathways. *Nucleic Acids Research*, *34*(21), 6170–6182. https://doi.org/10.1093/nar/gkl840

- Wang, M., Yuan, Z., Xie, R., Ma, Y., Liu, X., & Yu, X. (2018). Structure–function analyses reveal the mechanism of the ARH3-dependent hydrolysis of ADP-ribosylation. *Journal of Biological Chemistry*, *293*(37), 14470–14480. https://doi.org/10.1074/jbc.RA118.004284
- Wang, S., Lv, W., Li, T., Zhang, S., Wang, H., Li, X., Wang, L., Ma, D., Zang, Y., Shen, J., Xu, Y., & Wei, W. (2022). Dynamic regulation and functions of mRNA m6A modification. *Cancer Cell International*, *22*(1), 48. https://doi.org/10.1186/s12935-022-02452-x
- Wang, X., Feng, J., Xue, Y., Guan, Z., Zhang, D., Liu, Z., Gong, Z., Wang, Q., Huang, J., Tang, C., Zou, T., & Yin, P. (2016). Structural basis of N6-adenosine methylation by the METTL3–METTL14 complex. *Nature*, *534*(7608), 575–578. https://doi.org/10.1038/nature18298
- Wang, X., Lu, Z., Gomez, A., Hon, G. C., Yue, Y., Han, D., Fu, Y., Parisien, M., Dai, Q., Jia, G., Ren, B., Pan, T., & He, C. (2014). N6-methyladenosine-dependent regulation of messenger RNA stability. *Nature*, *505*(7481), 117–120. https://doi.org/10.1038/nature12730
- Wang, X., Zhao, B. S., Roundtree, I. A., Lu, Z., Han, D., Ma, H., Weng, X., Chen, K., Shi, H., & He, C. (2015). N6-methyladenosine Modulates Messenger RNA Translation Efficiency. *Cell*, *161*(6), 1388–1399. https://doi.org/10.1016/j.cell.2015.05.014
- Wang, Y., Huang, J.-W., Li, M., Cavenee, W. K., Mitchell, P. S., Zhou, X., Tewari, M., Furnari, F. B., & Taniguchi, T. (2011). MicroRNA-138 Modulates DNA Damage Response by Repressing Histone H2AX Expression. *Molecular Cancer Research*, *9*(8), 1100–1111. https://doi.org/10.1158/1541-7786.MCR-11-0007
- Wang, Y., Li, Y., Yue, M., Wang, J., Kumar, S., Wechsler-Reya, R. J., Zhang, Z., Ogawa, Y., Kellis, M., Duester, G., & Zhao, J. C. (2018). N6-methyladenosine RNA modification regulates embryonic neural stem cell self-renewal through histone modifications. *Nature Neuroscience*, *21*(2), 195–206. https://doi.org/10.1038/s41593-017-0057-1
- Wang, Z., Michaud, G. A., Cheng, Z., Zhang, Y., Hinds, T. R., Fan, E., Cong, F., & Xu, W. (2012). Recognition of the *iso* -ADP-ribose moiety in poly(ADP-ribose) by WWE domains suggests a general mechanism for poly(ADP-ribosyl)ation-dependent ubiquitination. *Genes & Development*, *26*(3), 235–240. https://doi.org/10.1101/gad.182618.111
- Wei, J., Liu, F., Lu, Z., Fei, Q., Ai, Y., He, P. C., Shi, H., Cui, X., Su, R., Klungland, A., Jia, G., Chen, J., & He, C. (2018). Differential m6A, m6Am, and m1A Demethylation Mediated by FTO in the Cell Nucleus and Cytoplasm. *Molecular Cell*, *71*(6), 973-985.e5. https://doi.org/10.1016/j.molcel.2018.08.011
- Wei, W., Ba, Z., Gao, M., Wu, Y., Ma, Y., Amiard, S., White, C. I., Rendtlew Danielsen, J. M., Yang, Y.-G., & Qi, Y. (2012). A Role for Small RNAs in DNA Double-Strand Break Repair. *Cell*, *149*(1), 101–112. https://doi.org/10.1016/j.cell.2012.03.002
- Wei, W., Huo, B., & Shi, X. (2019). miR-600 inhibits lung cancer via downregulating the expression of METTL3. *Cancer Management and Research*, *Volume 11*, 1177–1187. https://doi.org/10.2147/CMAR.S181058
- Weixler, L., Feijs, K. L. H., & Zaja, R. (2022). ADP-ribosylation of RNA in mammalian cells is mediated by TRPT1 and multiple PARPs. *Nucleic Acids Research*, *50*(16), 9426–9441. https://doi.org/10.1093/nar/gkac711
- Wen, J., Lv, R., Ma, H., Shen, H., He, C., Wang, J., Jiao, F., Liu, H., Yang, P., Tan, L., Lan, F., Shi, Y. G., He, C., Shi, Y., & Diao, J. (2018). Zc3h13 Regulates Nuclear RNA m6A Methylation and Mouse Embryonic Stem Cell Self-Renewal. *Molecular Cell*, *69*(6), 1028-1038.e6. https://doi.org/10.1016/j.molcel.2018.02.015
- Woodcock, C. B., Yu, D., Hajian, T., Li, J., Huang, Y., Dai, N., Corrêa, I. R., Wu, T., Vedadi, M., Zhang, X., & Cheng, X. (2019). Human MettL3–MettL14 complex is a sequence-specific DNA adenine methyltransferase active on single-strand and unpaired DNA in vitro. *Cell Discovery*, *5*(1), 63. https://doi.org/10.1038/s41421-019-0136-4
- Woolley, P. R., Wen, X., Conway, O. M., Ender, N. A., Lee, J.-H., & Paull, T. T. (2024). Regulation of transcription patterns, poly(ADP-ribose), and RNA-DNA hybrids by the ATM protein kinase. *Cell Reports*, *43*(3), 113896. https://doi.org/10.1016/j.celrep.2024.113896
- Wu, L., Wu, D., Ning, J., Liu, W., & Zhang, D. (2019). Changes of N6-methyladenosine modulators promote breast cancer progression. *BMC Cancer*, *19*(1), 326. https://doi.org/10.1186/s12885-019-5538-z
- Wu, W., Hill, S. E., Nathan, W. J., Paiano, J., Callen, E., Wang, D., Shinoda, K., Van Wietmarschen, N., Colón-Mercado, J. M., Zong, D., De Pace, R., Shih, H.-Y., Coon, S., Parsadanian, M., Pavani, R., Hanzlikova, H., Park, S., Jung, S. K., McHugh, P. J., … Nussenzweig, A. (2021). Neuronal enhancers are hotspots for DNA single-strand break repair. *Nature*, *593*(7859), 440–444. https://doi.org/10.1038/s41586-021-03468-5
- Xiang, Y., Laurent, B., Hsu, C.-H., Nachtergaele, S., Lu, Z., Sheng, W., Xu, C., Chen, H., Ouyang, J., Wang, S., Ling, D., Hsu, P.-H., Zou, L., Jambhekar, A., He, C., & Shi, Y. (2017). RNA m6A methylation regulates the ultraviolet-induced DNA damage response. *Nature*, *543*(7646), 573–576. https://doi.org/10.1038/nature21671

- Xiao, W., Adhikari, S., Dahal, U., Chen, Y.-S., Hao, Y.-J., Sun, B.-F., Sun, H.-Y., Li, A., Ping, X.-L., Lai, W.-Y., Wang, X., Ma, H.-L., Huang, C.-M., Yang, Y., Huang, N., Jiang, G.-B., Wang, H.-L., Zhou, Q., Wang, X.-J., … Yang, Y.-G. (2016). Nuclear m 6 A Reader YTHDC1 Regulates mRNA Splicing. *Molecular Cell*, *61*(4), 507–519. https://doi.org/10.1016/j.molcel.2016.01.012
- Xu, C., Wang, X., Liu, K., Roundtree, I. A., Tempel, W., Li, Y., Lu, Z., He, C., & Min, J. (2014). Structural basis for selective binding of m6A RNA by the YTHDC1 YTH domain. *Nature Chemical Biology*, *10*(11), 927–929. https://doi.org/10.1038/nchembio.1654
- Xu, W., He, C., Kaye, E. G., Li, J., Mu, M., Nelson, G. M., Dong, L., Wang, J., Wu, F., Shi, Y. G., Adelman, K., Lan, F., Shi, Y., & Shen, H. (2022). Dynamic control of chromatin-associated m6A methylation regulates nascent RNA synthesis. *Molecular Cell*, *82*(6), 1156-1168.e7. https://doi.org/10.1016/j.molcel.2022.02.006
- Yamada, T., Horimoto, H., Kameyama, T., Hayakawa, S., Yamato, H., Dazai, M., Takada, A., Kida, H., Bott, D., Zhou, A. C., Hutin, D., Watts, T. H., Asaka, M., Matthews, J., & Takaoka, A. (2016). Constitutive aryl hydrocarbon receptor signaling constrains type I interferon–mediated antiviral innate defense. *Nature Immunology*, *17*(6), 687–694. https://doi.org/10.1038/ni.3422
- Yang, H., Lachtara, E. M., Ran, X., Hopkins, J., Patel, P. S., Zhu, X., Xiao, Y., Phoon, L., Gao, B., Zou, L., Lawrence, M. S., & Lan, L. (2023). The RNA m5C modification in R-loops as an off switch of Alt-NHEJ. *Nature Communications*, *14*(1), 6114. https://doi.org/10.1038/s41467-023-41790-w
- Yang, J. (2003). ATM, ATR and DNA-PK: Initiators of the cellular genotoxic stress responses. *Carcinogenesis*, *24*(10), 1571–1580. https://doi.org/10.1093/carcin/bgg137
- Yankova, E., Blackaby, W., Albertella, M., Rak, J., De Braekeleer, E., Tsagkogeorga, G., Pilka, E. S., Aspris, D., Leggate, D., Hendrick, A. G., Webster, N. A., Andrews, B., Fosbeary, R., Guest, P., Irigoyen, N., Eleftheriou, M., Gozdecka, M., Dias, J. M. L., Bannister, A. J., … Kouzarides, T. (2021). Small-molecule inhibition of METTL3 as a strategy against myeloid leukaemia. *Nature*, *593*(7860), 597–601. https://doi.org/10.1038/s41586-021-03536-w
- Ye, B. J., Kang, H. J., Lee-Kwon, W., Kwon, H. M., & Choi, S. Y. (2021). PARP1-mediated PARylation of TonEBP prevents R-loop–associated DNA damage. *DNA Repair*, *104*, 103132. https://doi.org/10.1016/j.dnarep.2021.103132
- Yu, D., Horton, J. R., Yang, J., Hajian, T., Vedadi, M., Sagum, C. A., Bedford, M. T., Blumenthal, R. M., Zhang, X., & Cheng, X. (2021). Human MettL3-MettL14 RNA adenine methyltransferase complex is active on double-stranded DNA containing lesions. *Nucleic Acids Research*, *49*(20), 11629–11642. https://doi.org/10.1093/nar/gkab460
- Yu, W., Ginjala, V., Pant, V., Chernukhin, I., Whitehead, J., Docquier, F., Farrar, D., Tavoosidana, G., Mukhopadhyay, R., Kanduri, C., Oshimura, M., Feinberg, A. P., Lobanenkov, V., Klenova, E., & Ohlsson, R. (2004). Poly(ADP-ribosyl)ation regulates CTCF-dependent chromatin insulation. *Nature Genetics*, *36*(10), 1105–1110. https://doi.org/10.1038/ng1426
- Zhang, C., Chen, L., Peng, D., Jiang, A., He, Y., Zeng, Y., Xie, C., Zhou, H., Luo, X., Liu, H., Chen, L., Ren, J., Wang, W., & Zhao, Y. (2020). METTL3 and N6-Methyladenosine Promote Homologous Recombination-Mediated Repair of DSBs by Modulating DNA-RNA Hybrid Accumulation. *Molecular Cell*, *79*(3), 425-442.e7. https://doi.org/10.1016/j.molcel.2020.06.017
- Zhang, F., Chen, Y., Li, M., & Yu, X. (2014). The oligonucleotide/oligosaccharide-binding fold motif is a poly(ADP-ribose)-binding domain that mediates DNA damage response. *Proceedings of the National Academy of Sciences*, *111*(20), 7278–7283. https://doi.org/10.1073/pnas.1318367111
- Zhang, F., Wang, Y., Wang, L., Luo, X., Huang, K., Wang, C., Du, M., Liu, F., Luo, T., Huang, D., & Huang, K. (2013). Poly(ADP-ribose) Polymerase 1 Is a Key Regulator of Estrogen Receptor α-dependent Gene Transcription. *Journal of Biological Chemistry*, *288*(16), 11348–11357. https://doi.org/10.1074/jbc.M112.429134
- Zhang, J., Chen, F., Tang, M., Xu, W., Tian, Y., Liu, Z., Shu, Y., Yang, H., Zhu, Q., Lu, X., Peng, B., Liu, X., Xu, X., Gullerova, M., & Zhu, W.-G. (2024). The ARID1A-METTL3-m6A axis ensures effective RNase H1-mediated resolution of R-loops and genome stability. *Cell Reports*, *43*(2), 113779. https://doi.org/10.1016/j.celrep.2024.113779
- Zhang, S., Zhao, B. S., Zhou, A., Lin, K., Zheng, S., Lu, Z., Chen, Y., Sulman, E. P., Xie, K., Bögler, O., Majumder, S., He, C., & Huang, S. (2017). M 6 A Demethylase ALKBH5 Maintains Tumorigenicity of Glioblastoma Stem-like Cells by Sustaining FOXM1 Expression and Cell Proliferation Program. *Cancer Cell*, *31*(4), 591-606.e6. https://doi.org/10.1016/j.ccell.2017.02.013
- Zhang, Z., Hildebrandt, E. F., Simbulan-Rosenthal, C. M., & Anderson, M. G. (2002). Sequence-Specific Binding of Poly(ADP-Ribose) Polymerase-1 to the Human T Cell Leukemia Virus Type-I Tax Responsive Element. *Virology*, *296*(1), 107–116. https://doi.org/10.1006/viro.2002.1385

- Zheng, G., Dahl, J. A., Niu, Y., Fedorcsak, P., Huang, C.-M., Li, C. J., Vågbø, C. B., Shi, Y., Wang, W.-L., Song, S.-H., Lu, Z., Bosmans, R. P. G., Dai, Q., Hao, Y.-J., Yang, X., Zhao, W.-M., Tong, W.-M., Wang, X.-J., Bogdan, F., … He, C. (2013). ALKBH5 Is a Mammalian RNA Demethylase that Impacts RNA Metabolism and Mouse Fertility. *Molecular Cell*, *49*(1), 18–29. https://doi.org/10.1016/j.molcel.2012.10.015
- Zhong, L., Liao, D., Zhang, M., Zeng, C., Li, X., Zhang, R., Ma, H., & Kang, T. (2019). YTHDF2 suppresses cell proliferation and growth via destabilizing the EGFR mRNA in hepatocellular carcinoma. *Cancer Letters*, *442*, 252–261. https://doi.org/10.1016/j.canlet.2018.11.006
- Zhou, J., Wan, J., Gao, X., Zhang, X., Jaffrey, S. R., & Qian, S.-B. (2015a). Dynamic m6A mRNA methylation directs translational control of heat shock response. *Nature*, *526*(7574), 591–594. https://doi.org/10.1038/nature15377
- Zobeck, K. L., Buckley, M. S., Zipfel, W. R., & Lis, J. T. (2010). Recruitment Timing and Dynamics of Transcription Factors at the Hsp70 Loci in Living Cells. *Molecular Cell*, *40*(6), 965–975. https://doi.org/10.1016/j.molcel.2010.11.022
- Zong, W., Gong, Y., Sun, W., Li, T., & Wang, Z.-Q. (2022). PARP1: Liaison of Chromatin Remodeling and Transcription. *Cancers*, *14*(17), 4162. https://doi.org/10.3390/cancers14174162

Appendix 1: Affidavit

LMU LUDWIG-MAXIMILIANS-UNIVERSITÄT MÜNCHEN

Dekanat Medizinische Fakultät
Promotionsbüro

Affidavit

Gonzalez Leal, Claudia Patricia

Surname, first name

I hereby declare, that the submitted thesis entitled:

The role of METTL3 and ADP-ribosylation in DNA repair

is my own work. I have only used the sources indicated and have not made unauthorised use of services of a third party. Where the work of others has been quoted or reproduced, the source is always given.

I further declare that the dissertation presented here has not been submitted in the same or similar form to any other institution for the purpose of obtaining an academic degree.

Basel, 15.Feb.2025

Place, Date

Claudia Patricia Gonzalez Leal

Signature doctoral candidate

Appendix 2: Confirmation of congruency

LMU LUDWIG-MAXIMILIANS-UNIVERSITÄT MÜNCHEN

Dekanat Medizinische Fakultät
Promotionsbüro

Confirmation of congruency between printed and electronic version of the doctoral thesis

Gonzalez Leal, Claudia Patricia

name, first name

I hereby declare that the electronic version of the submitted thesis, entitled:

The role of METTL3 and ADP-ribosylation in DNA repair

is congruent with the printed version both in content and format.

Basel, 18.Feb.2026

Place, Date

Claudia Patricia Gonzalez Leal

Signature doctoral candidate

Appendix 3: List of publications

Gonzalez-Leal, C., Cai, Jin, de Groot B.A.F.F., Wegerer, A., Preisser, J., Luijsterburg, M.S., Ladurner, A.G. “Poly-(ADP-ribose) serves as a scaffold for the methyltransferase METTL3/14 complex in the DNA damage response. *Nucleic Acids Res.* (2025):53(7):gkaf244. doi: 10.1093/nar/gkaf244.

Gonzalez-Leal, C. and Andreas G Ladurner. “A triskelion of nucleic acids drives protein aggregation in A-T.” *Molecular cell* vol. 81,7 (2021): 1367-1369. doi:10.1016/j.molcel.2021.03.017

Blessing, C., Apelt, K., van den Heuvel, D., **Gonzalez-Leal, C**., Rother, M., van der Woude, M., Gonzalez-Prieto, R., Yifrach, A., Parnas, A., Shah, R., Tyrsett Kuo, T., Boer, D., Cai, J., Kragten, A., Suk Kim, Hyun., Orlando, S., Vertegaal, A., Shah, G., Adar, S., Lans, H., van Attikum, H., Ladurner, A.G., Luijsterburg, M. “XPC-PARP complexes engage the chromatin remodeler ALC1 to catalyze global genome DNA damage repair.” *Nature communications* vol. 13,1 4762. 13 Aug. 2022, doi:10.1038/s41467-022-31820-4

Blessing, C., Mandemaker, I.K., **Gonzalez-Leal, C**., Preisser, J., Schomburg, A., and Ladurner, A.G. “The Oncogenic Helicase ALC1 Regulates PARP Inhibitor Potency by Trapping PARP2 at DNA Breaks.” *Molecular cell* vol. 80,5 (2020): 862-875.e6. doi:10.1016/j.molcel.2020.10.009

Dankers, W., **Gonzalez-Leal, C.,** Davelaar, N., Asmawidjaja, P. S., Mus, A. M. C., Hazes, J. M. W., Colin, E. M., and Lubberts, E. “1,25$(OH)_2D_3$ and dexamethasone additively suppress synovial fibroblast activation by $CCR6^+$ T helper memory cells and enhance the effect of tumor necrosis factor alpha blockade.” *Arthritis research & therapy* vol. 20,1 212. 20 Sep. 2018, doi:10.1186/s13075-018-1706-9

Vazquez-Villegas, P., Ouellet, E., **González, C**., Ruiz-Ruiz, F., Rito-Palomares, M., Haynes, C. A., Aguilar, O. “A microdevice assisted approach for the preparation, characterization and selection of continuous aqueous two-phase systems: From micro to bench-scale” Lab on a Chip. 2016 16(14), doi:10.1039/C6LC00333H